NASA CR 165448

NASA

NATIONAL AERONAUTICS AND
SPACE ADMINISTRATION

KEVLAR/PMR-15 REDUCED DRAG DC-9 REVERSER STANG FAIRING

BY

R. T. KAWAI

DOUGLAS AIRCRAFT COMPANY
MCDONNELL DOUGLAS CORPORATION

AUGUST 1982

PREPARED FOR
NATIONAL AERONAUTICS AND SPACE ADMINISTRATION

NOTE:

Pages 58-59, 61-64, 68, 72-73, 77, 85, 89, 91, 93-94, 97-98, and Appendix pages A-1, 5-9, 33-34, 36-40, 42-46, 48-51, and 53 have been deleted from this document to remove data that is restricted For Early Domestic Dissemination (FEDD).

NASA LEWIS RESEARCH CENTER
CONTRACT NAS3-21763

FOREWORD

The work reported herein was conducted by the Douglas Aircraft Company component of McDonnell Douglas Corporation in Long Beach, California, for the Engine Component Improvement Program Office at the National Aeronautics and Space Administration Lewis Research Center in Cleveland, Ohio. The work was performed as Task 1 of Contract NAS3-21763 titled, "JT8D Nacelle Drag Reduction in DC-9 Aircraft and Engine Bleed Air Usage Reduction in DC-10 Aircraft ECI Performance Improvements." Task 1 was the development of an advanced composite thrust reverser stang fairing to reduce drag on the JT8D nacelles of DC-9 aircraft. Task 2 was the development of a cabin air recirculation system for the DC-10 and is reported in NASA CR159846, dated September 1980.

The Douglas Project Manager was R.T. Kawai with major support from: M.S. Willer and J.A. Bouey, Aerodynamics; N. Belevtsov, Flight Test; R.J. Palmer, R.M. Moore, and T.F. Morris, Materials and Process; A. Zsolnay and R.T. Hartunian, Manufacturing Research and Development; R.F. McCarthy and J.S. Ehret, Power Plant; R.L. Kinsey, Quality Assurance; F.J. Braun, Structural Mechanics. The Douglas Program Manager was M. Klotzsche.

The NASA Project Engineer was F.J. Hrach and NASA Program Managers J. A. Ziemianski and J.E. McAulay.

This program was initiated in September 1978 and completed in July 1982.

NOTE:

Pages 58-59, 61-64, 68, 72-73, 77, 85, 89, 91, 93-94, 97-98, and Appendix pages A-1, 5-9, 33-34, 36-40, 42-46, 48-51, and 53 have been deleted from this document to remove data that is restricted For Early Domestic Dissemination (FEDD).

TABLE OF CONTENTS

		PAGE
1.0	SUMMARY	1
2.0	INTRODUCTION	3
3.0	DESIGN	6
	3.1 Aerodynamic Configuration Development	6
	3.2 Composite Design	46
4.0	FABRICATION	72
	4.1 Material and Process Evaluations	72
	4.2 Tooling	82
	4.3 Layup and Forming	85
	4.4 Curing	94
	4.5 Trimming	94
	4.6 Installation	104
5.0	ECONOMIC ASSESSMENT	110
6.0	CONCLUSION	113
	6.1 Accomplishment of Goals	114
7.0	PRODUCT ASSURANCE	116
	REFERENCES	120
	APPENDIX	
	Mechanical Properties of Kevlar-49/PMR-15	

SECTION 1

SUMMARY

A development program was conducted to reduce the fuel consumption of the DC-9 aircraft by decreasing the drag of the thrust reverser stang fairing on the JT8D nacelle. This was to be accomplished by improving the aerodynamic configuration of the fairing. The development included the use of composite materials in order to reduce system weight.

A series of stang fairing configurations were flight tested. The most desirable fairing reduced the airplane drag by an estimated 1% at cruise when compared with the current production baseline. This is approximately equivalent to a reduction in engine specific fuel consumption of 1%. The composite material selected and used in fabrication of the fairing was Kevlar-49/PMR-15. This material system resulted in a 40% weight savings compared to an equivalent system made from metal. It also proved to be capable of withstanding the 533°K (500°F) temperature exhaust flow during reverse thrust and exposure to hydraulic fluid (Skydrol), moisture, and vibration due to the high noise environment.

Material property tests were conducted on Kevlar-49/PMR-15 and the results are presented. They include the effects of temperature, hydraulic fluid, and moisture. The fatigue resistance of Kevlar-49/PMR-15 was judged to be satisfactory in the high noise environment that exists at the engine exhaust nozzle.

The stang fairing capable of reducing drag by 1% was complex in shape with sharp radii and reverse curvature. A multipiece retractable male mold was produced and an autoclave procedure was developed to provide a suitable fabrication technique.

SECTION 2
INTRODUCTION

At the request of Congress, the National Aeronautics and Space Administration established the Aircraft Energy Efficiency (ACEE) program to improve the fuel efficiency of commercial transport aircraft and thereby reduce the amount of fuel consumed by the air transportation industry. The program is described in References 1 and 2. The Engine Component Improvement (ECI) Project Office is an element of the ACEE program formed at the NASA Lewis Research Center. Its objective is to improve fuel consumption of current commercial transport engines, the General Electric CF6 and the Pratt & Whitney Aircraft JT8D and JT9D. As a first step in the ECI program, feasibility studies of potential engine improvements and propulsion-related aircraft improvements were conducted by two teams of engine, airframe, and airline companies. Results of their studies are reported in References 3 and 4.

One improvement that was evaluated, involved the JT8D engine exhaust system on the DC-9 nacelle. High drag was associated with the thrust reverser stangs. The fairings, which are the aft closure for the thrust reverser actuation system, extend beyond the exit plane of the exhaust nozzle. Figure 1 shows closeups of a production baseline and a modified reverser stang fairing. The modified fairing is fabricated using an advanced composite construction. There are two fairings per nacelle for a total of four per airplane. The DC-9 was originally designed when fuel was less expensive, and because the DC-9 was a short-haul airplane, emphasis was placed on simplicity and minimum weight. The reverser stang fairing was designed without exhaust flow scrubbing during forward thrust. While simple in design, this configuration results in supersonic base drag at cruise, since the JT8D nozzle pressure ratio is supercritical at cruise. Elimination of this supersonic base area was identified as a means to reduce fuel consumption with DC-9 aircraft powered by JT8D engines. The reduction in fuel consumption with an improved fairing was calculated, and an economic evaluation was made and reported in Reference 3.

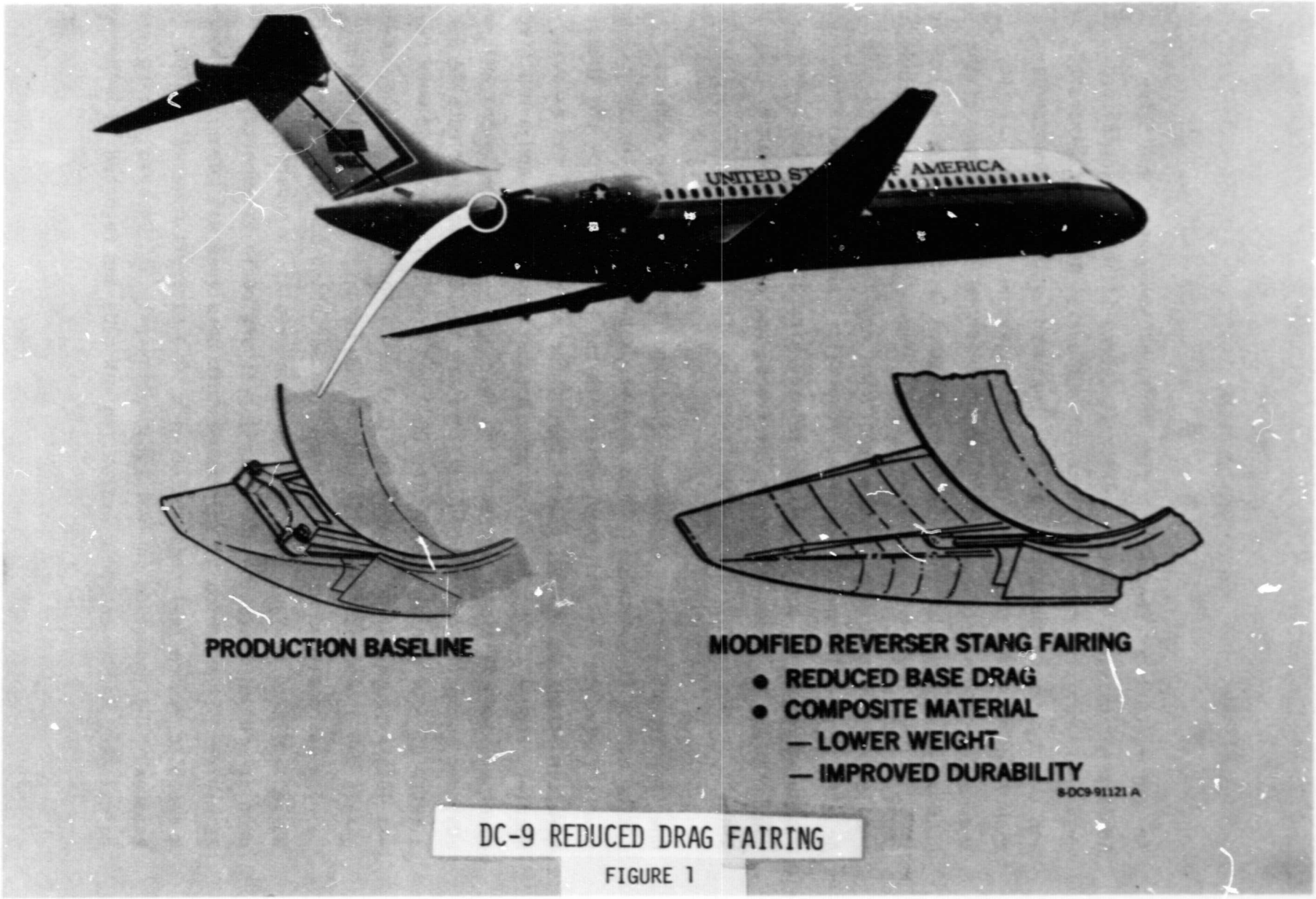

DC-9 REDUCED DRAG FAIRING

FIGURE 1

As reported in Reference 3, the initial modification configuration evaluated was estimated to reduce the total airplane drag by 1/2%. The economic evaluation conducted which assessed the effect of production cost for the modification showed use of the reduced drag fairing would have a payback of 0.7 years and result in a 0.1% reduction in airplane direct operating cost. The favorable fuel savings and economic impact study results led to establishing a development plan. In the interest of weight savings, the plan was to develop a fairing constructed from an advanced composite material system. The plan was submitted to the NASA ECI Program Office. The NASA ECI Program Office approved the program, and development of a reduced drag fairing for JT8D nacelles constructed with an advanced composite material system was initiated.

SECTION 3

DESIGN

3.1 AERODYNAMIC CONFIGURATION DEVELOPMENT

Development of the aerodynamic configuration of the DC-9 thrust reverser stang fairing to reduce drag was conducted using flight test data from a series of DC-9 flights. Initially, surface static pressure measurements were made to determine flow quality. These measurements were taken as a part of an instrumented flight test program to also measure the stang fairing temperature and dynamic loads environment. This was followed by inflight tuft surveys to determine flow quality visually. The tuft surveys were recorded on video tape, 16 mm movie film and 35 mm still film. These tuft surveys were studied to determine the flow quality over the fairing surface. The drag differences were then calculated using empirical drag coefficients for similar shapes and flow quality.

Initial Configuration

The initial aerodynamic modification to reduce drag was a relatively simple change to the production baseline design. The production baseline is shown in Figure 2. The stang fairing is the aft aerodynamic closure for the thrust reverser stang. The thrust reverser stang is the structural support frame for the thrust reverser four bar linkage. In the production baseline, a part of this structural frame is exposed and scrubbed by the engine exhaust flow. A base area that is an aft facing step to the engine exhaust flow exists. During cruise, the exhaust flow is slightly supersonic causing supersonic base drag.

The initial modification was designed to reduce this base drag. As shown in Figure 3, the initial modification faired out the base area.

One (1) nacelle set of these fairings was made and installed on a DC-9 airplane. The tested DC-9 was instrumented, a trailing cone was installed for measuring airspeed, and an air data computer and onboard data system was used to record flight data. The flight test instrumentation is further described in Section 3.2.

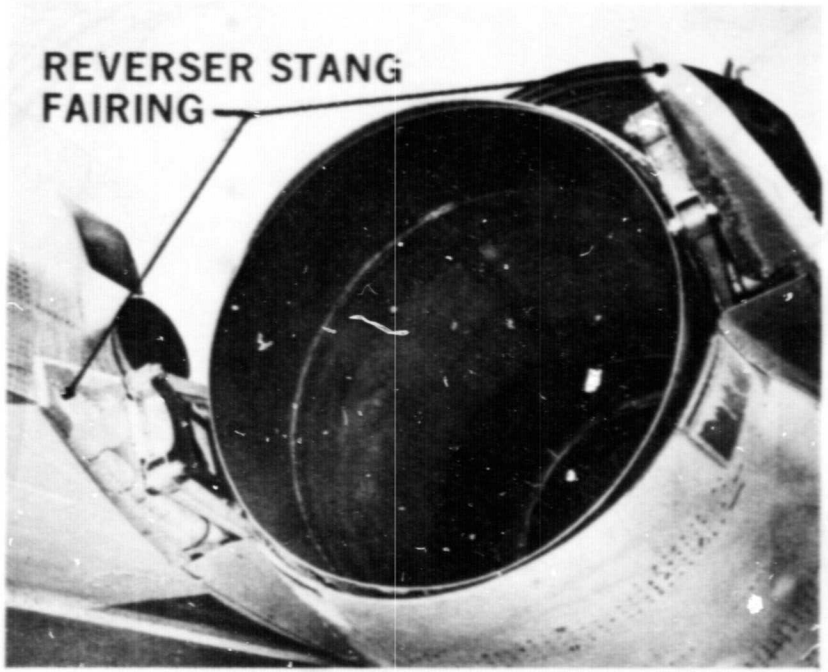

DC-9 NACELLE WITH PRODUCTION BASELINE
REVERSER STANG FAIRINGS

Figure 2

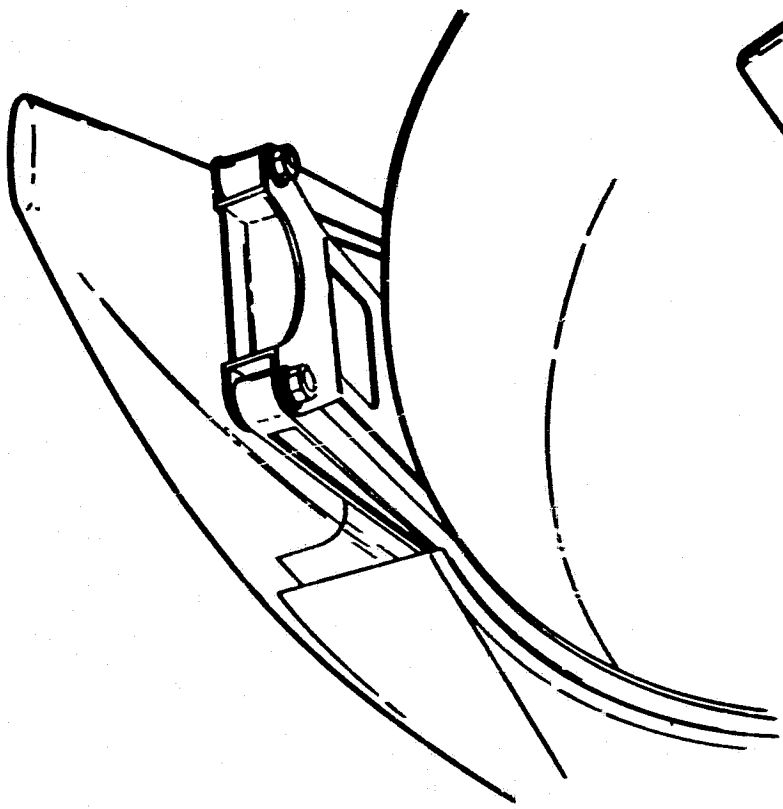

PRODUCTION BASELINE FAIRING

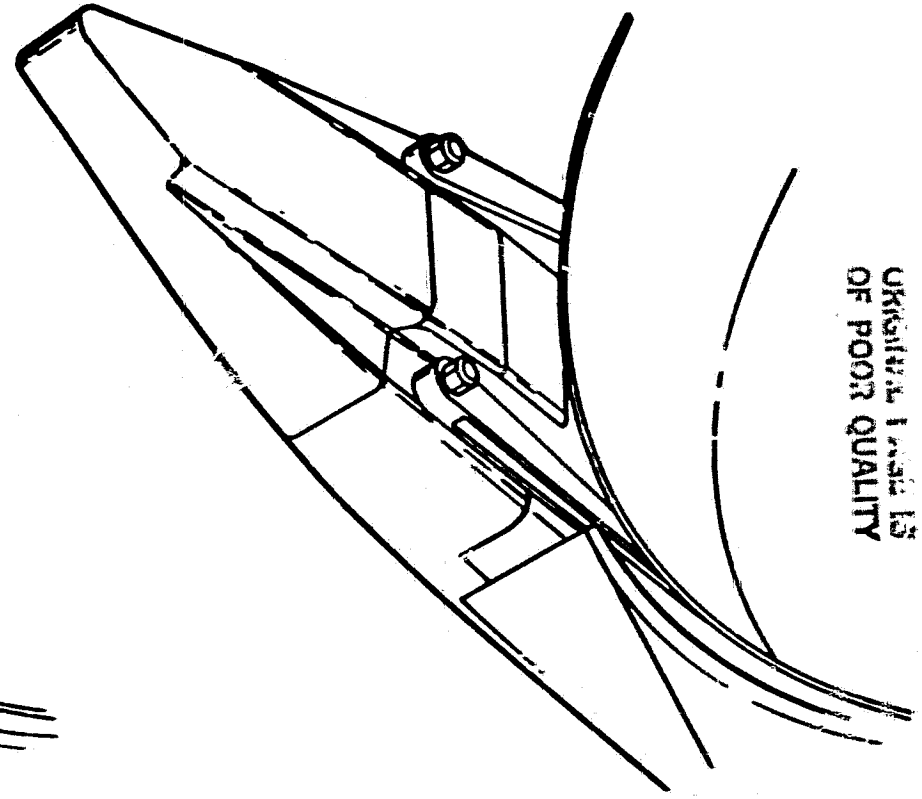

INITIAL MODIFICATION FAIRING

COMPARISON OF PRODUCTION BASELINE
AND INITIAL MODIFICATION

Figure 3

The initial modification fairing lines and static pressure tap locations are shown in Figures 4 and 5. The static pressure tap locations on axial station cuts are shown on Figure 6. The lines of the production baseline fairing and static pressure tap locations are shown in Figures 7 and 8. The static tap locations on axial station cuts for this fairing is shown on Figure 9.

Evaluation of Initial Configuration

The static pressure lines were connected to a Scanivalve with measurements made on a pressure transducer. The data were taken at constant flight conditions by using a split throttle operation in which the left and right throttles are advanced and retarded differentially to maintain constant total thrust while the individual engine power settings are varied. The initial modification pressure instrumentation was on the left outboard fairing while the production baseline pressure instrumentation was on the right outboard fairing as shown in Figure 10.

The data was recorded in flight and processed on the ground through a data reduction system that calculates the pressure coefficients. The pressure coefficient is:

$$C_p = \frac{P_S - P_\infty}{q_\infty}$$

where:

C_p = Pressure Coefficient

P_S = Local Static Pressure

P_∞ = Freestream Static Pressure

q_∞ = Freestream Dynamic Pressure

Figures 11, 12, and 13 show the pressure coefficients on the inboard (engine exhaust flow) side, top and outboard (freestream) side respectively for the engine exhaust nozzle pressure ratio of 2.61 during flight at Mach 0.79 and 9144 m (30,000 ft.) altitude. The data shown for the same flight conditions but at an engine exhaust nozzle pressure ratio of 2.99, are shown in Figures 14, 15, and 16.

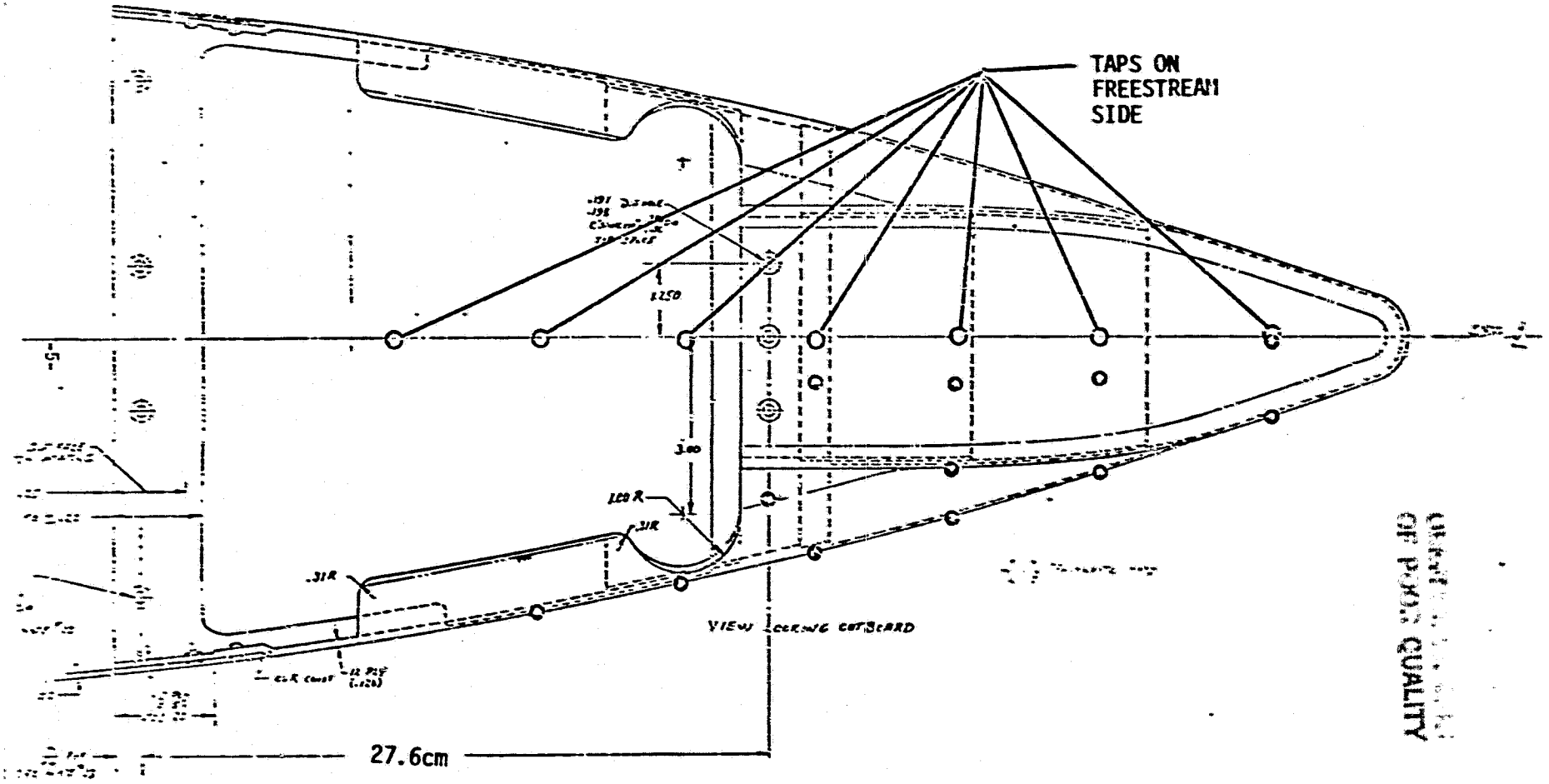

INITIAL MODIFICATION VERTICAL PLANE VIEW -
STATIC PRESSURE TAP LOCATIONS

Figure 4

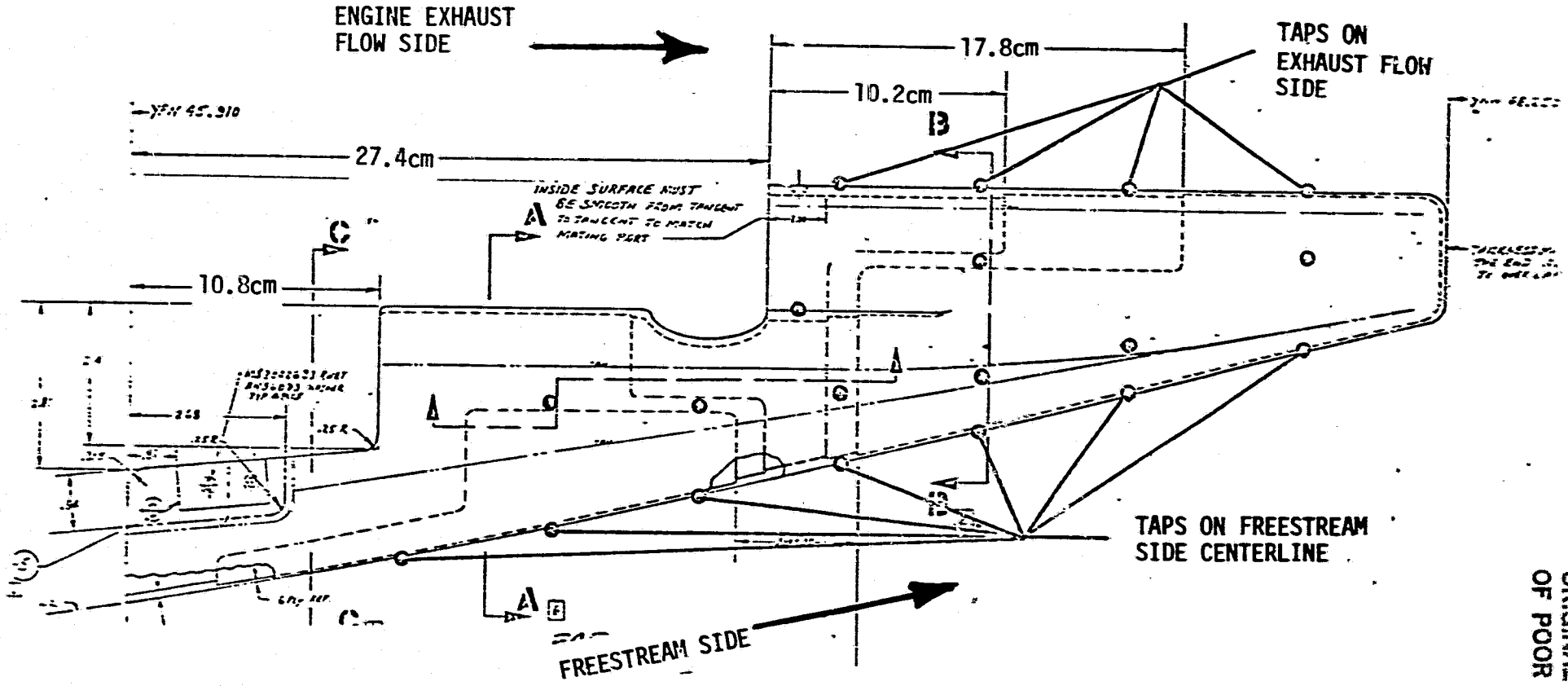

INITIAL MODIFICATION HORIZONTAL PLANE VIEW -
STATIC PRESSURE TAP LOCATIONS

Figure 5

INITIAL MODIFICATION STATION CUTS
WITH STATIC PRESSURE TAP LOCATIONS

Figure 6

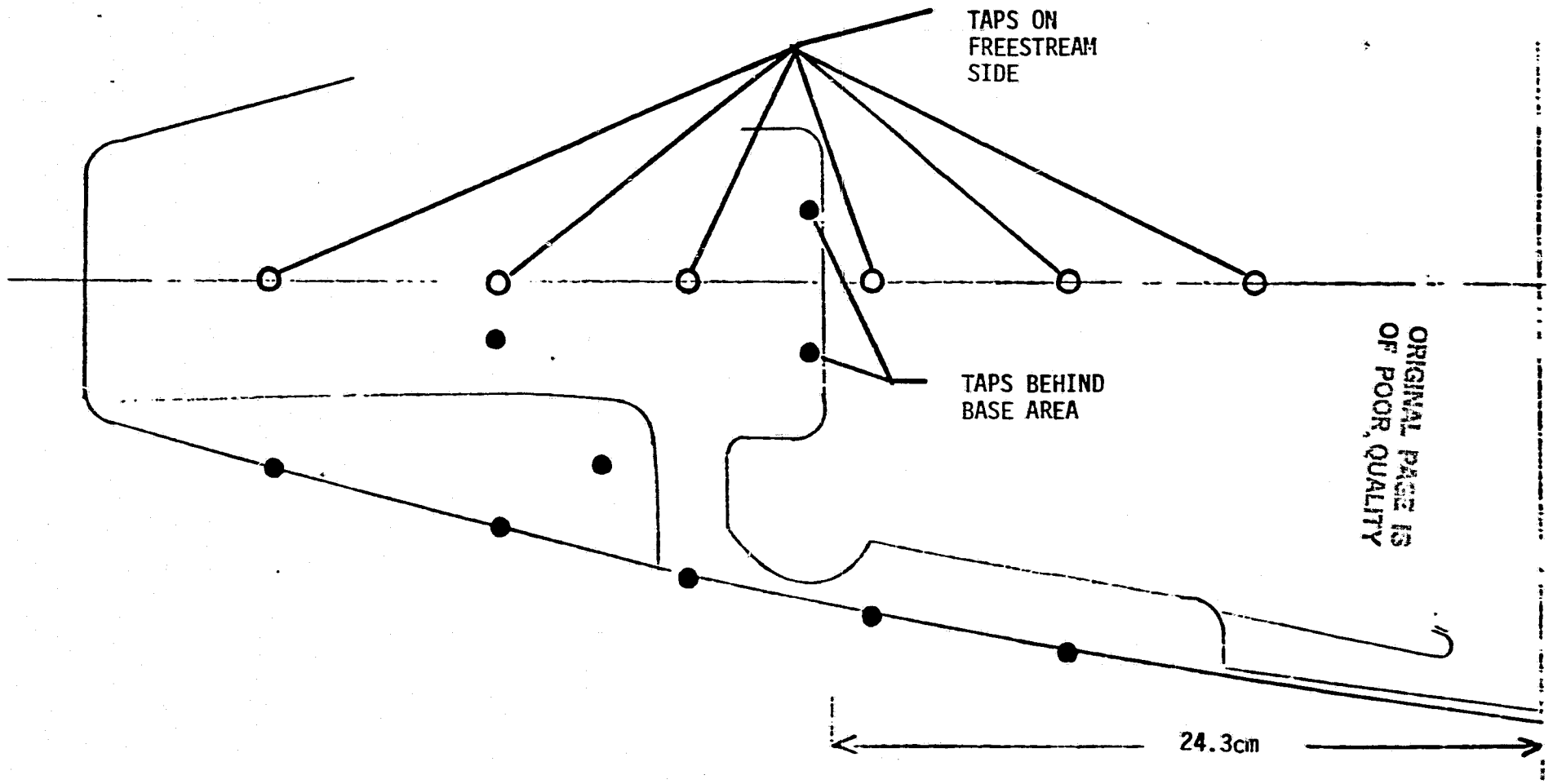

PRODUCTION BASELINE FAIRING VERTICAL PLANE VIEW -
STATIC PRESSURE TAP LOCATIONS

Figure 7

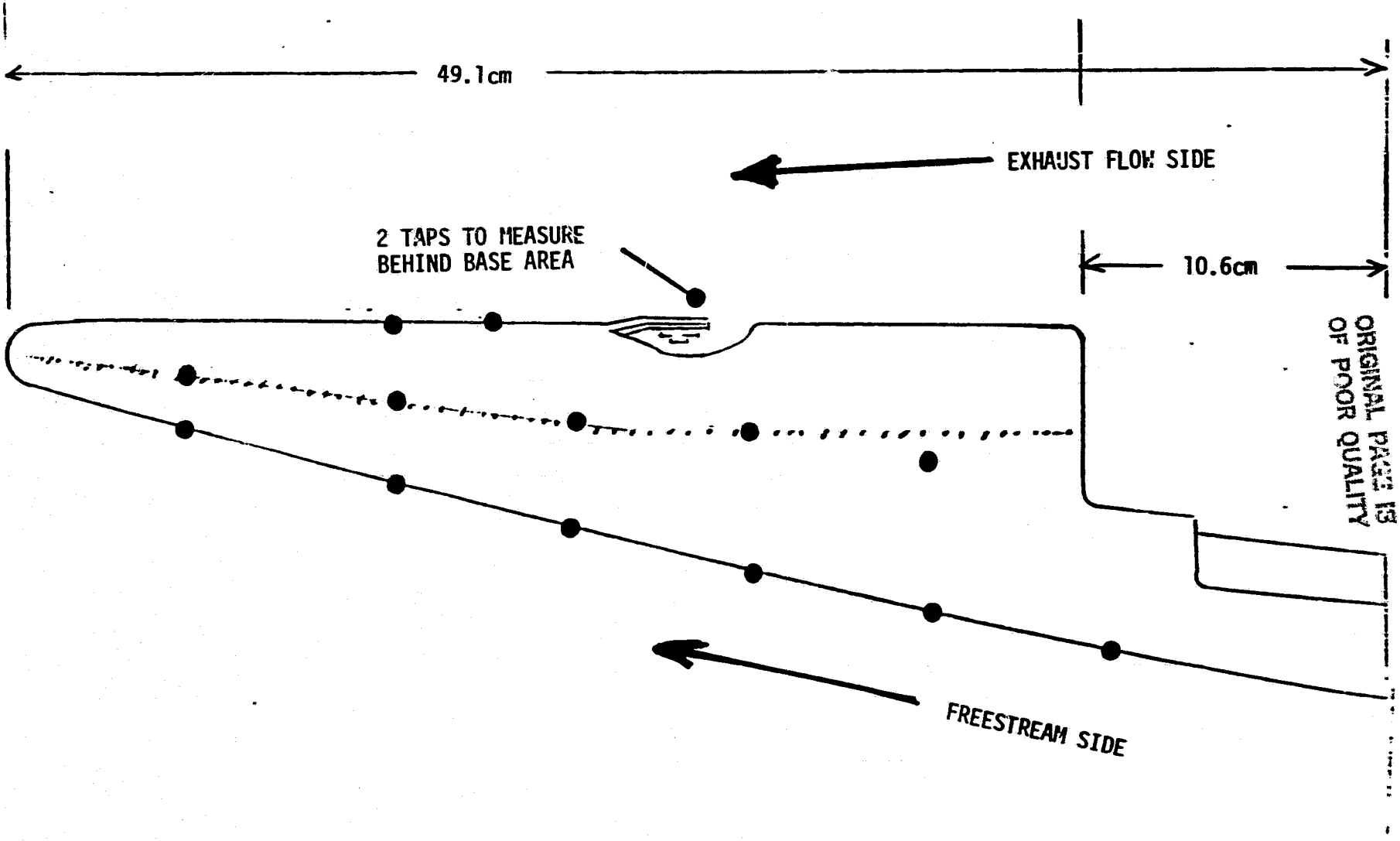

PRODUCTION BASELINE FAIRING HORIZONTAL PLANE VIEW -
STATIC PRESSURE TAP LOCATIONS

Figure 8

PRODUCTION BASELINE FAIRING STATION CUTS
WITH STATIC PRESSURE TAP LOCATIONS

Figure 9

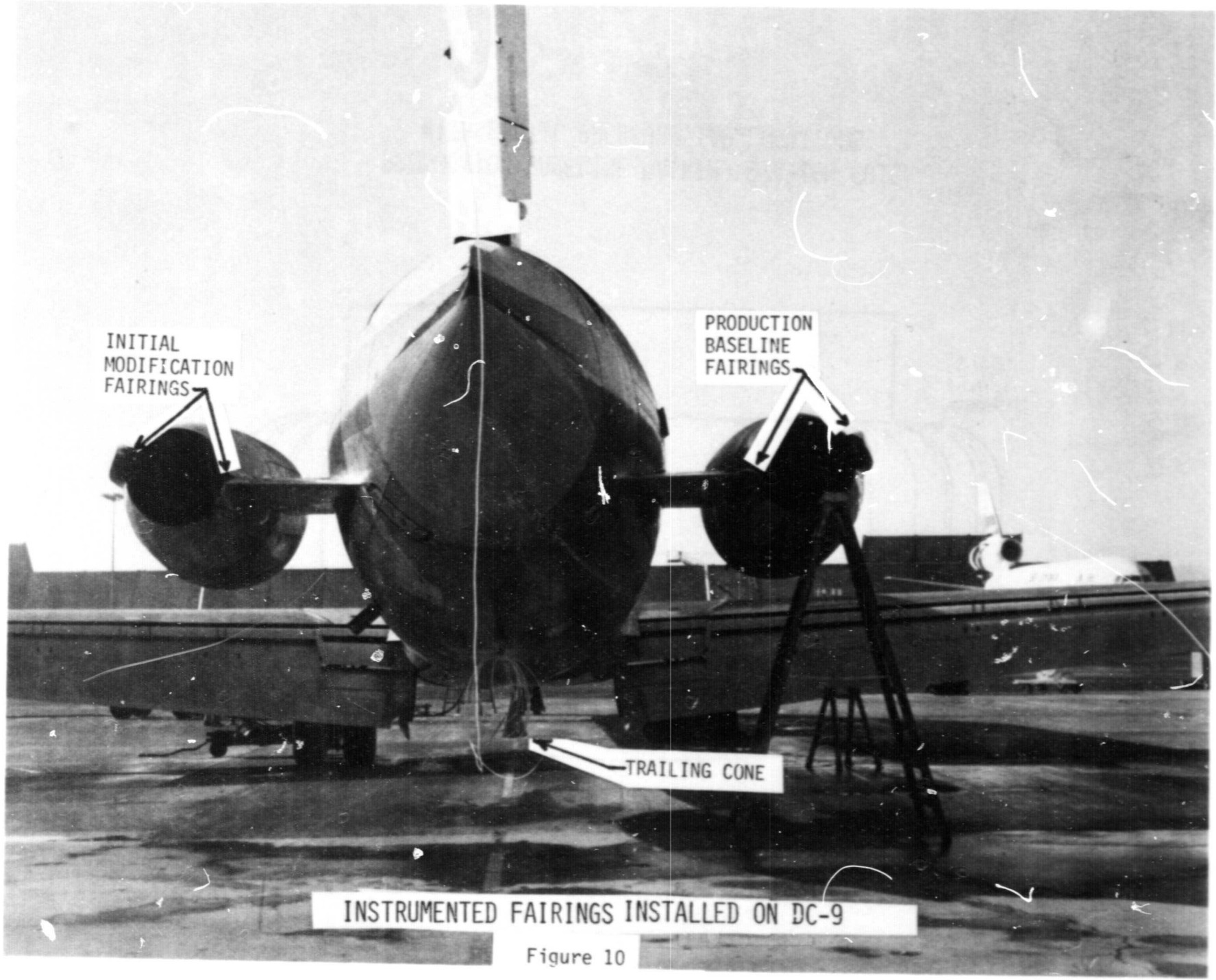

INSTRUMENTED FAIRINGS INSTALLED ON DC-9

Figure 10

Flight Mach No. = 0.79, Altitude - 9144 m

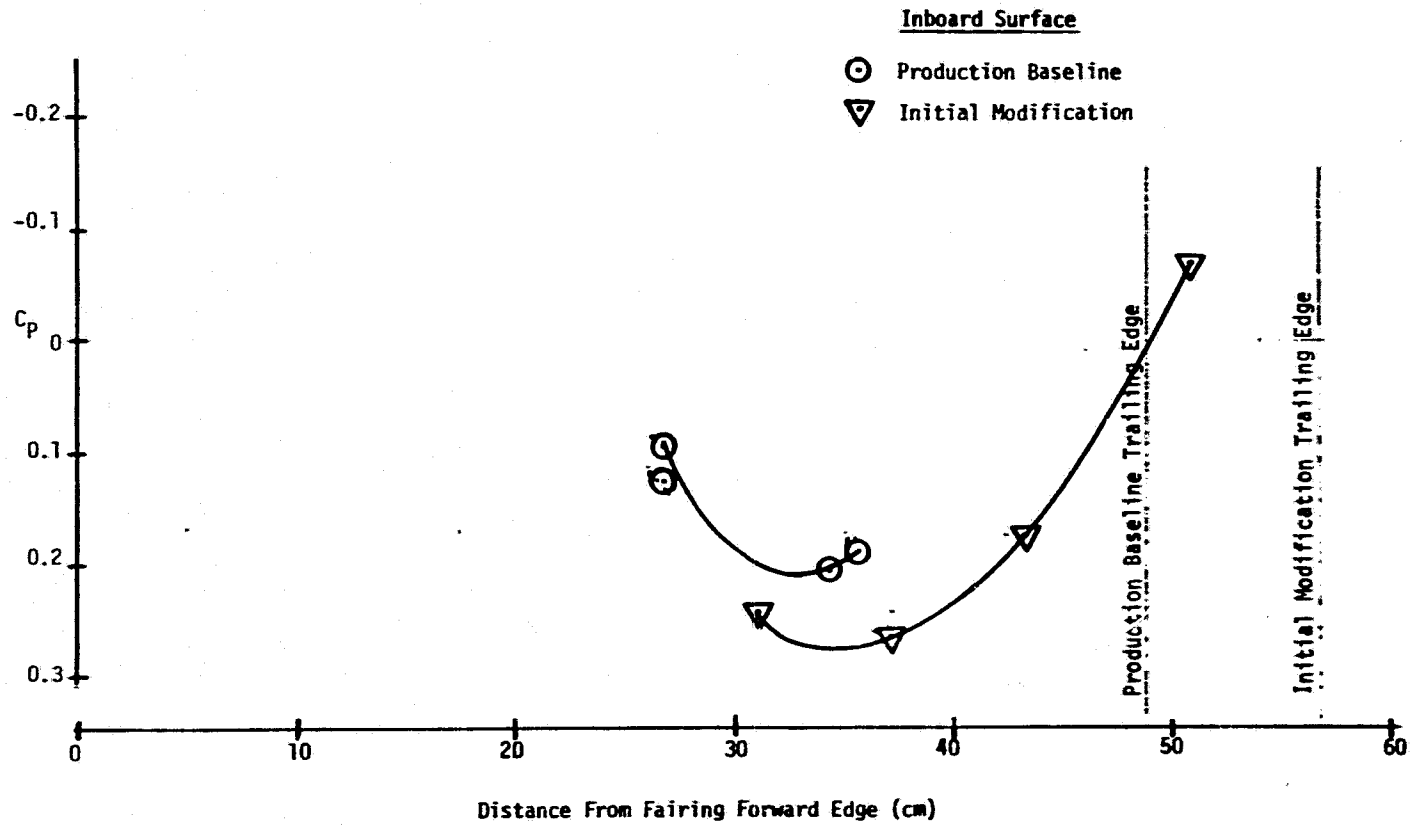

ORIGINAL PAGE IS
OF POOR QUALITY

INBOARD SURFACE STATIC PRESSURE SURVEY
PRESSURE RATIO = 2.61

Figure 11

Flight Mach No. = 0.79, Altitude - 9144 m

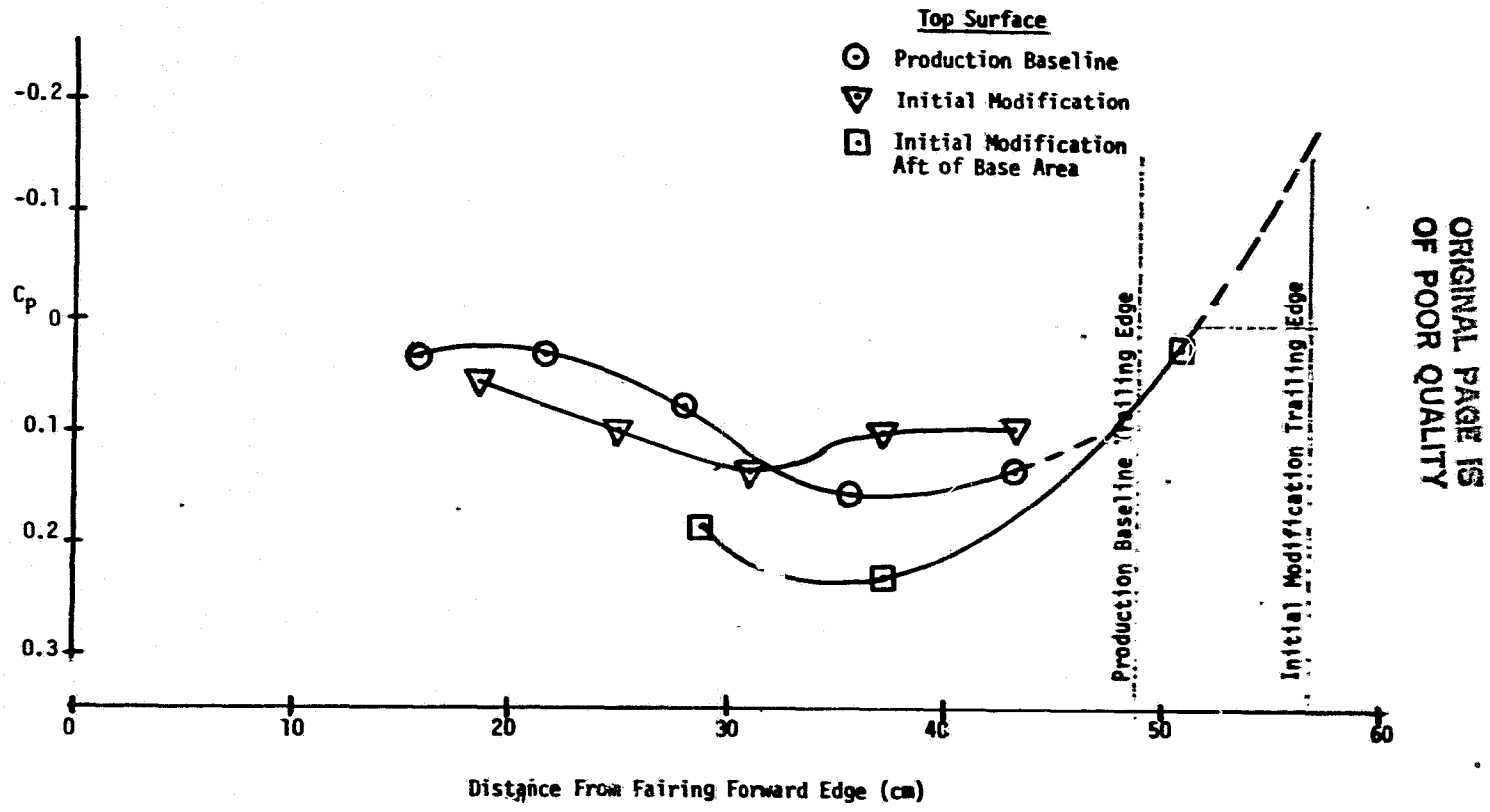

TOP SURFACE STATIC PRESSURE SURVEY
PRESSURE RATIO = 2.61

Figure 12

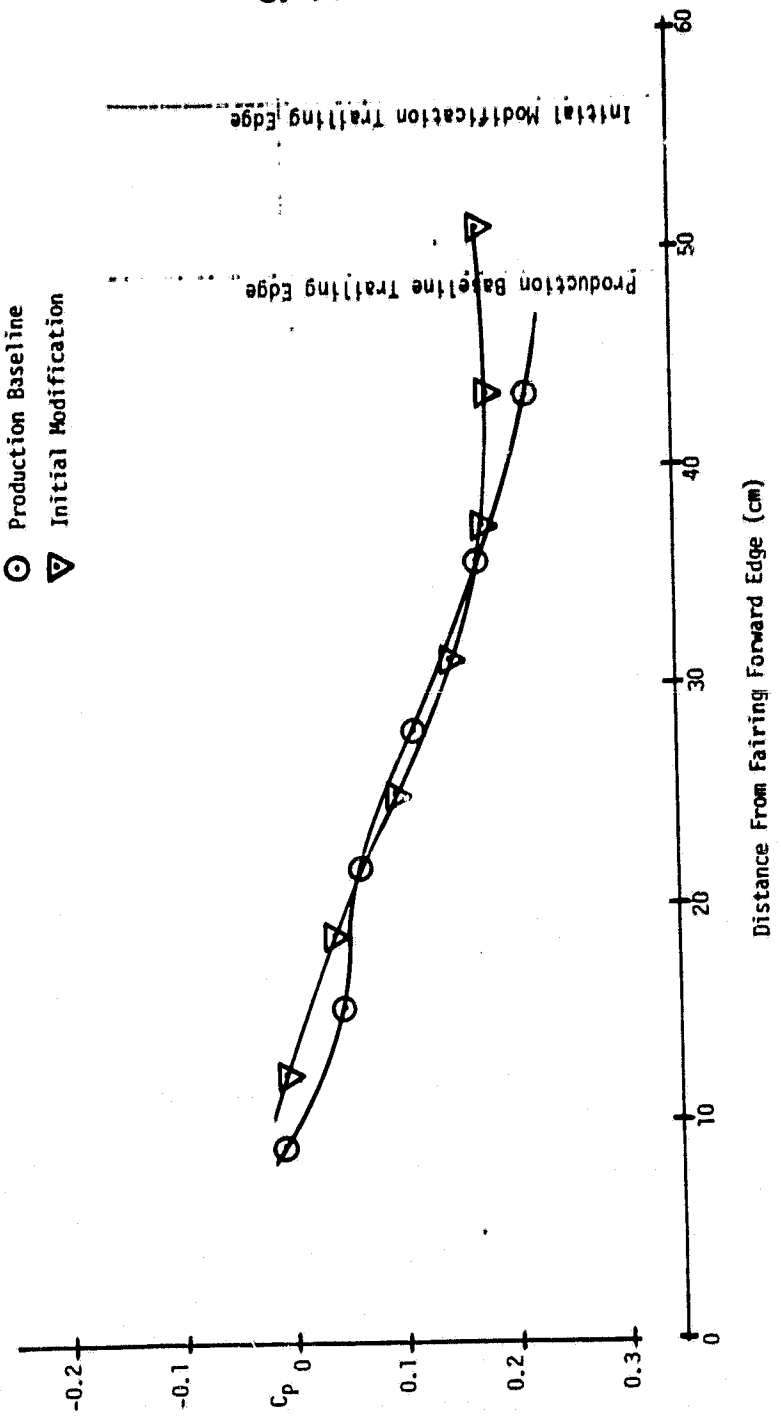

OUTBOARD SURFACE STATIC PRESSURE SURVEY
PRESSURE RATIO = 2.61

Figure 13

Flight Mach No. = 0.79, Altitude - 9144 m

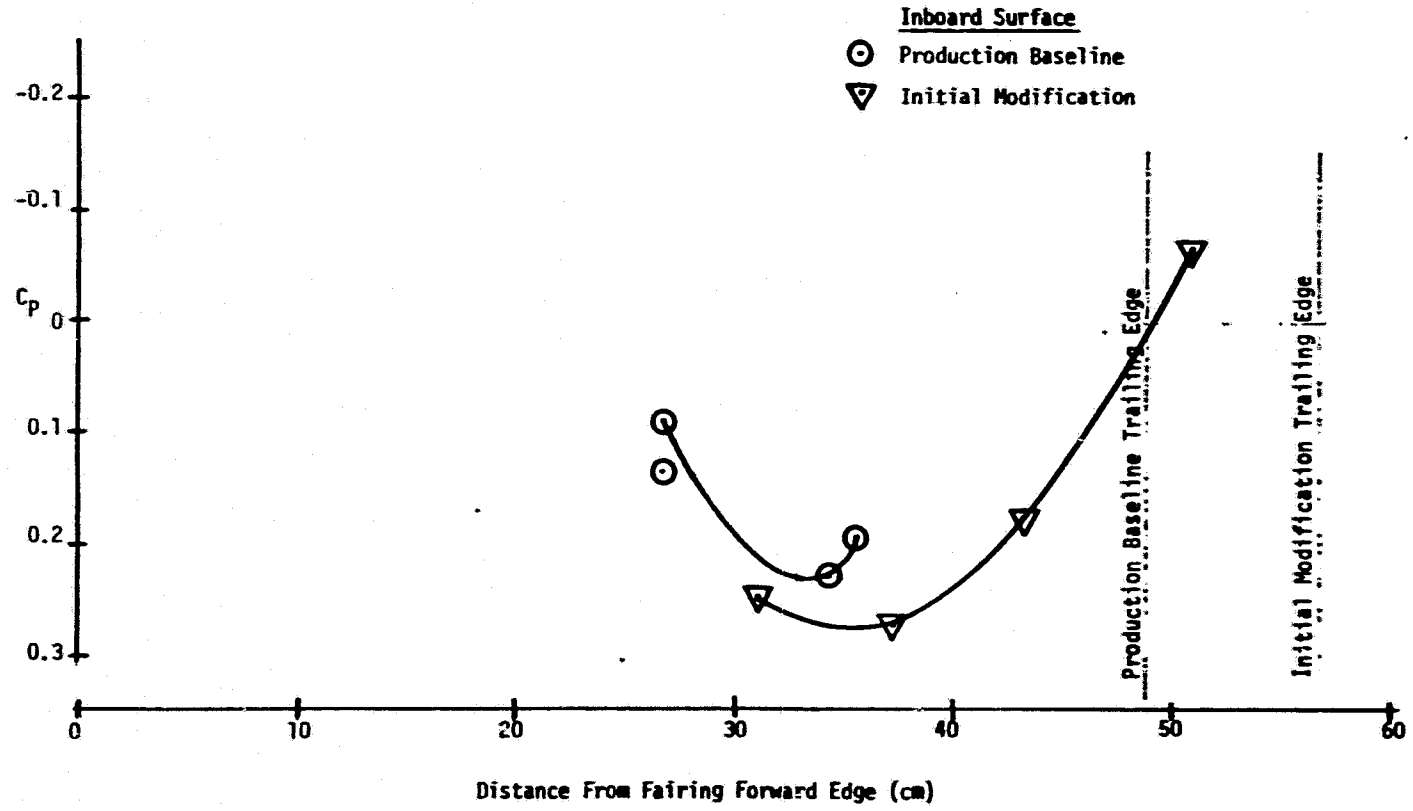

INBOARD SURFACE STATIC PRESSURE SURVEY
PRESSURE RATIO = 2.99

Figure 14

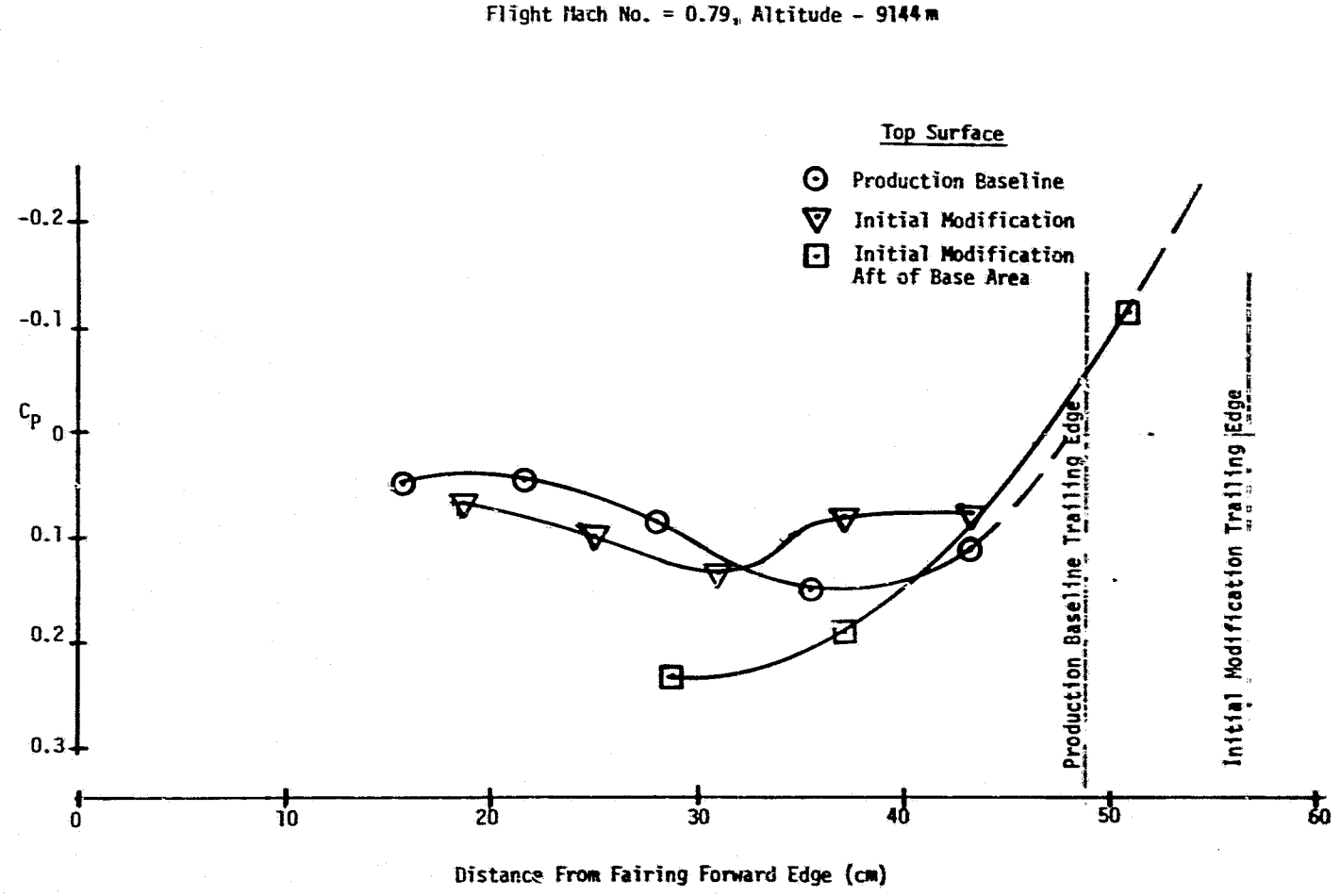

ORIGINAL PAGE IS
OF POOR QUALITY

TOP SURFACE STATIC PRESSURE SURVEY
PRESSURE RATIO = 2.99

Figure 15

Flight Mach No. = 0.79, Altitude - 9144 m

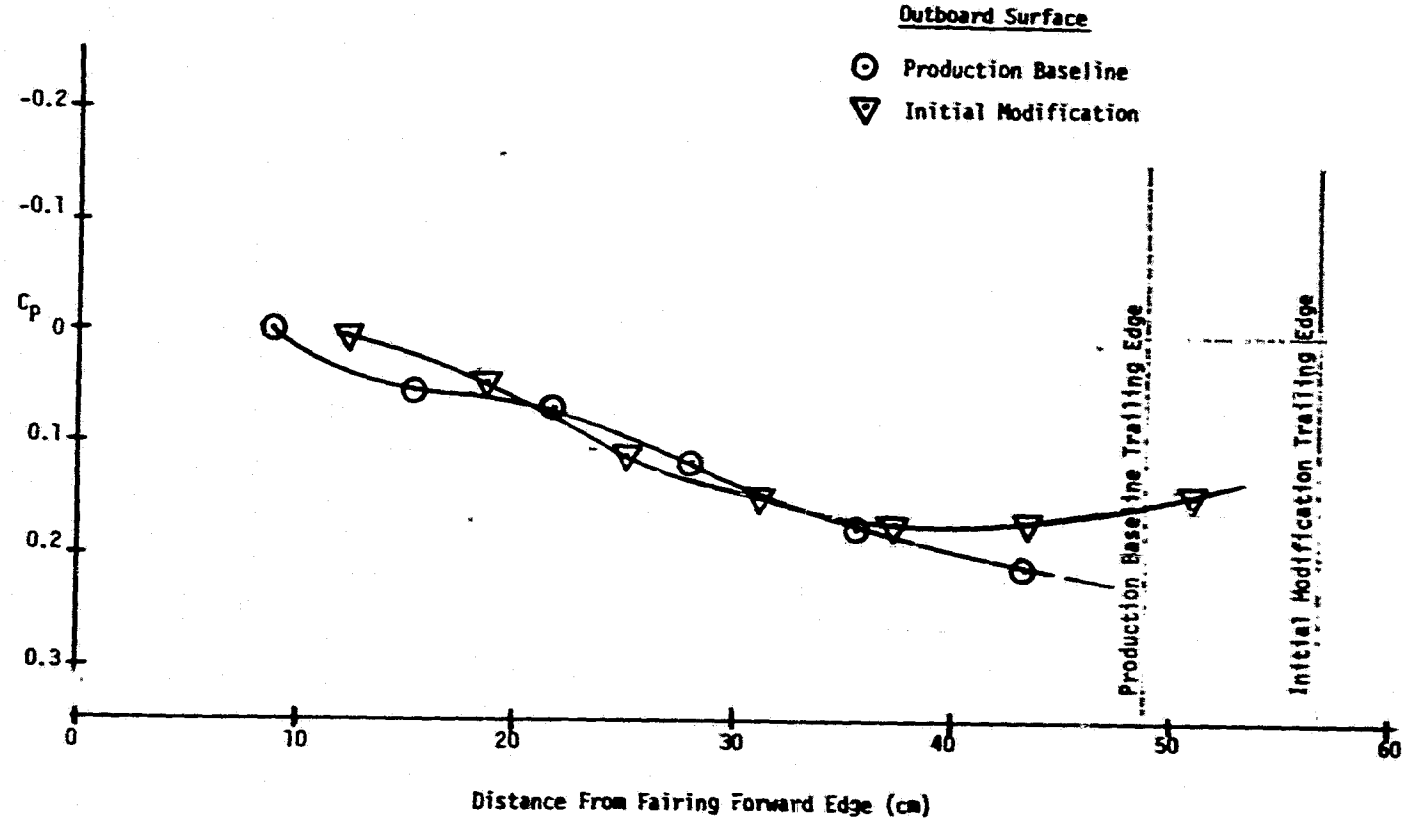

OUTBOARD SURFACE STATIC PRESSURE SURVEY
PRESSURE RATIO = 2.99

Figure 16

Review of the pressure coefficient data indicated that flow separation was occuring on the aft section of the initial modification fairing. However, since the exhaust nozzle is supercritical, an alternative possibility was that an over expansion of exhaust flow was occuring. An inflight tuft survey was therefore conducted in order to determine flow quality by visual means.

Nylon tufts were attached to the initial modification and the production baseline fairing. The tufts were 7.6 cm (3 in.) long and spaced at 6.3 cm (2.5 in.) starting from the trailing edge and going forward. The DC-9 with these tufted fairings was flown at Mach 0.77 and 0.79. The tufts were observed and video taped, also 16 mm movie and 35 mm still photographs were taken by a photographer using hand held cameras and observing through the side window from a Learjet chase airplane. Figure 17 shows a typical photo of the production baseline. It is apparent from the photo that there is flow separation at the base area of the production baseline fairing by observing the tufts hanging loosely in that area.

The typical tuft survey photographs of the initial modification is seen in Figure 18. The tufts on the upper and lower aft section undergo some motion but it appears to be caused by recirculation in a separated flow region. These flow visualization tests confirmed the presence of flow separation which was indicated by the static pressure survey.

Alternate Configurations

Since the initial modification fairing design showed a relatively large area of separated flow, redesign was undertaken to improve the lines. New lines were developed to reduce boattail angles on the upper and lower surfaces where the flow visualization tests show flow separation was occuring. Establishing the new configurations was an iterative development between aerodynamic desires, and structural and mechanical interference requirements. Configuration A lines were developed to maintain ease of fabrication. Ease of fabrication required that there was no reverse curvature and continuous positive draft so that the part could be removed from a single piece mold.

Figure 17

ORIGINAL PAGE
BLACK AND WHITE PHOTOGRAPH

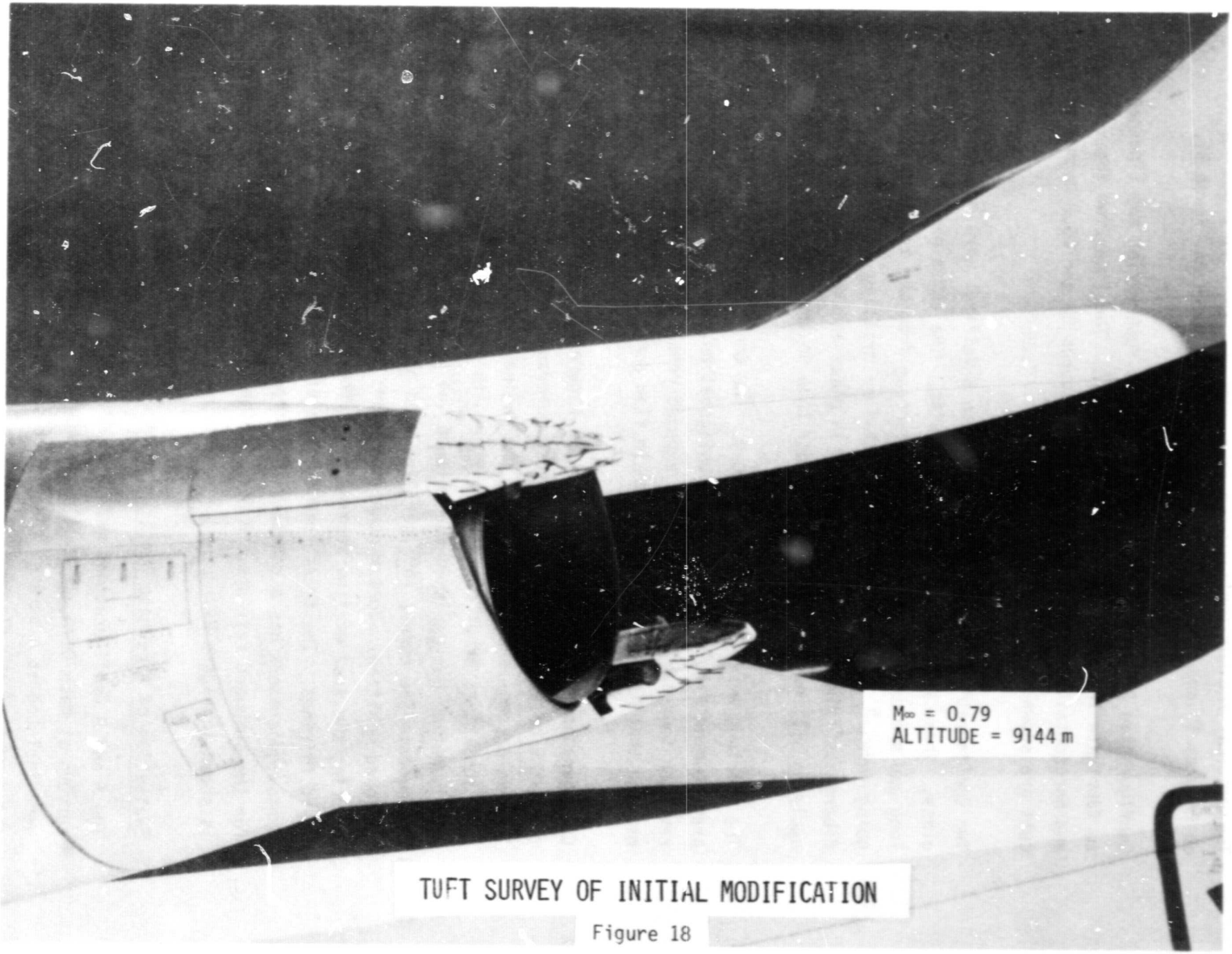

TUFT SURVEY OF INITIAL MODIFICATION

Figure 18

The vertical and horizontal plane view lines for Configuration A are shown on Figures 19 and 20. Normal station cuts are shown on Figure 21.

Configuration B lines were developed without restricting the lines so as to fabricate the part in a single piece mold. The lines for the vertical and horizontal plane views are shown on Figures 22 and 23. Normal station cuts are shown on Figure 24.

Two Configuration A and two Configuration B fairings were made of fiberglass. These were tufted with nylon tufts. The tufts were 7.6 cm (3 in.) long and spaced at 6.3 cm (2.5 in.) starting from the trailing edge and going forward. The tufts were installed by drilling holes into the fiberglass fairings and holding them in place and sealing the holes by applying silicon rubber and high speed tape on the inside of the fairing.

The fairings were installed on a DC-9. The Configuration A tufted fairings are shown in Figure 25. In this configuration, the aft pivot for the thrust reverser four-bar linkage remains exposed resulting in some base area remaining that is scrubbed by transonic flow during cruise.

Configuration B with tufts is shown in Figure 26. This configuration reduces the base area behind the thrust reverser four-bar linkage aft pivots. This is accomplished by extending the engine exhaust flow side surface over the aft reverser pivots. This results in a wider trailing edge. The configuration has recessed channels on the upper and lower surfaces to accommodate the thrust reverser link when the thrust reverser is in the deployed position. Vortex generators were used in one test as a means of reducing the area of flow separation on the freestream surface of the inboard fairings. The freestream surface of the inboard fairings without vortex generators has a considerably larger area of separated flow than for the outboard fairings. A description of the vortex generators used is shown in Figure 27.

Evaluation of Alternate Configurations

The A and B Configurations were evaluated by again conducting inflight tuft surveys at Mach 0.79 and 9144 m (30,000 ft.) altitude. Some modifications were included as a part of these tuft surveys and are described in the assessment of the flight test results.

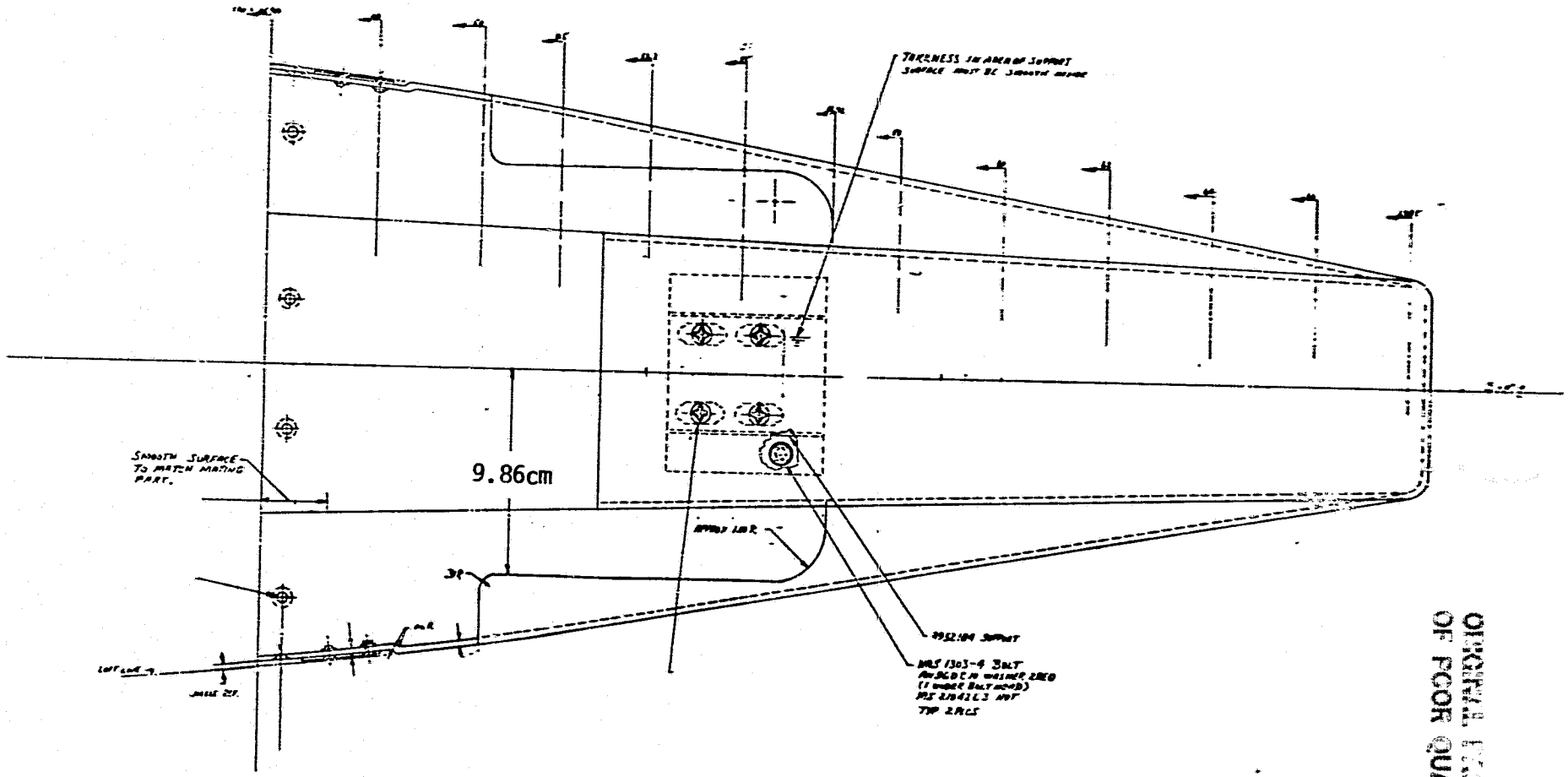

CONFIGURATION A
VERTICAL PLANE VIEW

Figure 19

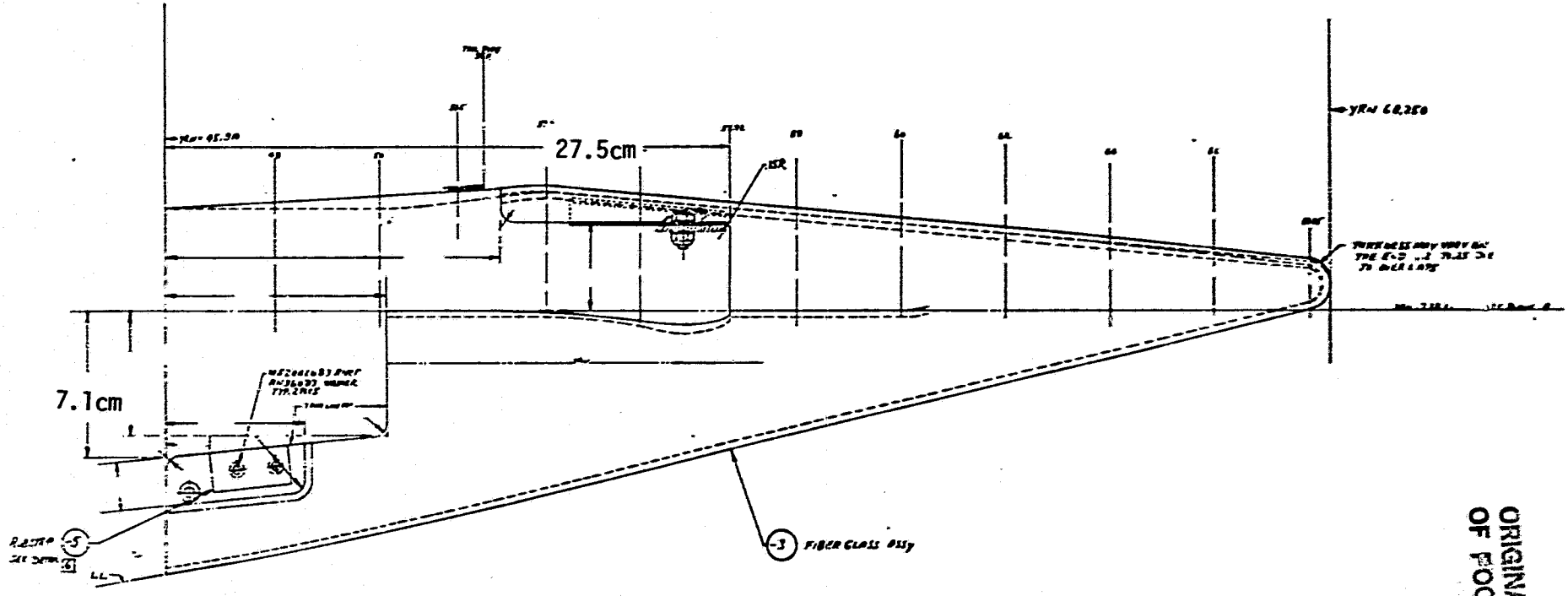

CONFIGURATION A
HORIZONTAL PLANE VIEW

Figure 20

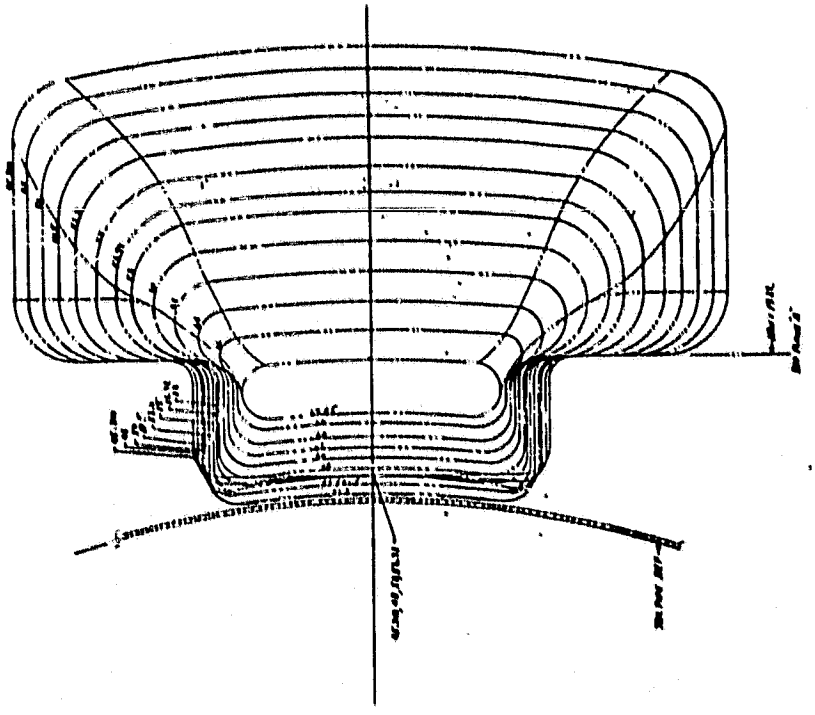

CONFIGURATION A
STATION CUTS

Figure 21

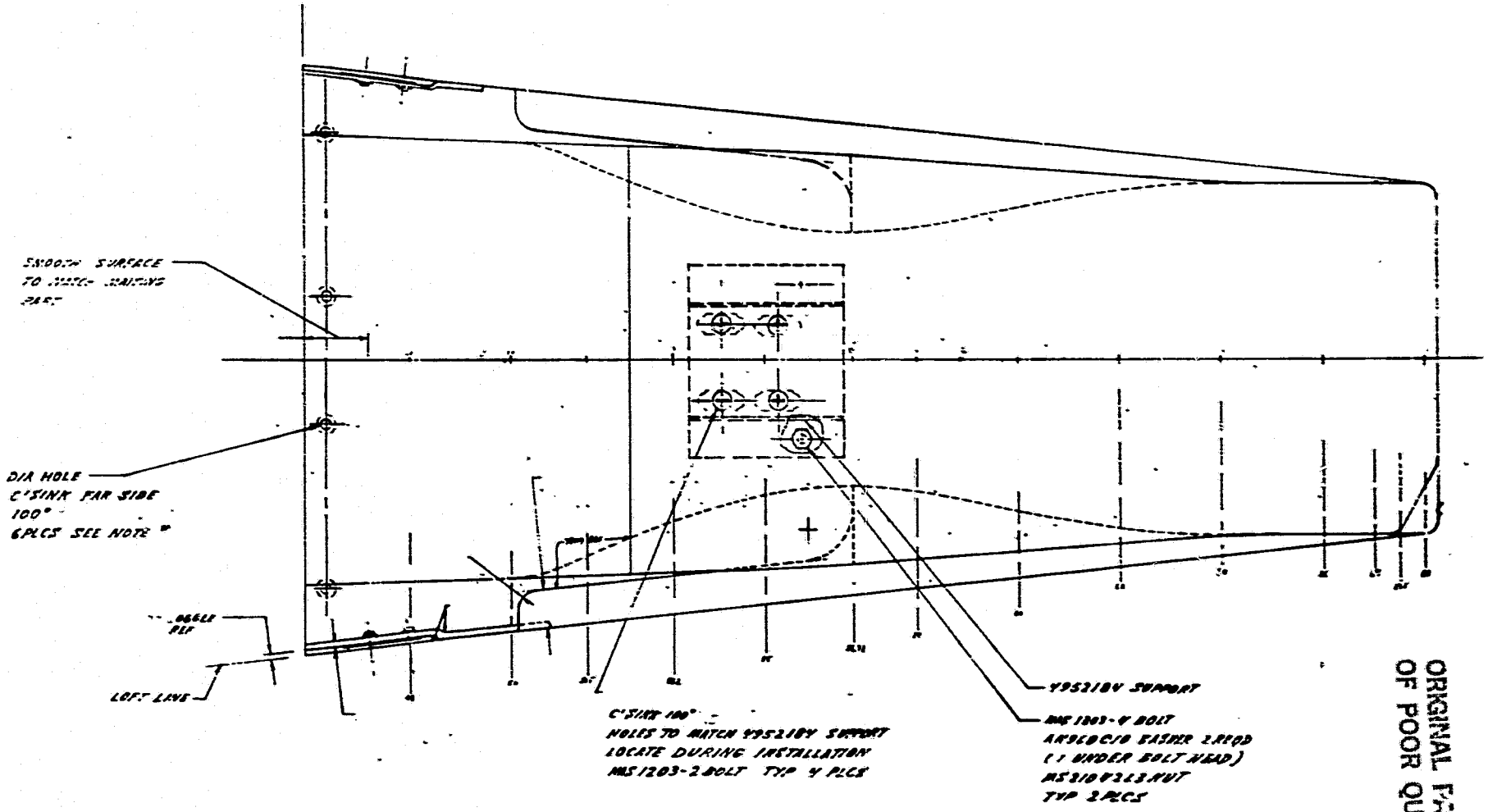

CONFIGURATION B
VERTICAL PLANE VIEW

Figure 22

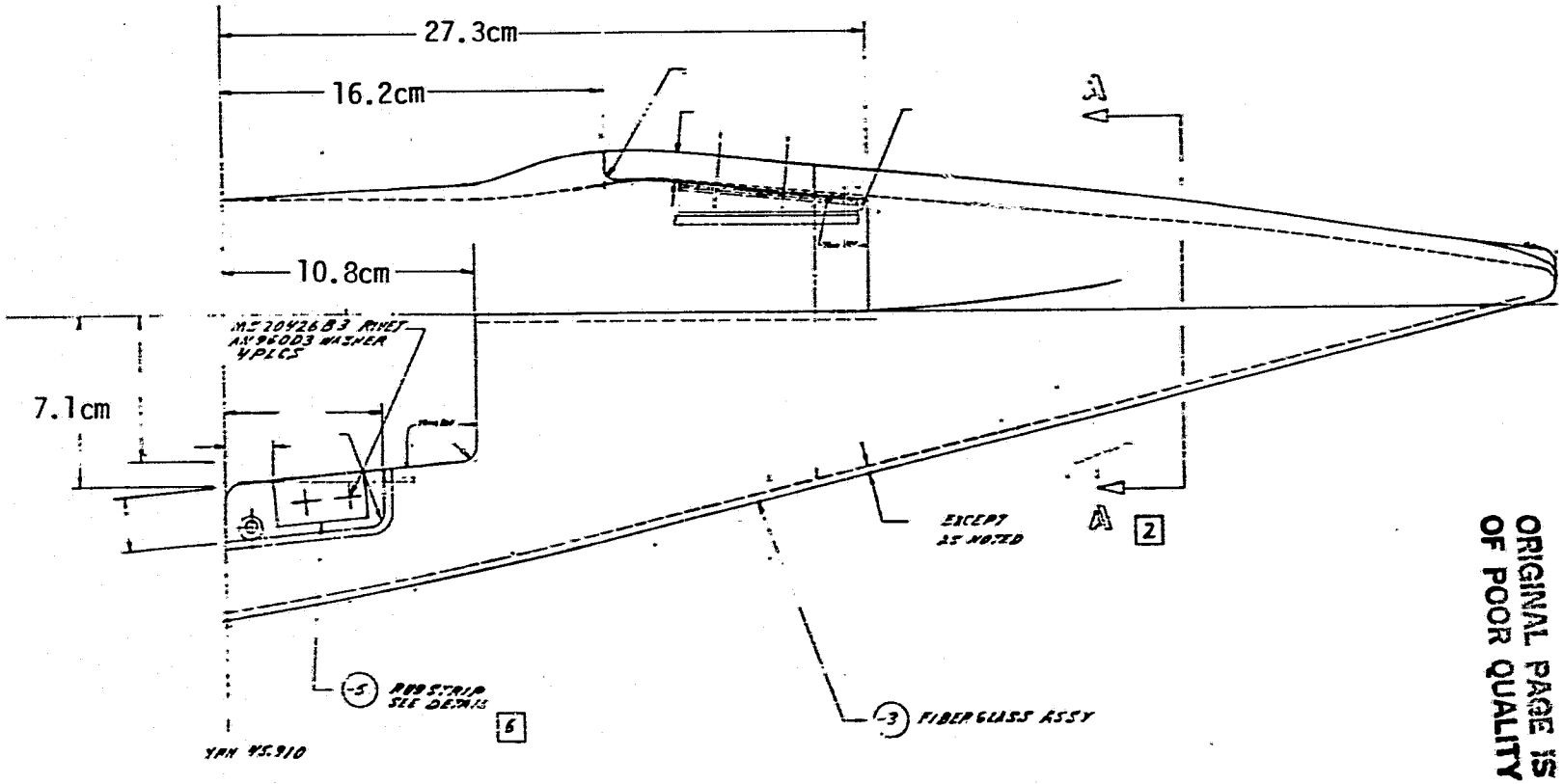

CONFIGURATION B
HORIZONTAL PLANE VIEW

Figure 23

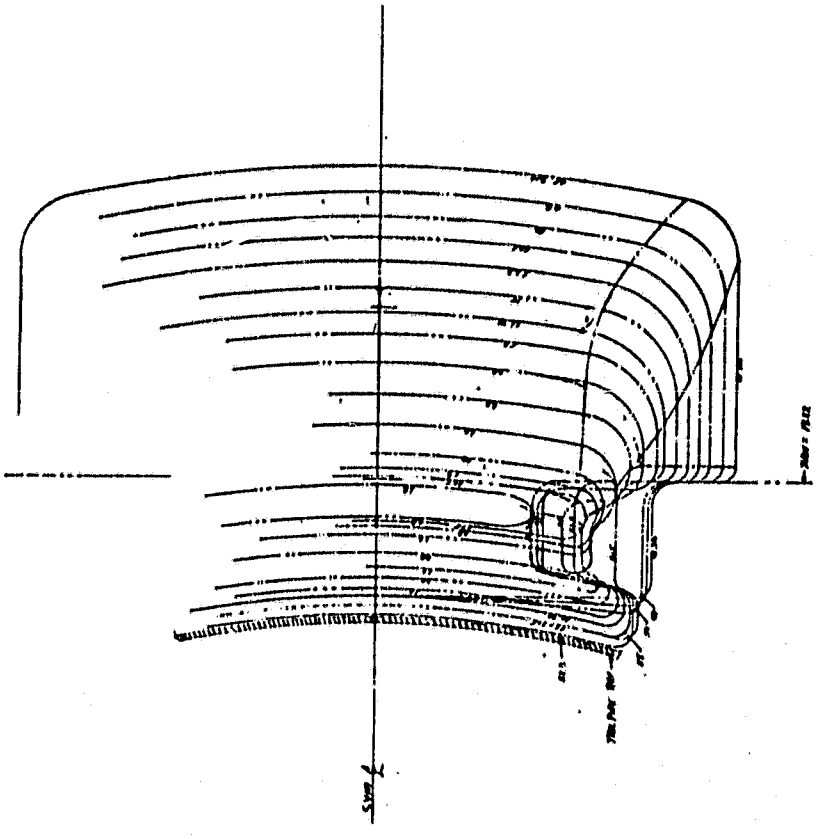

CONFIGURATION B
STATION CUTS

Figure 24

CONFIGURATION A WITH TUFTS

Figure 25

Figure 26

ORIGINAL PAGE
BLACK AND WHITE PHOTOGRAPH

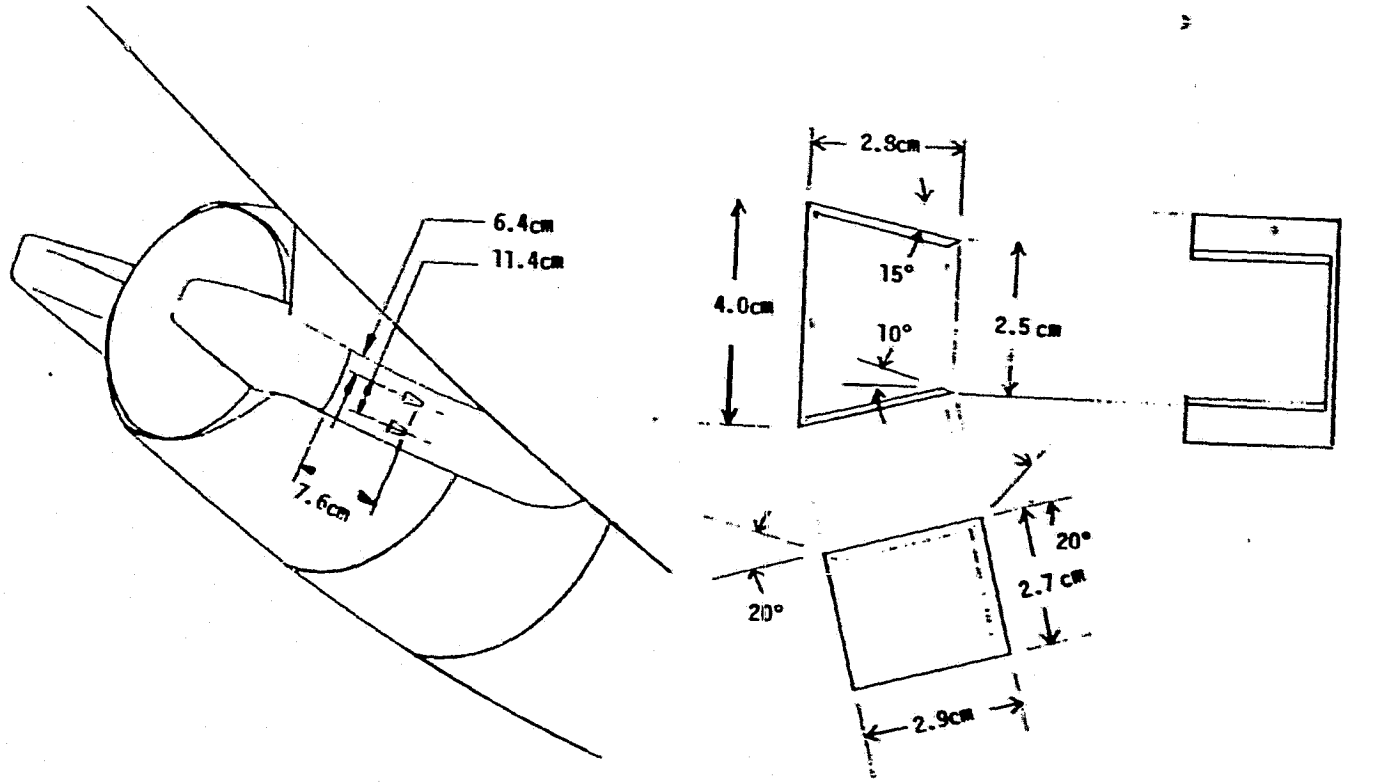

VORTEX GENERATOR DESCRIPTION

Figure 27

The evaluation of the configurations was made by calculating drag differences relative to the production baseline. This was done by using empirical drag coefficients for similar shapes, the applicable area as determined by studying the tuft survey visual recordings and the appropriate flow dynamic pressure. The magnitude of the drag improvements under investigation, i.e., 1/2% to 1%, could not be determined from airplane specific range measurements. A powered model wind tunnel test of a mixed flow exhaust that duplicated the intrinsic features of the configurations with proper consideration for Reynolds number effects was not practicable.

The flow visualization recordings were studied and boundaries estimated for stang fairing scrubbed surface areas where flow was attached and where flow was separated. The incremental drag was then calculated for: skin friction for surfaces scrubbed by the freestream flow and the engine exhaust or jet flow; and base drag where flow separation existed from surfaces scrubbed by the freestream and jet flow. The incremental drag was calculated from:

$$D = q_\infty (A_{FF} C_{FF} + A_{BG} C_{DG} + A_{BF} C_{DF}) + q_J (A_{FJ} C_{FJ} + A_{BJ} C_{DJ})$$

where:

D = Drag
q_∞ = Freestream Dynamic Pressure
q_J = Jet Flow Dynamic Pressure
A_{FF} = Surface Area Scrubbed by Freestream Flow
A_{BG} = Base Area of Gaps Scrubbed by Freestream Flow
A_{BF} = Base Area of Separated Surfaces Scrubbed by Freestream Flow
A_{FJ} = Surface Area Scrubbed by Jet Flow
A_{BJ} = Base Area of Separated Surfaces Scrubbed by Jet Flow
C_{FF} = Freestream Skin Friction Coefficient
C_{DG} = Base Drag Coefficient for Gaps in Freestream
C_{DF} = Base Drag Coefficient for Separated Areas in Freestream Flow
C_{FJ} = Jet Flow Skin Friction Coefficient
C_{DJ} = Base Drag Coefficient for Separated Flow in Jet

The exhaust flow Mach number for a typical airplane cruise Mach number of 0.78 (30,000 ft.) of 1.26 was used for calculating base drag due to the supersonic flow of the exhaust.

The base drag coefficients were from Figure 28 which are empirically determined NACA data.

From visual inspection of the stang fairing, the base area behind the thrust reverser four-bar linkage support frame or stang most closely resembles a two dimensional base immersed in the engine supersonic exhaust flow. The complete expansion jet flow Mach number is 1.26 for the typical flight condition evaluated. The base drag coefficient of 0.42 was therefore used.

The base area scrubbed by freestream flow resemble bodies that are between two dimensional and three dimensional shapes. The three dimensional base drag coefficient was used as a conservative estimate for separated area and for calculating the drag due to gaps that exist in the configurations.

For typical cruise flight conditions evaluated:

q_∞	$= 1.22 \times 10^4$ N/m^2 (254 psf)	calculated for standard stmosphere for Mach 0.78, 9144 m (30,000 ft.) altitude
q_J	$= 3.40 \times 10^4$ N/m^2 (710 psf)	calculated using flow thermodynamic data from engine simulation computer program
C_{FF}	$= 0.0027$	
C_{FJ}	$= 0.0031$	
C_{DG}	$= 0.12$	from Figure 28 for 3D base drag
C_{DF}	$= 0.12$	from Figure 28 for 3D base drag
C_{DJ}	$= 0.42$	from Figure 28 for 2D base drag

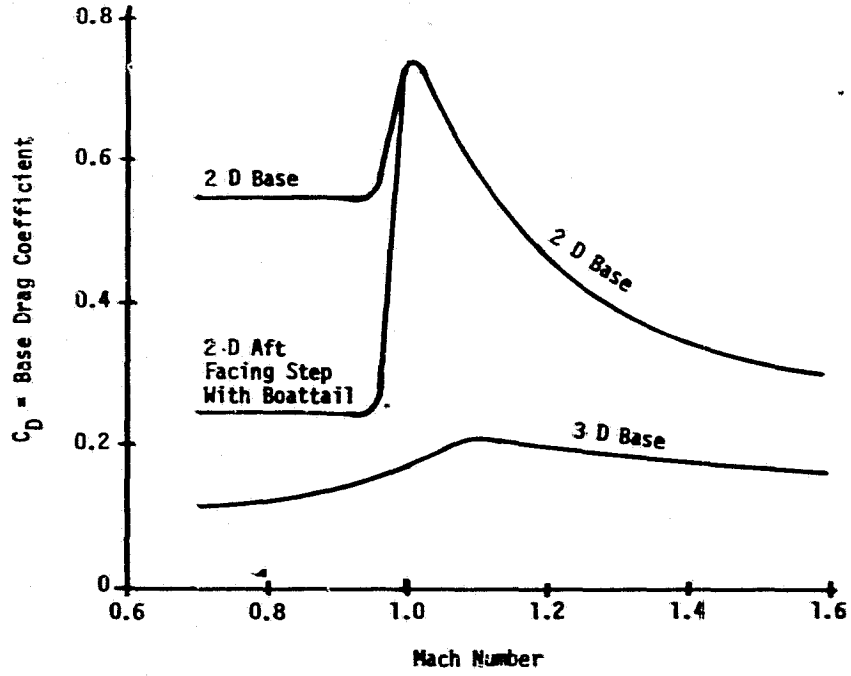

Data Sources

Type Flow	Type Base	NACA References
Subsonic	2D Base	RMA52E01 RML50E19A
	2D Aft Facing Step or 2D Base With Boattail	RM3384 RM3344
	3D Base	TMX1960 TN4201 RM3323
Supersonic	2D Base	RMA52E01 RML50E19A TN3819 TN3548 RM3468
	3D Base	TN3819 RM3323

BASE DRAG COEFFICIENT

Figure 28

Typical flow quality assessment is shown in Figures 29 and 30 where the areas for different flow zones are shown. This was done for each configuration with a separate assessment for the inboard (relative to the airplane) and outboard fairing on a nacelle. The area assessment results are shown on Table 1. The results from the incremental drag calculations using these areas are shown on Table 2 as a percent reduction in total airplane drag relative to the production baseline fairing. Positive values are drag reductions and negative values are drag increases relative to the production baseline configuration. The total is for four fairings on an airplane.

The first configuration listed is the production baseline. The next is the initial modification which had greater separated flow areas than expected. Configuration A was the redesign which maintained ease of manufacturing while Configuration B was the redesign for minimum drag. Configuration B 4° VG was tested with two vortex generators located just upstream of the fairing on the inboard (relative to the airplane) fairing. The fairings were installed canted away from the engine centerline by 4° relative to the basic Configuration B fairing. This canting was done to determine the effect of reducing the outboard boattail angle by 4°. Configuration B "filled" was tested to determine the effect of the recessed channels which are for clearance of the thrust reverser links in the reverse mode. Although not practical, these were filled with foam to create a smooth aerodynamic shape. Configuration A 6° was tested to determine the effect of reducing the outside or free-stream side boattail angles by 6°. This was done by installing the fairings canted 6° away from the engine centerline.

The last two configurations were not tested, but are the estimated performance if vortex generators were used with Configurations A and B based on the incremental drag reduction due to vortex generator. In-flight tuft survey photographs of Configurations A and B are shown in Figures 31 and 32. The superior aerodynamic performance of Configuration B is evident in the photographs.

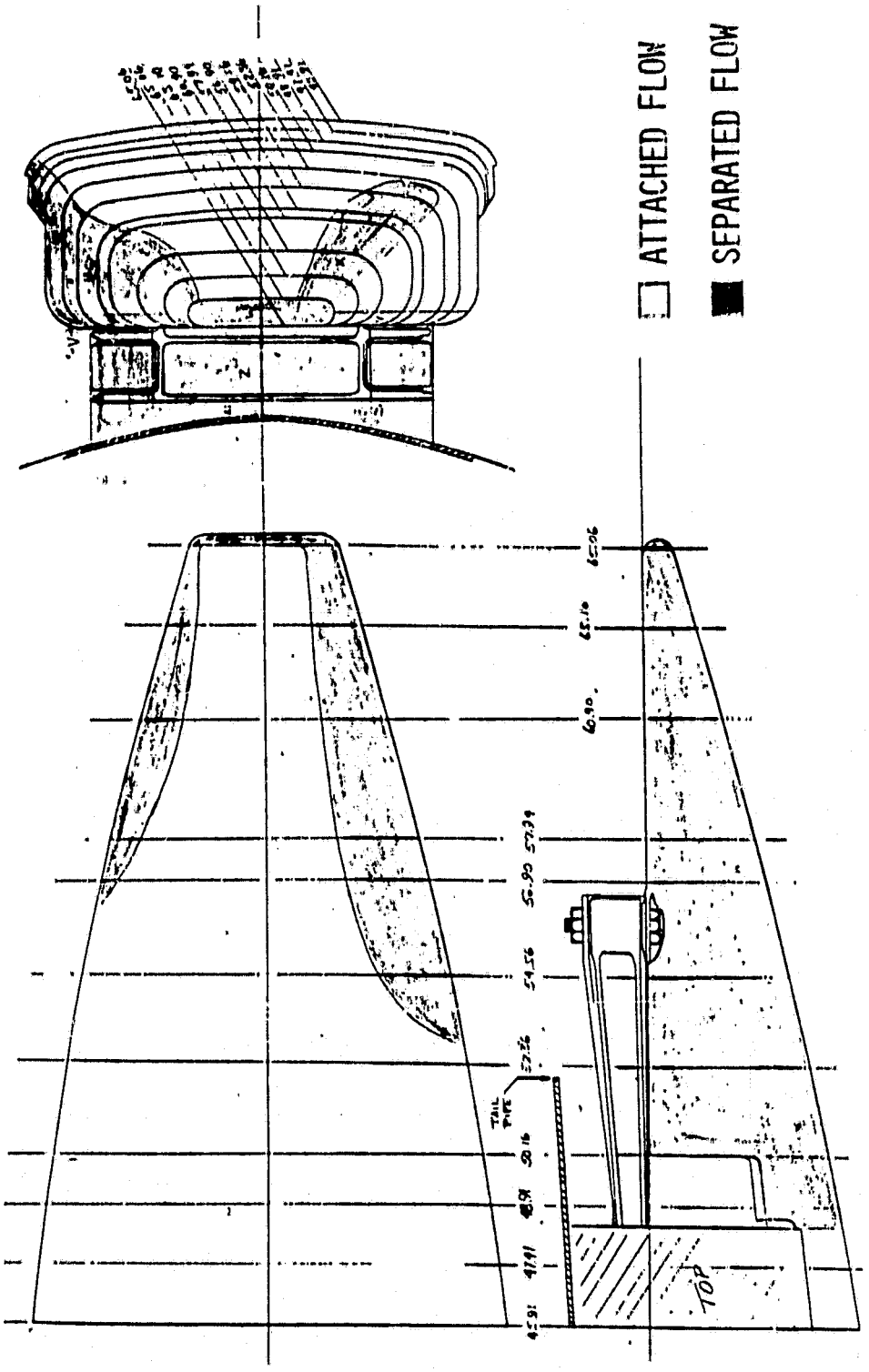

FLOW QUALITY ASSESSMENT
INBOARD PRODUCTION BASELINE

Figure 29

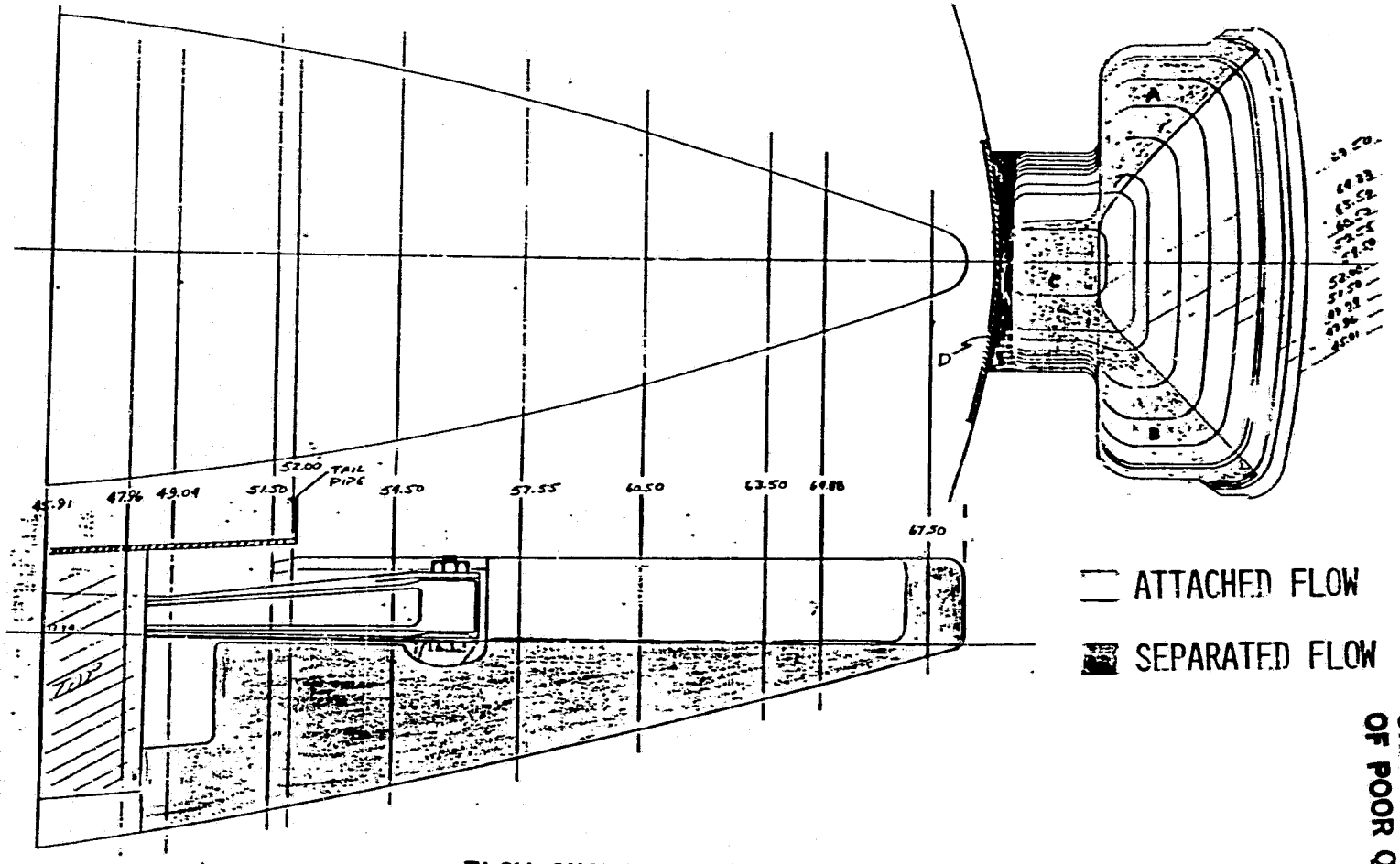

FLOW QUALITY ASSESSMENT
OUTBOARD INITIAL MODIFICATION

Figure 30

TABLE 1

FLOW ZONE AREAS (cm^2)

	OUTBOARD FAIRING					INBOARD FAIRING				
	BASE AREAS			WETTED AREAS		BASE AREAS			WETTED AREAS	
	A_{BG} (GAP)	A_{BJ} (JET)	A_{BF} (FREE STREAM)	A_{FJ} (JET)	A_{FF} FREE) STREAM)	A_{BG} (GAP)	A_{BJ} (JET)	A_{BF} FREE) STREAM)	A (JET)	A (FREE STREAM)
Production Baseline	33.2	94.7	101.0	0	1205	33.2	94.7	113.0	0	1138
Initial Modification	31.4	81.0	104.0	373	1080	31.4	74.3	63.7	309	1426
Configuration A	17.9	61.9	62.2	473	1338	17.9	61.9	164.0	473	1010
Configuration B	0.0	17.5	42.6	864	1648	0.0	19.6	158.0	864	1280
Configuration B 4° VG	0.0	17.5	42.6	864	1648	0.0	23.5	39.4	864	1937
Configuration B Filled	0.0	10.3	10.3	864	1926	0.0	10.3	10.3	864	1926
Configuration A 6°	17.9	60.6	48.6	520	1425	17.9	60.6	128.0	473	1226
Configuration A* VG	17.9	61.9	62.2	473	1338	17.9	61.9	64.5	473	1436
Configuration B* VG	0.0	17.5	42.6	864	1648	0.0	19.6	32.9	864	1937

*Not Tested

TABLE 2

INCREMENTAL DRAG REDUCTION CALCULATIONS

(% Relative to Production Baseline)

	OUTBOARD FAIRINGS					INBOARD FAIRINGS						
	BASE AREAS			WETTED AREAS		BASE AREAS			WETTED AREAS		VORTEX GEN	TOTAL
	GAP	JET	FREE STREAM	JET	FREE STREAM	GAP	JET	FREE STREAM	JET	FREE STREAM		
C_D / C_F	0.12	0.42	0.12	0.0031	0.0027	0.12	0.42	0.12	0.0031	0.0027		
Drag Reduction (% Airplane)												
Initial Mod.	0.0015	0.111	-0.0023	-0.0220	0.0025	0.0015	0.166	0.0413	-0.0182	-0.0056	--	0.28
Configuration A	0.0127	0.266	0.0327	-0.0278	-0.0025	0.0127	0.266	-0.0420	-0.0278	0.0025	--	0.49
Configuration B	0.0276	0.626	0.0489	-0.0509	-0.0086	0.0276	0.610	-0.0372	-0.0509	-0.0028	--	1.19
Configuration B 4 deg VG	0.0276	0.626	0.0489	-0.0509	-0.0086	0.0276	0.578	0.0615	-0.0509	-0.0157	-0.0043	1.24
Configuration B Filled	0.0276	0.685	0.0757	-0.0509	-0.0142	0.0276	0.685	0.0858	-0.0509	-0.0154	--	1.46
Configuration A 6 deg	0.0127	0.276	0.0438	-0.03-6	-0.0043	0.0127	0.276	-0.0119	-0.0278	-0.0018	--	0.55
Configuration A* VG	0.0127	0.266	0.0327	-0.0278	-0.0025	0.0127	0.266	0.0408	-0.0278	-0.0058	-0.0043	0.56
Configuration B* VG	0.0276	0.626	0.0489	-0.0509	-0.0086	0.0276	0.610	0.0671	-0.0509	-0.0157	-0.0043	1.28

*Estimated based on a combination of other tested configurations

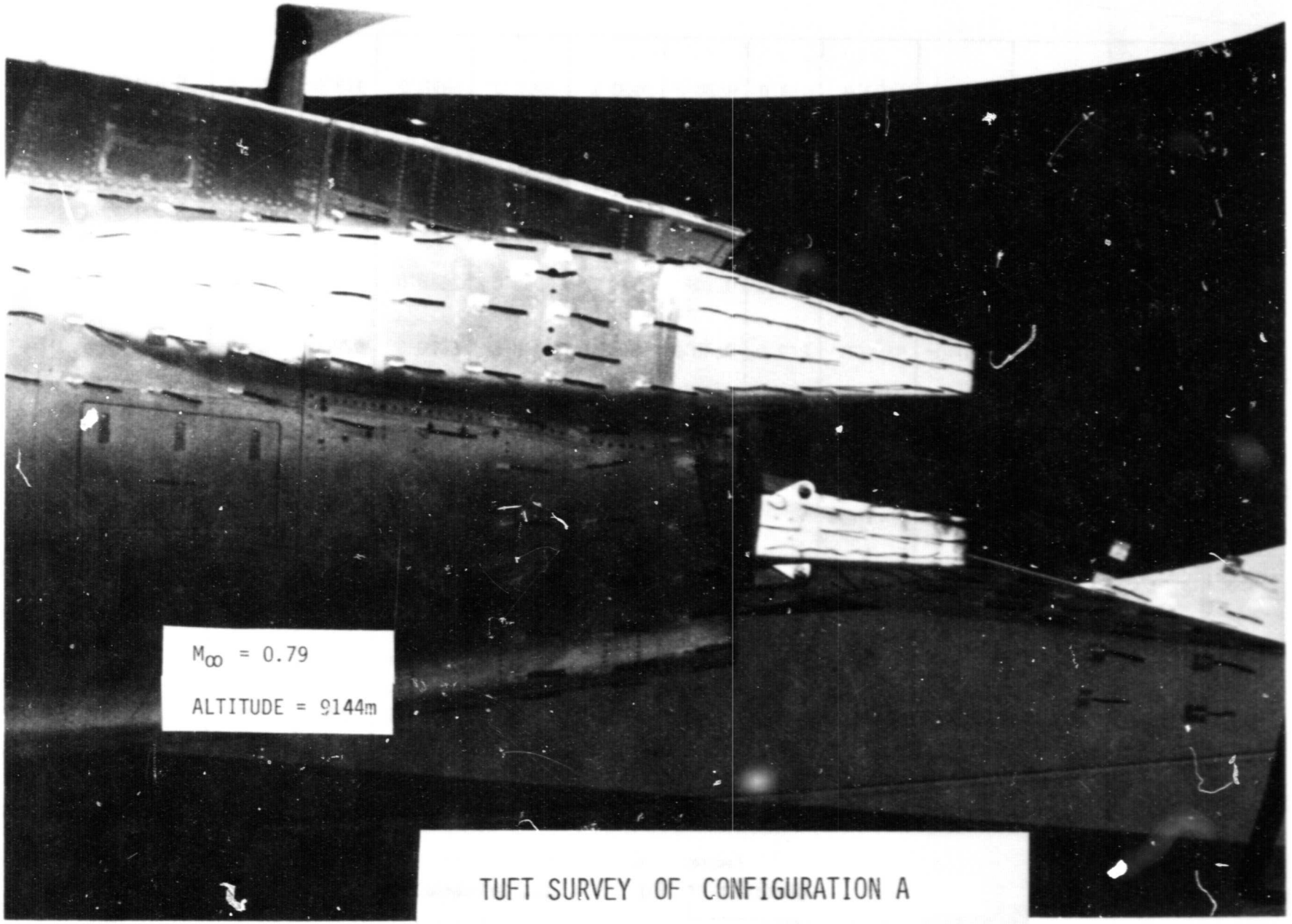

TUFT SURVEY OF CONFIGURATION A

Figure 31

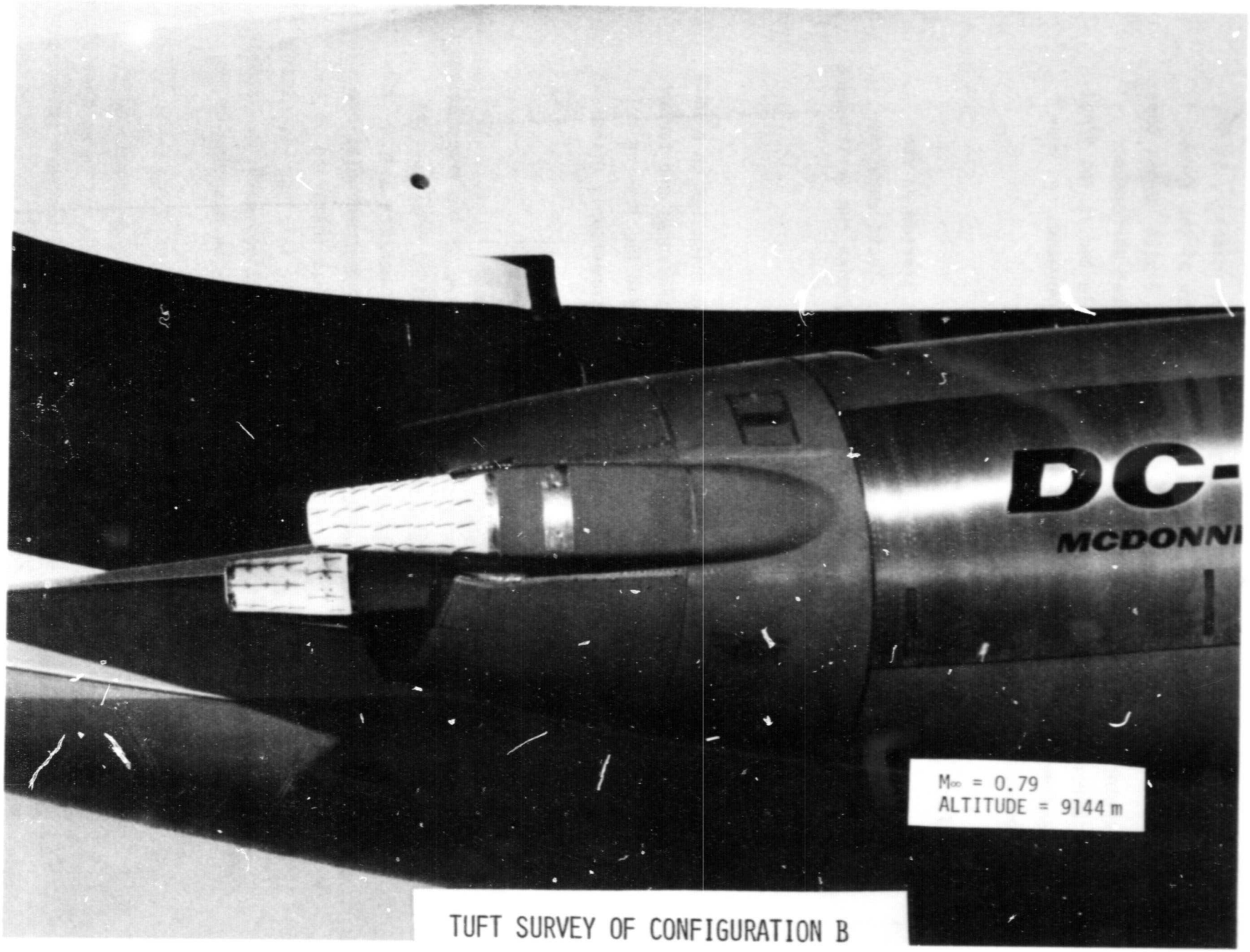

TUFT SURVEY OF CONFIGURATION B

Figure 32

The best tested configuration is B filled. This, however, is not considered to be practical since it precludes use of the thrust reversers. The best practical configuration is B with vortex generators. Configuration B had twice the calculated performance improvement as Configuration A, and thus was selected as the final aerodynamic configuration. The performance improvement has been estimated to be 1% of airplane drag.

3.2 COMPOSITE DESIGN

Structural design using advanced composites was started on the initial modification aerodynamic configuration. Tests were conducted with this configuration in order to determine the environment that the fairing would be exposed to.

Environmental Requirements

Instrumented initial modification fairings were installed on a DC-9 airplane and measurements made of the dynamic pressures and temperatures. Data was taken during takeoff and during the landing roll with reverse thrust. The static pressure data previously discussed were also taken during this test program.

Instrumentation

Dynamic pressures were measured by installing two Kulite transducers flush mounted on the inboard surface of the initial modification fairing. Three thermocouples were installed to measure surface temperatures. The location of the transducers and thermocouples are shown in Figure 33. This instrumented fairing was installed on the left engine nacelle on the inboard position. The fairings with static pressure taps were located on the outboard positions with the initial modifications on the left nacelle and the production baseline on the right nacelle.

All static tap pressures were measured with Douglas pneumatic multiplexer assembly, P/N 3893671-1. This module consists of three type 09 24 port Scanivalves with Statham PM 131TC differential pressure transducers

ORIGINAL PAGE IS
OF POOR QUALITY

LOCATION OF TRANSDUCERS
AND THERMOCOUPLES

Figure 33

and motor and drive train, heater blankets, pneumatic and electrical connectors. Each Scanivalve DP transducer was referenced to the flight test trailing cone static pressure. Each Scanivalve is capable of measuring 24 separate pressures with a single pressure transducer, thus only two of the three available Scanivalves were utilized - one for the production reverser stang pressure taps and the other for the modified reverser stang.

The instrumentation used is listed in Table 3. Figure 34 shows the data recording system schematic for the flight performance evaluation. The pressure lines were passed through the fuselage skin by using existing drain fittings. The drain lines were disconnected for purposes of this test.

Dynamic Pressure

The dynamic pressure data was recorded during takeoff and landing, and reduced in the acoustic data reduction center. The maximum sound pressure level measurements are shown in Figure 35. The peak value during reverse thrust corresponds to 165 db. The second peak during landing is attributed to an engine throttle excursion during taxiing.

The acoustic spectral density during takeoff is shown in Figure 36 and during reverse in Figure 37. The acoustic power is seen to be primarily below 1000 cycles per second.

Temperatures

Temperatures were measured using the thermocouples located on the exhaust flow side of a fairing along the centerline with the aft thermocouple about 2.54 cm (1 in.) from the trailing edge. The data was recorded during takeoff and landing, and reduced in ground facilities. Typical reduced data is shown in Figure 38. These data indicated the maximum temperature on the fairing would be 445°K (343°F) during reverse thrust. However, when the inflight tuft tests were conducted, some of the tufts were found to melt during reverse thrust. The tufts were made of nylon 6/6 which melts

Table 3

INSTRUMENTATION LIST

T/WR 197 - DC-9 NO 898

PARAM NO	PARAM DESCRIP	UNITS	RANGE	INSTRUMENTATION TYPE	SIGNAL TYPE	RESOLUTION
34-0000	AUX TOTAL PRESSURE	IN. HG	5/40	SPERRY ADC-1	DIG	.001
90-0052	FLT TEST T/C STATIC PRESS.	IN. HG	5/31	SPERRY ADC-1	DIG	.0005
34-1101	CAPTAIN'S AIRSPEED	KTS	0/450	SADC-2	DIG	.25
34-1103	CAPTAIN'S ALTITUDE	FEET	0/50000	SADC-2	DIG	1.0
34-1102	CAPTAIN's MACH NUMBER		0/1	SADC-2	DIG	.002
34-1100	PROD RAM AIR TEMP	°C	± 60	SADC-2/ROSEMT	DIG	1.0
34-1105	COMP STATIC AIR TEMP	°C	± 60	ROSEMT		1.0
77-1100	EPR ENG 1	RATIO	.8/2.4	PROD SYNCHRO	DIG	.005
77-2100	EPR ENG 2	RATIO	.8/2.4	PROD SYNCHRO	DIG	.005
77-1130	EGT ENG 1 - T_{T_7}	°C	0/800	TC-CA	VOLTAGE	2.0
77-2130	EGT ENG 2 - T_{T_7}	°C	0/800	TC-CA	VOLTAGE	2.0
71-1800	SCANI-VALVE PORT ID		1/24		DIG	
71-1801	SCANI-VALVE MODULE TEMP	°F	0/300	TC-CA	VOLTAGE	0.5
71-1804 THRU 71-1818	PRD STANG PRESSURES PLUMBED TO SINGLE S/V (15 TOTAL)	PSID	± 2.5	S/V TYPE 48J9 STATHM PM131TC	VOLTAGE	.005
71-1819 THRU 71-1837	MODIFIED STANG PRESSURES PLUMBED TO SINGLE S/V (19 TOTAL)	PSID	± 2.5	S/V TYPE 48J9 STATHM PM 131TC	VOLTAGE	.005
71-1838	MOD STANG FWD THERMOCOUPLE	°C	0/800	TC-CA	VOLTAGE	2.0
71-1839	MOD STANG CTR THERMOCOUPLE	°C	0/800	TC-CA	VOLTAGE	2.0
71-1840	MOD STANG AFT THERMOCOUPLE	°C	0/800	TC-CA	VOLTAGE	2.0
71-1841	MOD STANG FWD KULITE	PSIG	0/.3	XTEL-1-190-10	FM	
71-1842	MOD STANG AFT KULITE	PSIG	0/.3	XTEL-1-190-10	FM	
71-1843	MOD STANG CTR KULITE	PSIG	0/.3	XTEL-1-190-10	FM	
71-1844	MOD STANG ACCELEROMETER	GRMS	25GRMS/V	ENDEVCO 2221F	FM	

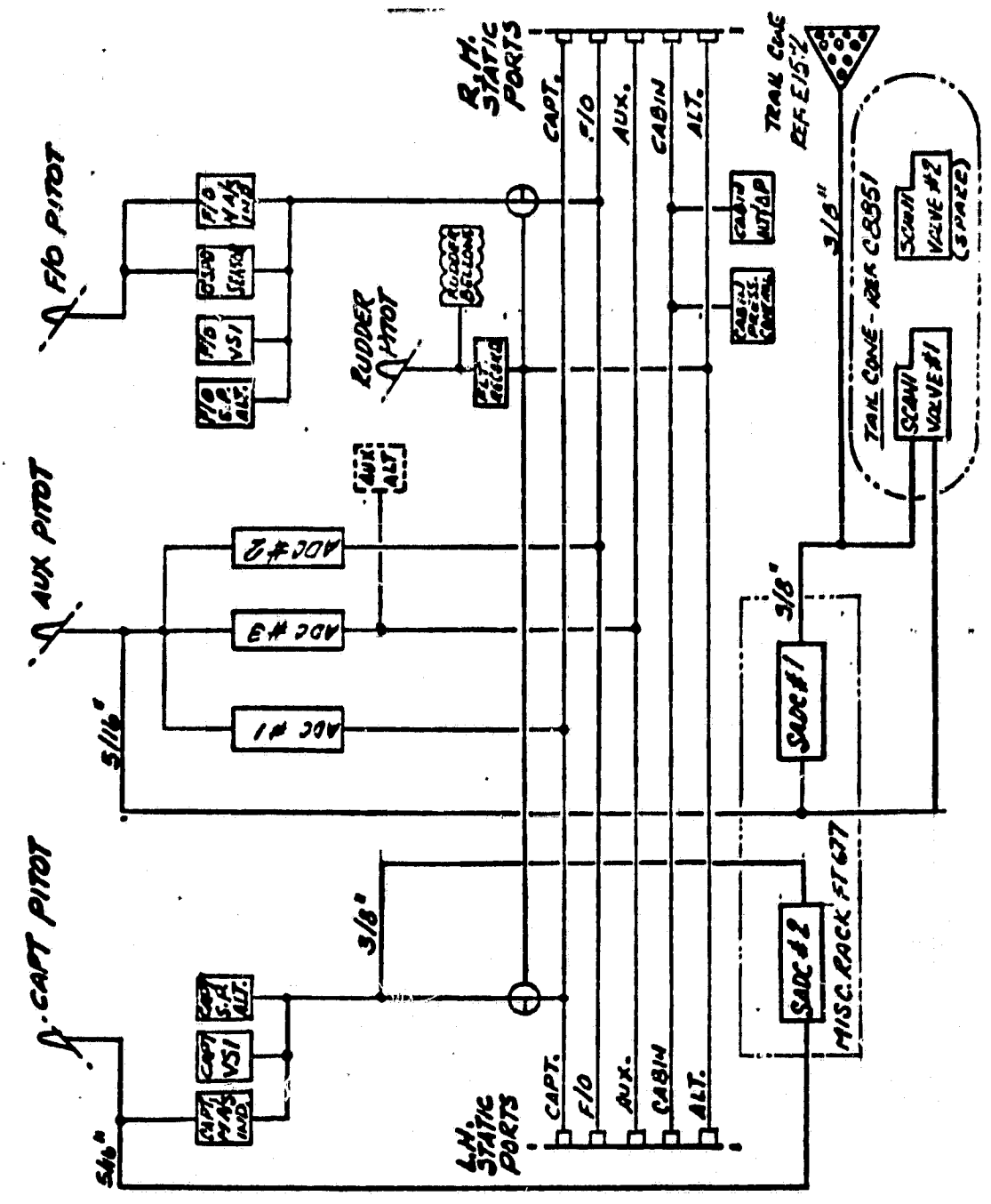

RECORDING SYSTEM SCHEMATIC

Figure 34

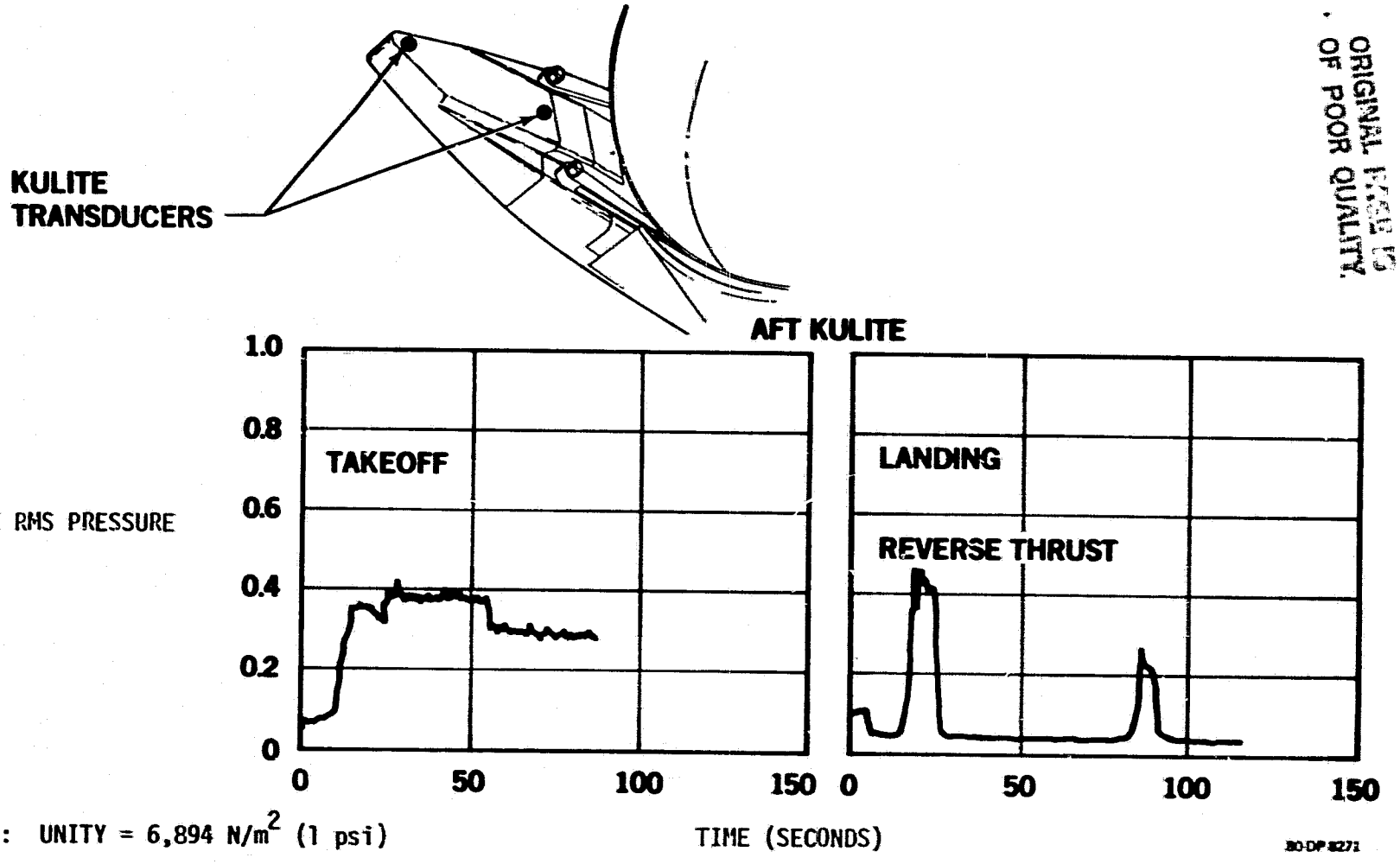

SOUND PRESSURE MEASUREMENTS

Figure 35

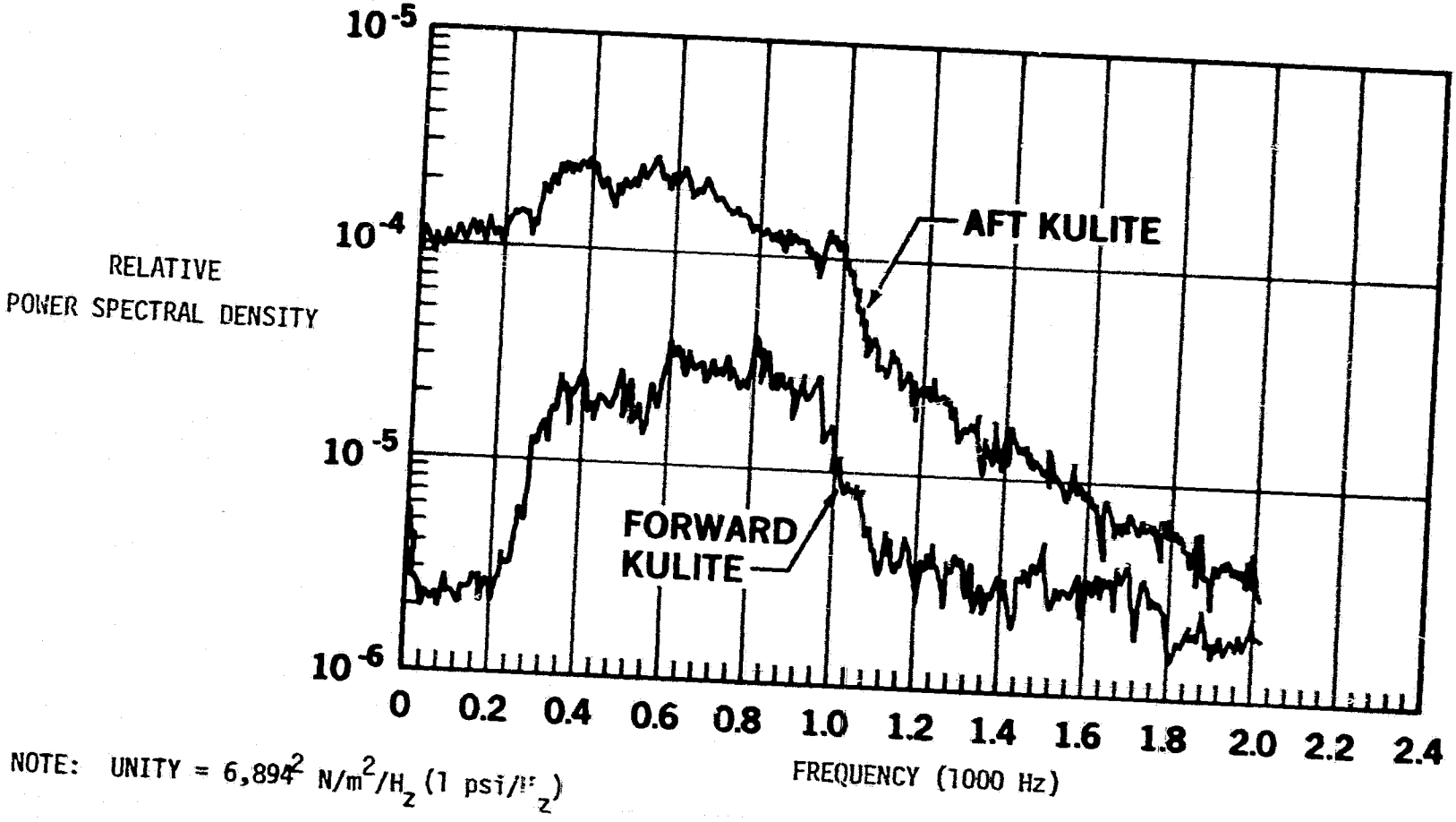

NOTE: UNITY = 6,894.2 $N/m^2/H_z$ (1 psi/H_z)

ACOUSTIC SPECTRAL DENSITY AT TAKEOFF

Figure 36

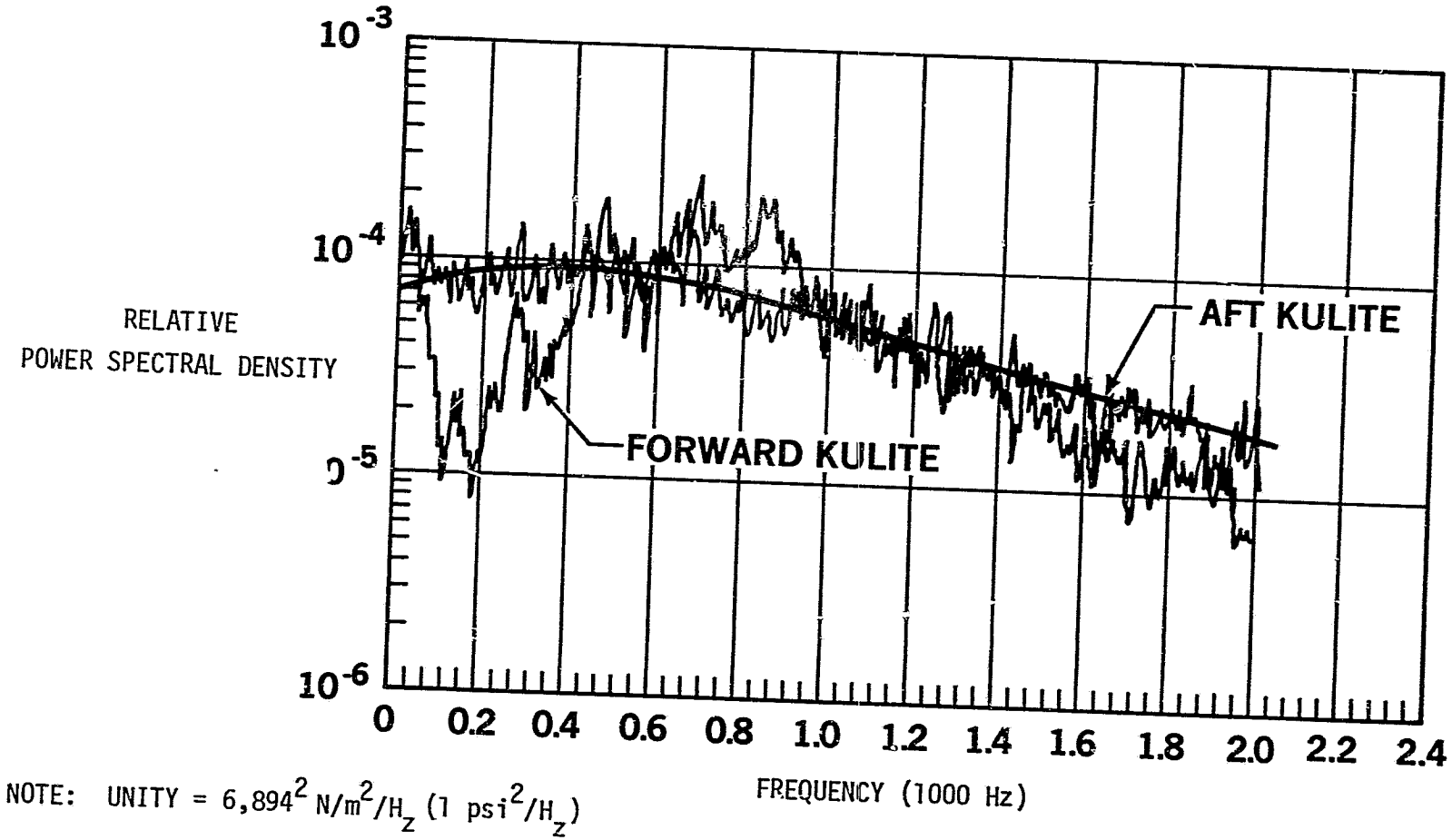

ACOUSTIC SPECIAL DENSITY DURING REVERSE

Figure 37

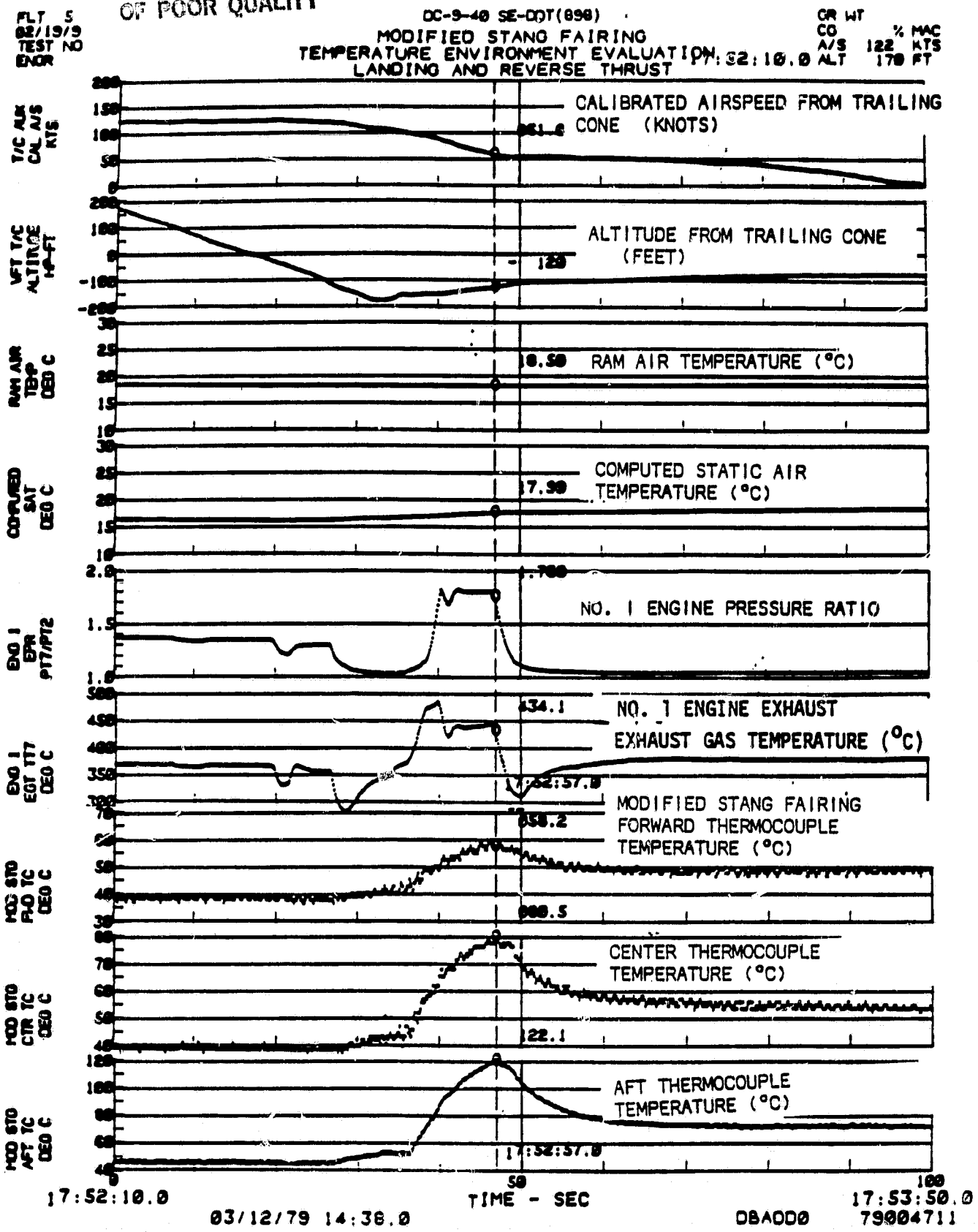

FAIRING SURFACE TEMPERATURE MEASUREMENTS

Figure 38

at 529°K (492°F). The tufts that melted were on the periphery of the trailing edge. Subsequently, temperature sensitive paint was applied to the trailing edge periphery during the aerodynamic development flight test program. Inspection of the temperature sensitive paint showed the trailing edge periphery reached around 533°K (500°F) during reverse thrust.

Material Selection

Use of an advanced composite system was selected in the interest of weight savings which would provide additional fuel savings, and to provide good fatigue resistance in a high sonic fatigue (165 db) environment. The fibrous nature of advanced composites minimizes crack propagation from defects.

The material system selection was based on the following considerations:

- Thermal Oxidative Stability
- Processability
- Material Availability/Assured Cost

Temperature measurements described above indicate surface temperature maximum of about 533°K (500°F) occurs during landing when the engines are in the reverse thrust mode. This established the need for a high temperature resin based composite material such as polyimide, since this resin is known to exhibit excellent thermal oxidative stability. PMR-15 was selected because it would provide the desired high temperature properties, processability, and was commercially available from a number of suppliers.

Originally developed by the NASA Lewis Research Center, The PMR-15 ("Polymerization of Monomeric Reactants") polyimide resins are compounded from three stable monomers (two ester-acids and a diamine), which are mixed together in a low-boiling alcohol. In the course of the prepregging operation, the precursors are reacted in place. Thus, the intractability often exhibited by other polyimide formulations, such as prepolymer instability, or high boiling solvent residuals in the prepreg, are absent with PMR-15.

The two step condensation-addition cure mechanism is characterized by:

- Imidization step during which the imide ring is closed, accompanied by the generation of condensation by-products (water and methanol).

- Chain propagation step via the opening of the polymer end cap, a "Reverse" Diels-Alder addition reaction.

Because the condensation process occurs relatively early in the cure cycle, most of the volatile removal problems associated with other polyimide formulations are eliminated. A more detailed discussion of the PMR-15 chemistry may be found in Reference 5.

On the DC-9, the elevated temperatures occur only during reverse thrust. The total time at temperature would be less than 100 hours after 50,000 flight hours. Results from long term 533°K (500°F) tests on Kevlar-49/PMR-15 composite materials conducted by the NASA Lewis Research Center and reported in Reference 6 show the stability in the present application.

Other investigators reported good retention of mechanical properties even after a 294 hour exposure at 589°K (600°F) with S-6581 Glass/PMR-15 as indicated in Reference 7.

Both of the above evaluations noted some reduction in composite properties in the course of the test, as evidenced by lower flexure strength values and weight loss determinations. However, the impact of this is relatively minor on the present application.

The use of Kevlar was also preferred for ease of forming. Experience has shown that the Kevlar does not exhibit the spring back that occurs with graphite. Consequently, although heating is required for forming to soften the resin, it does not require cool down to maintain conformity.

The final consideration for selecting the Kevlar-49/PMR-15 composite material was its ready availability from several commercial prepreggers.

All the prepreg utilized in this program was prepared by a commercial supplier using a hot-melt formulation on CS-353 Kevlar fabric. The widespread use of Kevlar provides an assured availability. In addition, at the time this material selection was made, there was a national concern about a potential free fiber problem with graphite which could jeopardize a graphite composite development program, particularly for an application in a hot area.

Properties of Kevlar-49/PMR-15

Material property tests were conducted on the Kevlar-49/PMR-15 to confirm the suitability of the use of this material system in aircraft secondary structures. While mechanical property data exists for graphite/polyimide and Kevlar/epoxy material systems, data for Kevlar/polyimide has not been available in literature. Tests were therefore conducted to determine the mechanical properties for Kevlar-49/PMR-15 through a temperature range of 219°K (-65°F) to 505°K (450°F). In addition, the effects of long term exposure to moisture, and aircraft hydraulic fluid (Skydrol) and moisture were determined. A description of the tests and resultant tabular data are presented in the Appendix. The mechanical properties are summarized here. The average values are shown based on nominal thicknesses for cross-sectional areas. Nominal thicknesses are used to determine cross-sectional areas as to actuals because the material strength is primarily in the fibers. The strength will be more directly related to the number of plies as to the thickness. The thickness varies after cure for a constant number of plies. The nominal is the average thickness for the number of plies as is more useful for design purposes.

The ultimate tensile strength and initial tangent tensile modulus are shown in Figures 39 and 40 for temperatures of 219°K (-65°F) to 505°K (450°F). The unidirectional data are for all plies with fibers oriented at 0°/90° and the isotropic data are for plies oriented at 0°/90°, ±45°. The wet data are for specimens conditioned in 95% humidity at 333°K (140°F) for 30 days. The Skydrol data are for specimens soaked in Skydrol at 333°K (140°F) for 7 days followed by 95% humidity at 333°K (140°F) for 30 days.

The ultimate compressive strength and initial tangent compressive modulus are shown in Figures 41 and 42. The unidirectional and isotropic data are for the same ply fiber orientations as described for the tensile data above. The environmental conditioning was also identical as for the tensile specimens.

The fatigue life characteristics are shown in Figure 43 for specimens subjected to an oscillating load. The strains were not measured during the fatigue tests, but were determined from load-strain data taken during the ultimate tension and compression tests.

The shear bearing strength is shown in Figure 44. Kevlar-49/PMR-15 exhibits a shear bearing strength which is greater than the tensile strength. The shear out strength shown in Figure 44 decreases with temperature as would be expected. The initial bearing failure data shows higher strength at 394°K (250°F) than at room temperature. The reason for this apparent anomaly is not understood.

The test results shows Kevlar-49/PMR-15 exhibits good mechanical properties. The effect of long term exposure to moisture and Skydrol is nominal. The shear bearing strength is good. For secondary structures where material thicknesses are determined by handling and stiffness requirements, the low density 13840 kg/m^3 (0.5 lbs/in^3) of Kevlar-49/PMR-15 should provide weight savings, while the material can be used at elevated temperatures.

Design Requirements

In order to maximize fuel savings, the final configuration is based on aerodynamic Configuration B, and must be retrofitable. To ease retrofitability, no airplane rework should be required. The structural design therefore uses the existing mechanical fastener locations. In order to properly fair, the thickness should match the metal thickness of the baseline production fairing. Using a male mold precludes use of doublers; the final fairing is therefore made from 16 plies to match the metal thickness of the baseline.

The reverser stang fairing is the aft closure for the thrust reverser four-bar linkage support that houses hydraulic actuators. The fairing can therefore be expected to be exposed to Skydrol as well as moisture.

In forward thrust there is very little load on the fairing. The maximum load occurs during reverse thrust at which time it is subjected to a bending load due to the reverse flow. The design conditions are depicted in Figures 45 & 46. The maximum temperatures occur around the trailing edge periphery and are about 500°F. The surface closest to the nozzle where the maximum bending moments occur will not exceed 405°K (270°F).

Strength Analysis

A conservative estimate of the loads were made assuming the exhaust flow would apply full total pressure to the aft section of the fairing. The maximum load would be less than 2224 N (500 Lbs.). The nominal thickness of the fairing using 16 plies is 0.325 cm (0.128"), and the flat surfaces are about 20.3 cm (8") wide providing a 6.45 cm^2 (1 sq. in.) cross sectional area. As determined from Figure 19, the compression and tension stresses will be less than 13.8×10^6 Pa (2000 PSI).

The maximum load in a fastener if all the load were taken in one of the three on the airflow side would be 1708 N (384 Lbs.). The number 10 fasteners made from 125 HT steel have a shear strength of over 8900 N (2000 Lbs.) each.

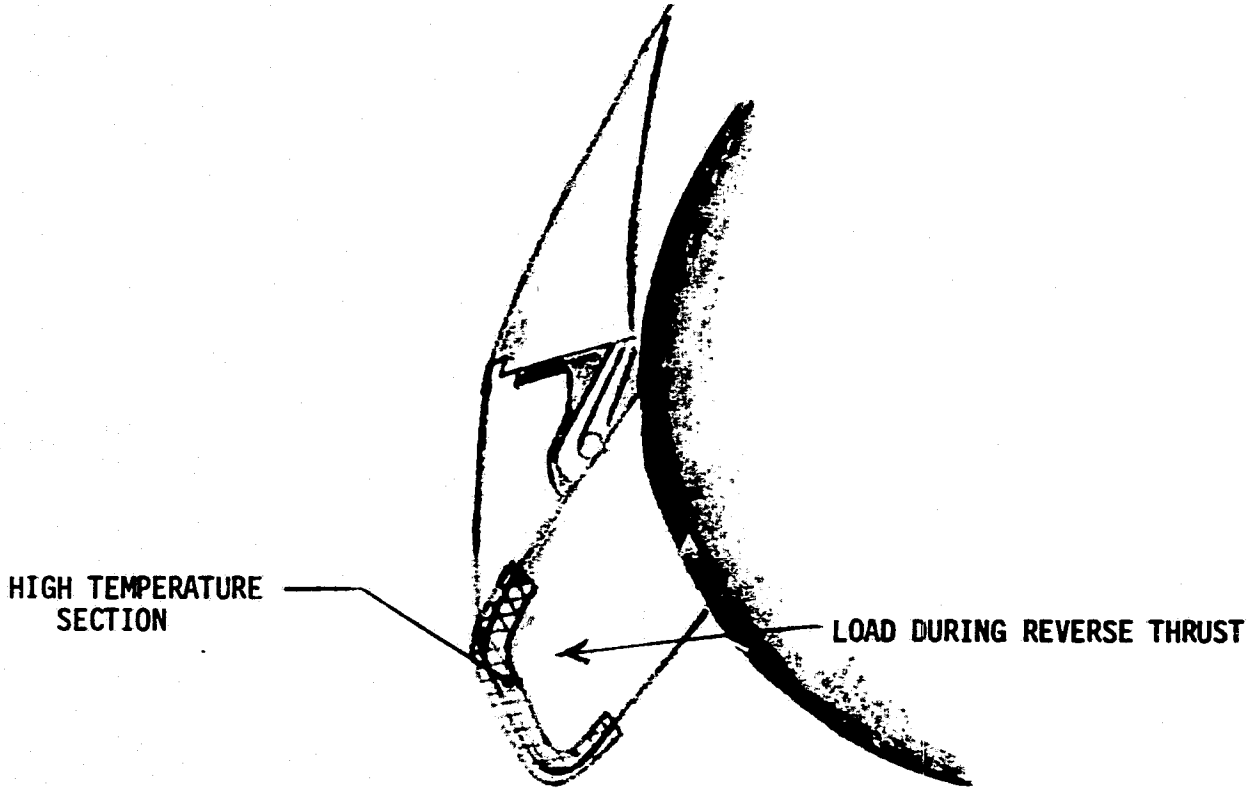

DESIGN CONDITIONS

Figure 45

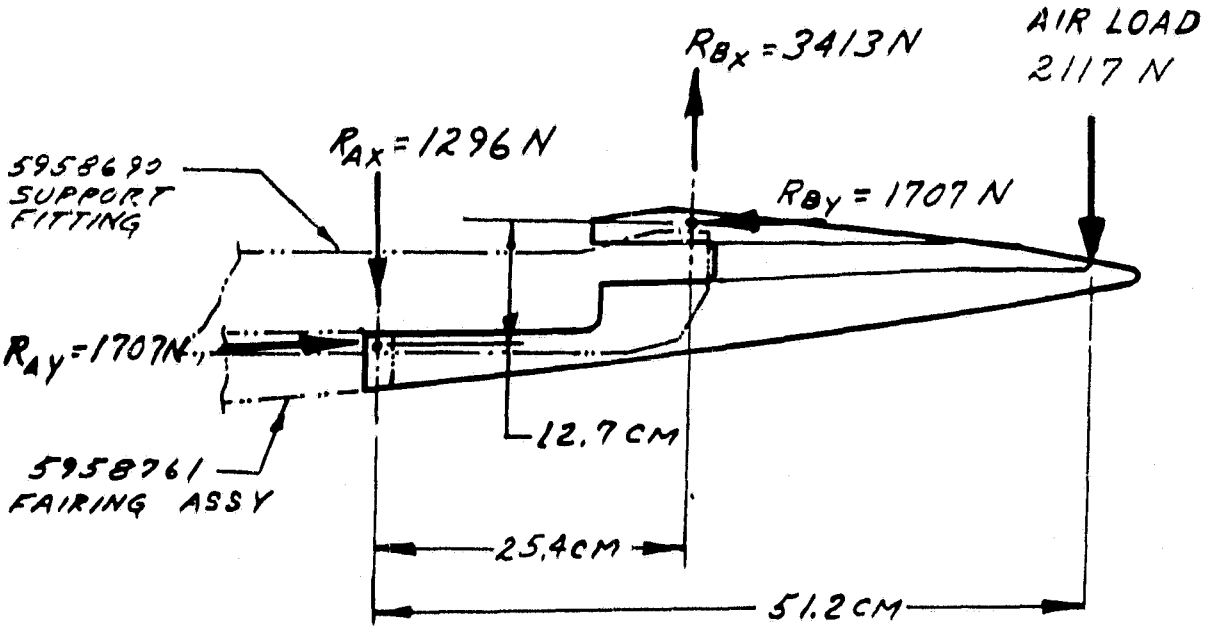

R_{Ax} IS REACTED IN COMPRESSION FROM THE STANG BEARING AGAINST THE 5958761 FAIRING ASSY

R_{Ay} IS REACTED IN SHEAR THROUGH FIVE #10 FLUSH HEAD SCREWS ATTACHING THE FAIRING TO THE 5958761 FAIRING ASSY.

R_{Bx} IS REACTED IN COMPRESSION FROM THE STANG BEARING AGAINST THE 5958690 SUPPORT FITTING.

R_{By} IS REACTED IN SHEAR THROUGH THREE #10 FLUSH HEAD SCREWS ATTACHING THE FAIRING TO THE 595-8690 SUPPORT FITTING.

MAXIMUM STATIC LOADS

Figure 46

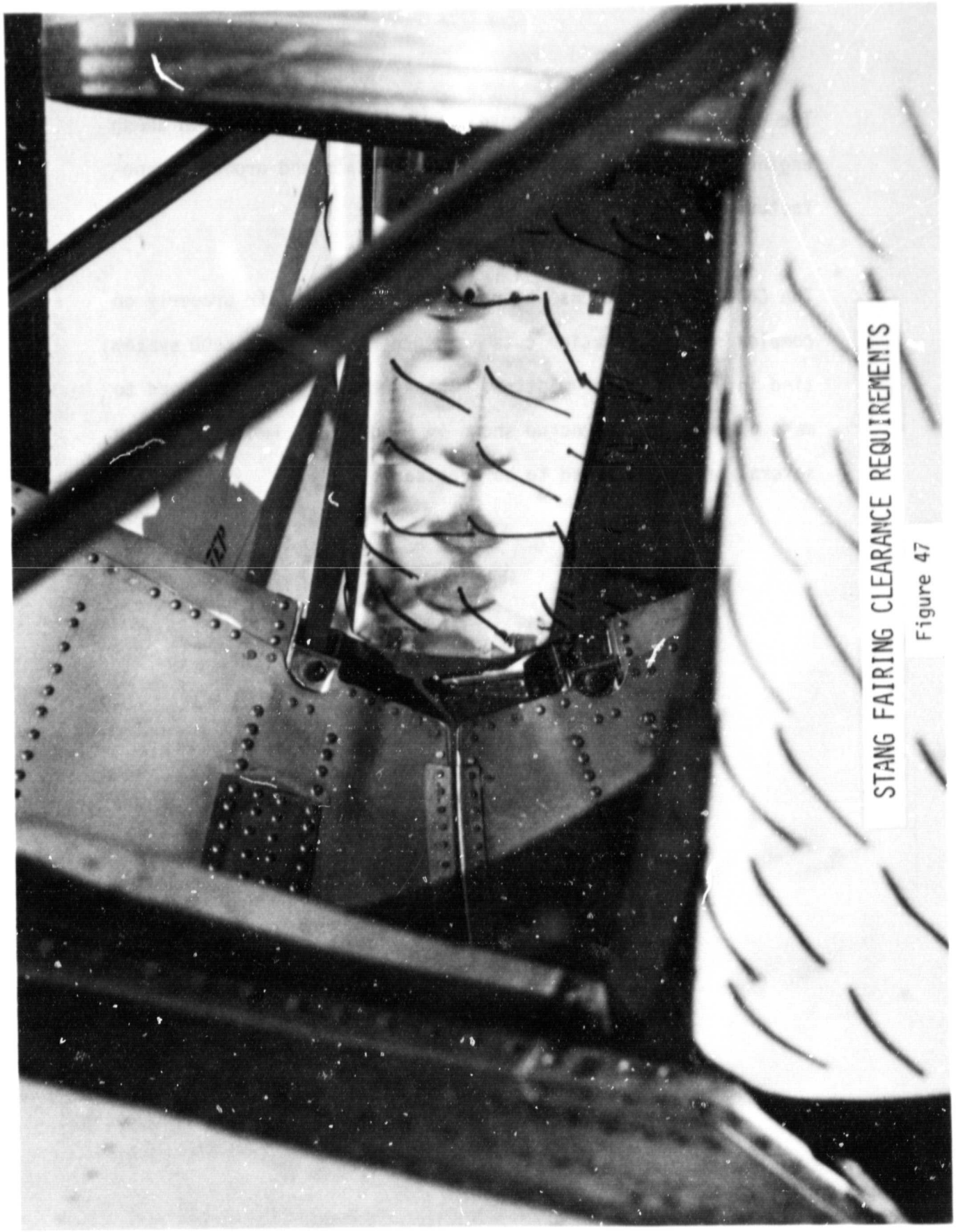

STANG FAIRING CLEARANCE REQUIREMENTS

Figure 47

The new configuration was developed by close coordination among engineers in design, aerodynamics, materials and process, manufacturing, and tool design.

The CADD uses equations which sometimes do not fair properly on complex shapes. Station cuts were generated by the CADD system tied in with a Gerber plotter. These station cuts were used to make an engineering mockup shown in Figure 48. Recontouring in several areas was found to be necessary.

ENGINEERING MOCK UP

Figure 48

would not cure properly. The cure temperature was elevated to 561°K (550°F) resulting in satisfactory cure. However, at this temperature the silicon rubber madrels used to develop molding pressure would crack. At this point, the decision was made to go to an autoclave cure cycle.

Autoclave Cure

Development of a molding and curing procedure was conducted on the initial modification aerodynamic configuration. A wood pattern was made of this initial modification configuration. A plaster mold was made from the pattern and a male layup tool cast. A layup on the layup tool is shown in Figure 49. Since the part was to be cured in a female mold which would establish the external lines of the final part, doublers were used to provide extra thickness for stiffness. The rise in the layup in Figure 49 is due to the doublers.

A female mold was made by using zinc spray on the wood pattern. Removable inserts were used to form the steps that are needed to properly mate with the airplane nacelle. The inserts are in place in the zinc spray mold shown in Figure 50. These inserts are removed with the cured part to preclude lockup in the mold.

Several autoclave cure cycles were evaluated on small specimens with the selected cycle shown in Figure 51. The cure cycle is followed by a post-cure at 561°K (550°F) after removal of the part from the mold.

Two initial modification fairings were made in an autoclave with the zinc spray female mold. The initial modification advanced composite fairing is shown in Figure 52.

Melt Out Tool

After the aerodynamic configuration development activities resulted in selection of a final design based on aerodynamic Configuration B, a review of molding requirements resulted in the conclusion that a male mold instead of a female mold should be used. The B Configuration has depressions for the thrust reverser linkage resulting in relatively thin

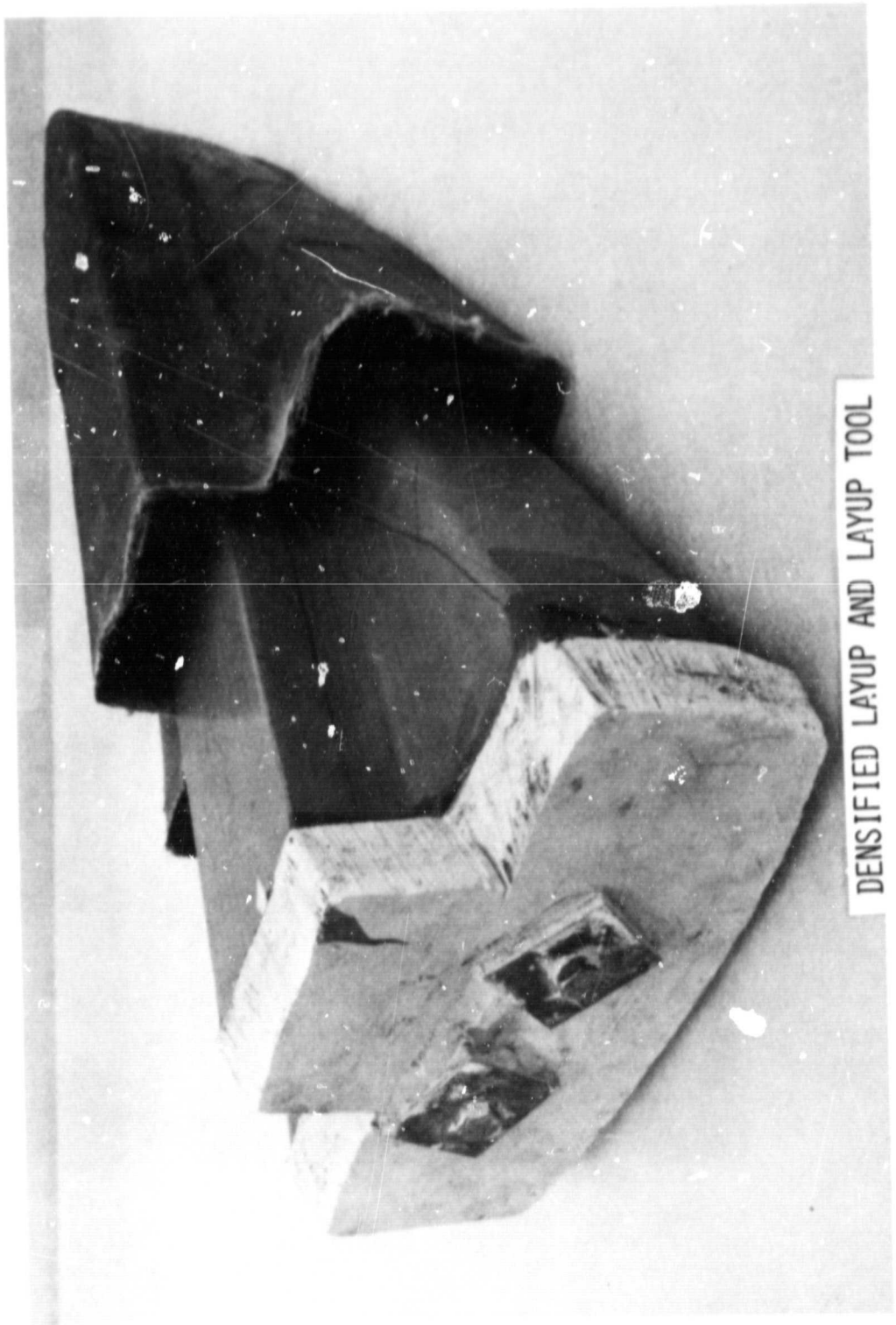

80-DP-8253

DENSIFIED LAYUP AND LAYUP TOOL

Figure 49

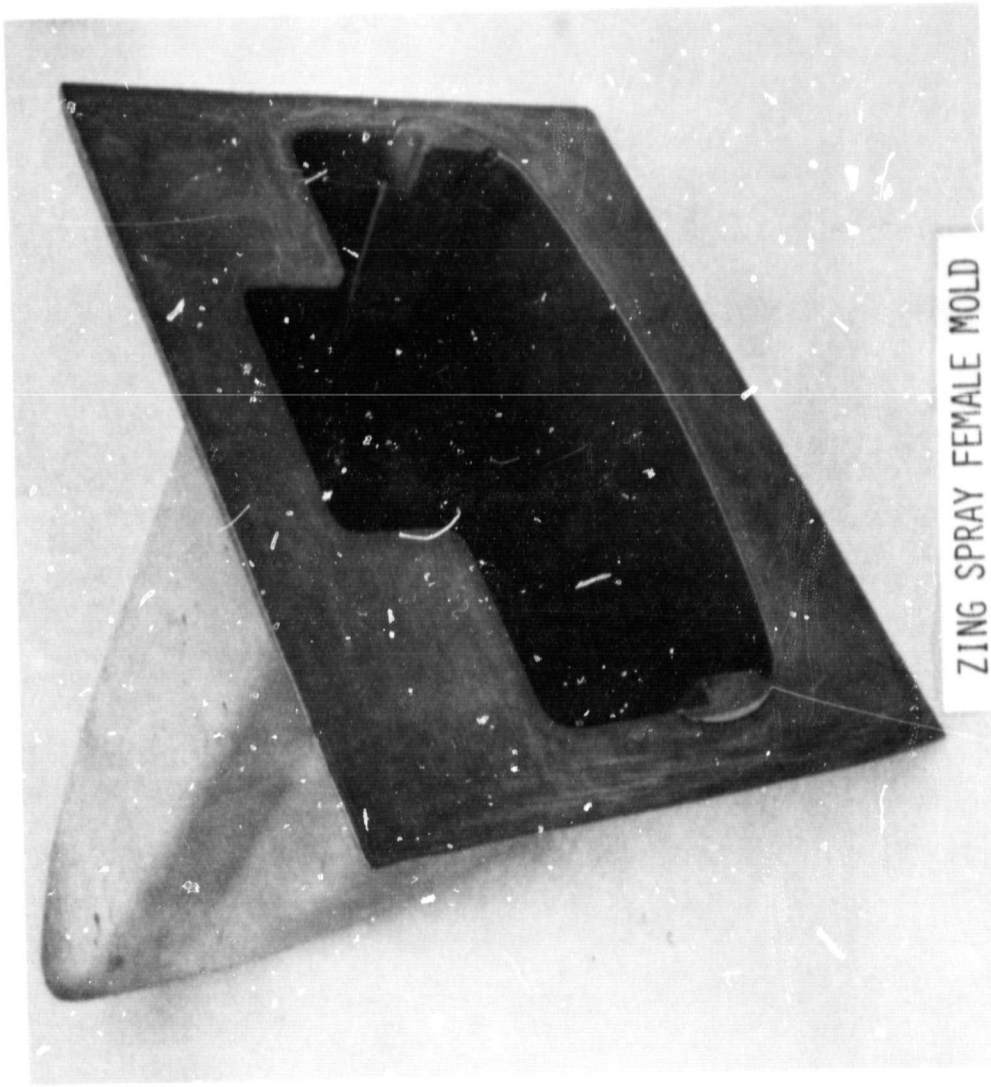

80-DP-8254

ZING SPRAY FEMALE MOLD

Figure 50

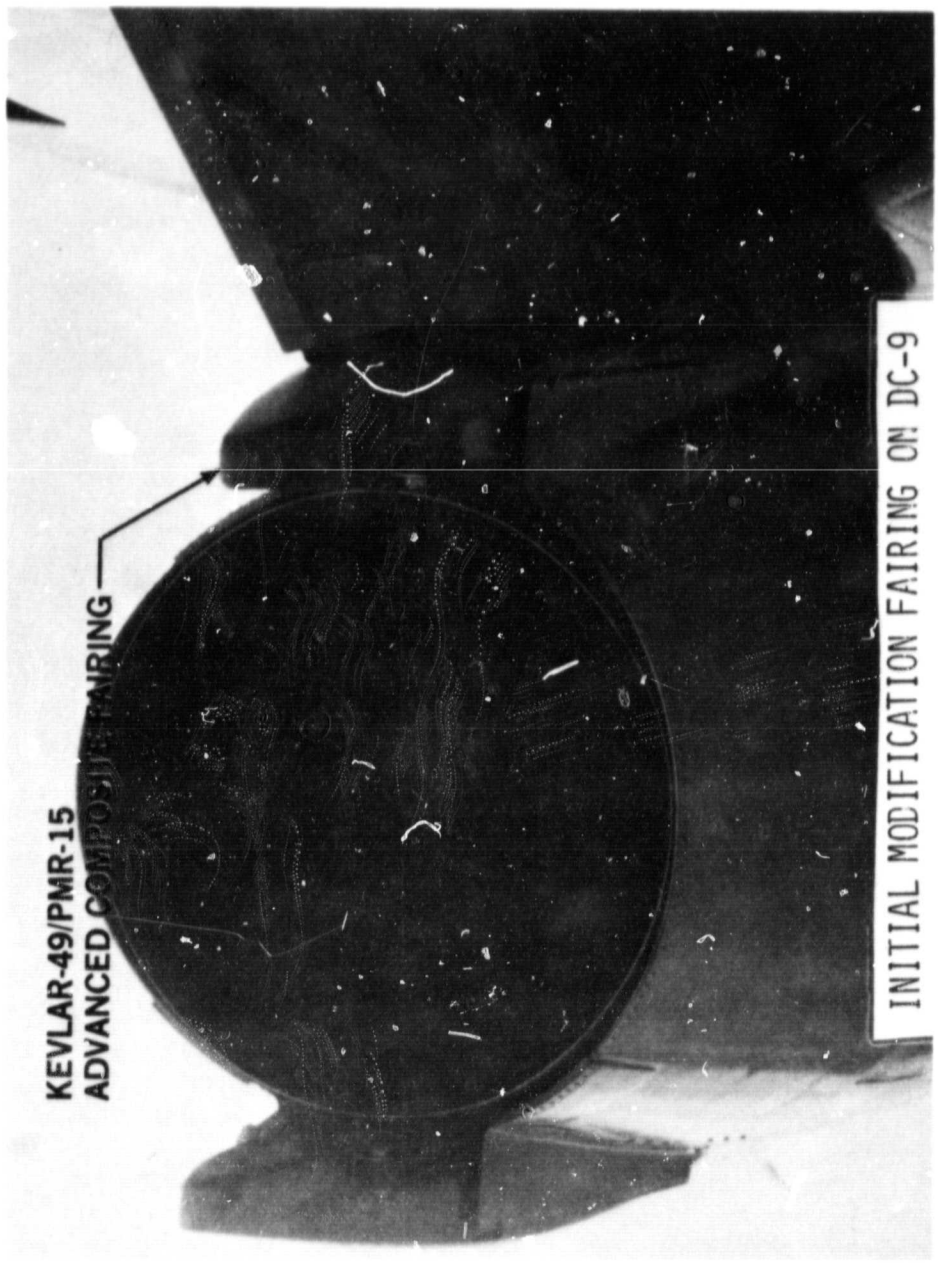

Figure 52

shelfs. Use of a female mold would require narrow depressions to create cavities to form these shelves. In a female mold, layup in a narrow cavity would be difficult and, based on previous experience, it was doubtful that suitable molding pressure would be developed in a narrow cavity. It was therefore decided to use a male mold.

Due to the long lead time required to obtain a multiple piece aluminum tool, use of a melt out tool was investigated. A simple mold was made from which a casting was then made with lead containing 3% antimony. This lead melts just above the cure temperature. The trial part is shown in Figure 53. This approach shows promise as a means to mold shapes that would be trapped in a 1 piece mold. This approach was not further pursued because the multi-piece aluminum tool became available. The multi-piece aluminum tool is relatively expensive and required several months to make, the melt out would be a promising approach for configuration development where a number of different mold shapes is required.

The weight of the Kevlar-49/PMR-15 was estimated to be 1.32 kg (2.9 lbs.). The weight of the same configuration made from aluminum 2024 and 2219 was estimated to be 2.27 kg (5.0 lbs.). A completed advanced composite fairing was weighed at 1.35 kg (2.97 lbs.). It was therefore determined that the use of Kevlar-49/PMR-15 advanced composites results in a 40% weight savings.

This material system therefore offers a 40% weight savings for fairings subjected to limited temperature exposures of 533°K (500°F) and should provide good fatigue resistence in a high sonic fatigue environment because of its fiberous nature. The material has good shear bearing strength for fasteners and can be molded into complex shapes. The Kevlar shapes well and if the protective film is left on, the prepreg until the adjacent layers are applied during layup, it exhibits good tack. This procedure minimizes evaporation of the solvent which provides the tack.

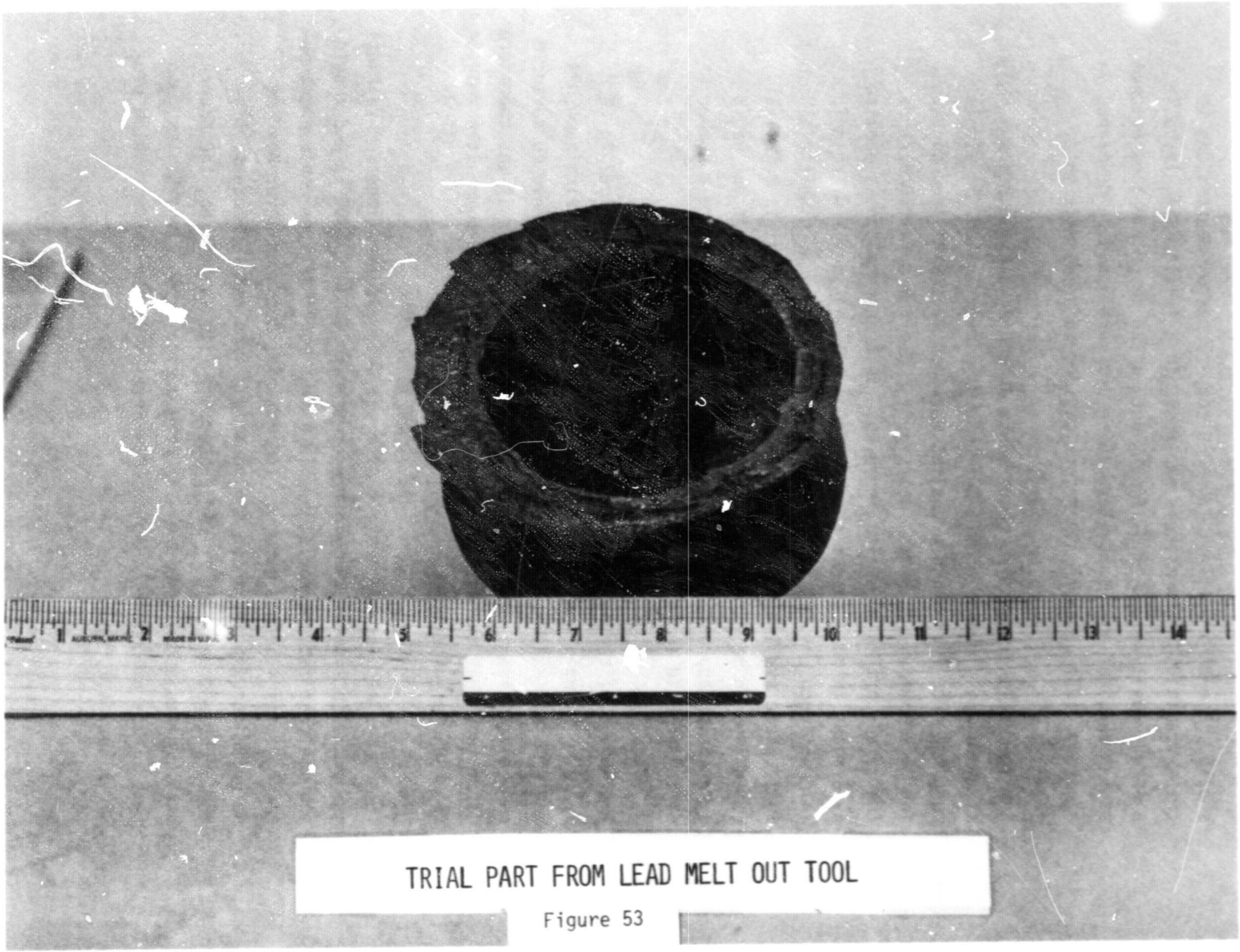

TRIAL PART FROM LEAD MELT OUT TOOL

Figure 53

Alternate Layup Methods

The first final design fairing was made by cutting out each layer from prepreg cloth in two halves which are placed on the front and back of the layup tool. The depressions or flutes are formed by cutting the edges to create fingers which allow shaping. This is done 16 times. The method being used required initially cutting prepreg cloth to a pattern. This pattern is oversized because each layer of prepreg is applied by hand and position placement on the layup varies. The edges and fingers in the depressions are then trimmed to form butt joints. With each subsequent layer, the position of the joints are staggered. This variation is needed to prevent any local area that does not have continuous fibers to preclude a structurally deficient joint. Butt joints are used to prevent excessive thickness buildup. Each layer thus then requires cutting two halves from prepreg cloth, trimming, bagging, and going through a forming compaction and partial densification cycle in an oven. Since this hand layup procedure used is labor intensive, evaluations were made on use of prepreg form fitting socks that would preclude the need for cutting each layer from a pattern and then trimming the butt joints.

Winding

Use of winding was evaluated but not pursued because use of a male mold would result in problems in achieving a suitable aerodynamic shape and finish. Winding on a bias results in thickness buildup as the fairing tapers down. The setup cost for trying this approach was considered to be excessive without any assurance of success.

Weaving

The use of weaving was evaluated. Discussions were held with a company specializing in weaving for composite structures and it was determined that a loom could be set up to weave Kevlar socks which could then be prepregged. In order to determine feasibility, socks were made by sewing together two halves. The CADD system was used to generate the perimeter versus axial station from which a pattern was made. Two halves were then cut from cloth and sewed together with Kevlar thread, and then impregnated with PMR-15.

Attempts to form a suitable layup were not successful. Wrinkles could not be avoided because of relative length changes required in the longitudinal direction. In addition, it is very difficult to pull a prepreg layer on over the previous layup.

Selected Layup Procedure

The hand layup procedure was refined and forming and compaction of multiple layers greatly reduced the time required to form a part.

4.2 Tooling

The retractable male tool was designed using lines from the CADD. A view on the CADD is shown in Figure 54. The CADD is particularly useful because the lines can be readily adjusted. Figure 55 identifies the requirements for adjusted lines. There are four sets of lines needed to make the composite fairings using a male mold. First, the aerodynamic lines are needed with station cuts for inspecting the finished part. These are the outside lines at room temperature. Another set of lines are needed to inspect the male tool. These lines are for the inside of the fairing, but corrected for thermal contraction of aluminum from 561°K down to room temperature. The aluminum male mold is sized so that the part is formed during cure at 561°K. The male mold surface lines, which are the inside lines of the fairing, are therefore needed after contraction to room temperature since this is when the tool is inspected for conformity.

Another set of lines is needed to make the sand mold to cast the aluminum tool. A wood pattern is made for making the sand casting cavity. This wood pattern is sized to account for the thermal contraction that occurs between the temperature at which aluminum sets during casting and the dimensions needed for making the fairings.

A fourth set of lines are needed to make the tool that is used for forming silicon rubber bags. The silicon rubber bags that are used are flexible and do not require accurate dimensions, but the tool should

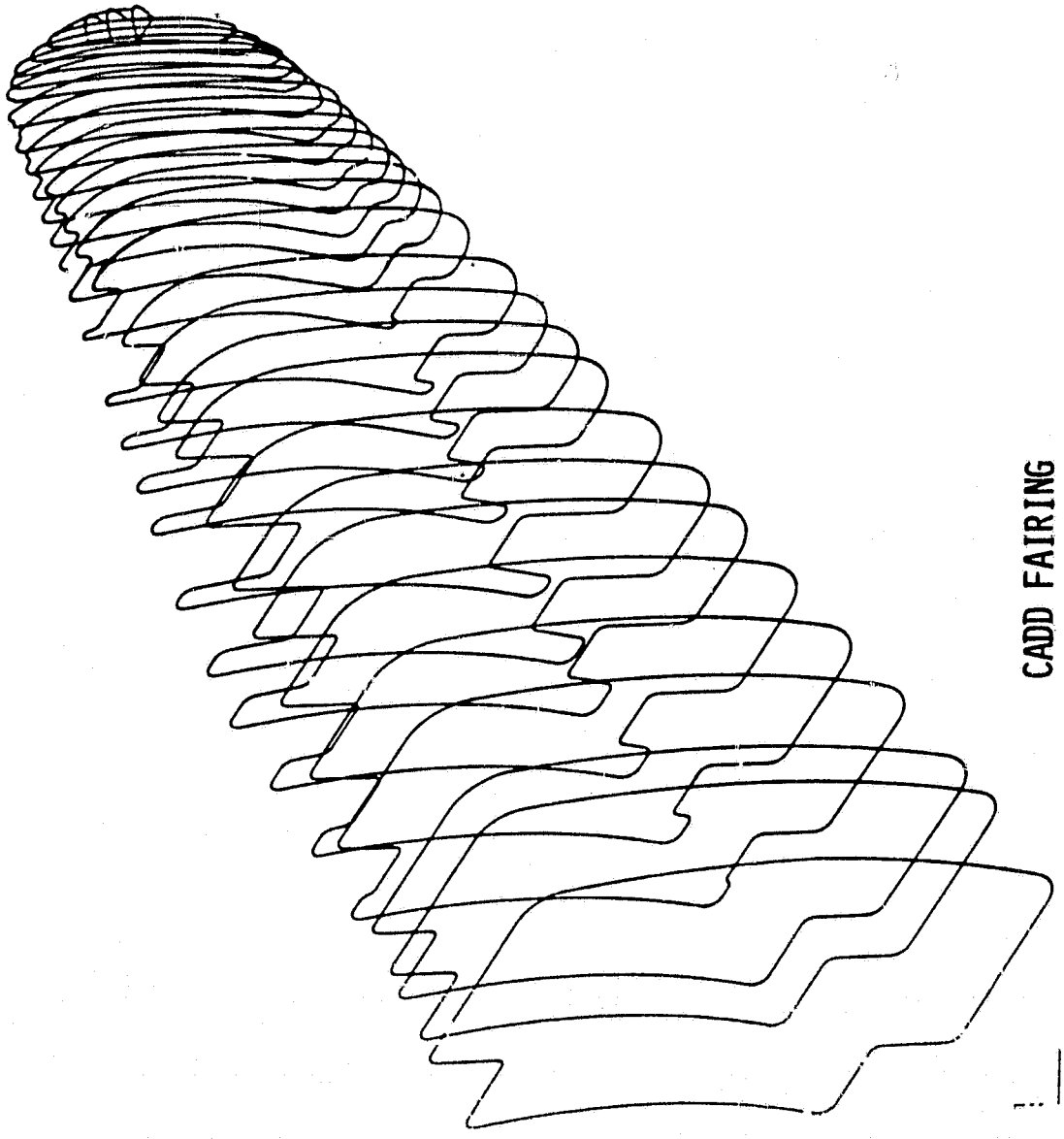

CADD FAIRING

Figure 54

Lines Development		Station Cuts
Fairing External Aerodynamic Lines	→	Inspection Templates for Finished Parts
↓		
Fairing Inside Lines for Male Mold		
↓		
Mold Lines at Room Temperature	→	Inspection Templates for Male Tool
↓		
Mold Lines at Casting Temperature for Tool	→	Templates for Wood Pattern to Cast Aluminum Tool
↓		
Lines for Forming Vacuum Bags	→	Lines for Bag Layup Tool

REQUIREMENTS FOR LINES

Figure 55

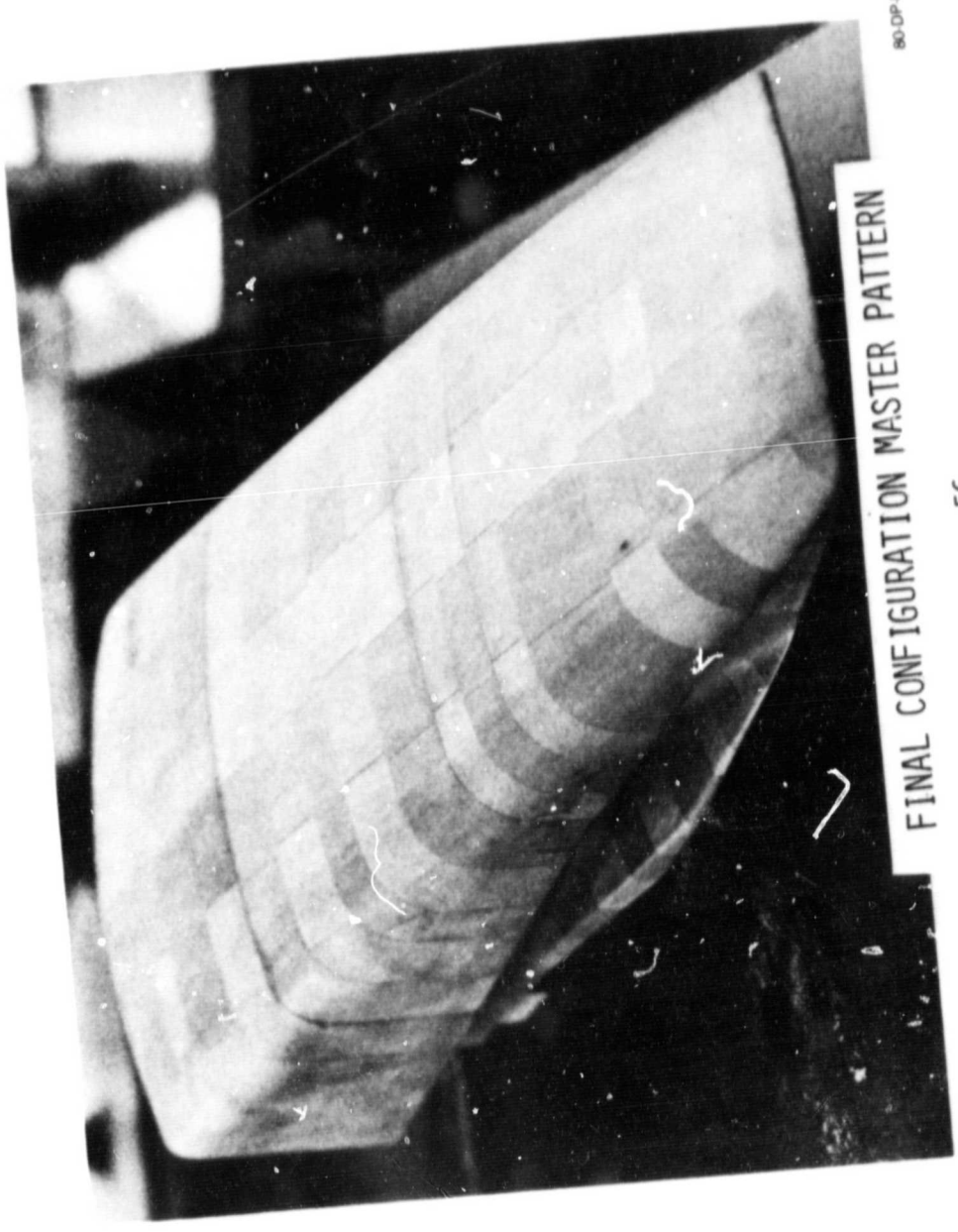

Figure 56

ASSEMBLED TOOL

Figure 57

TOOL DISASSEMBLED

Figure 58

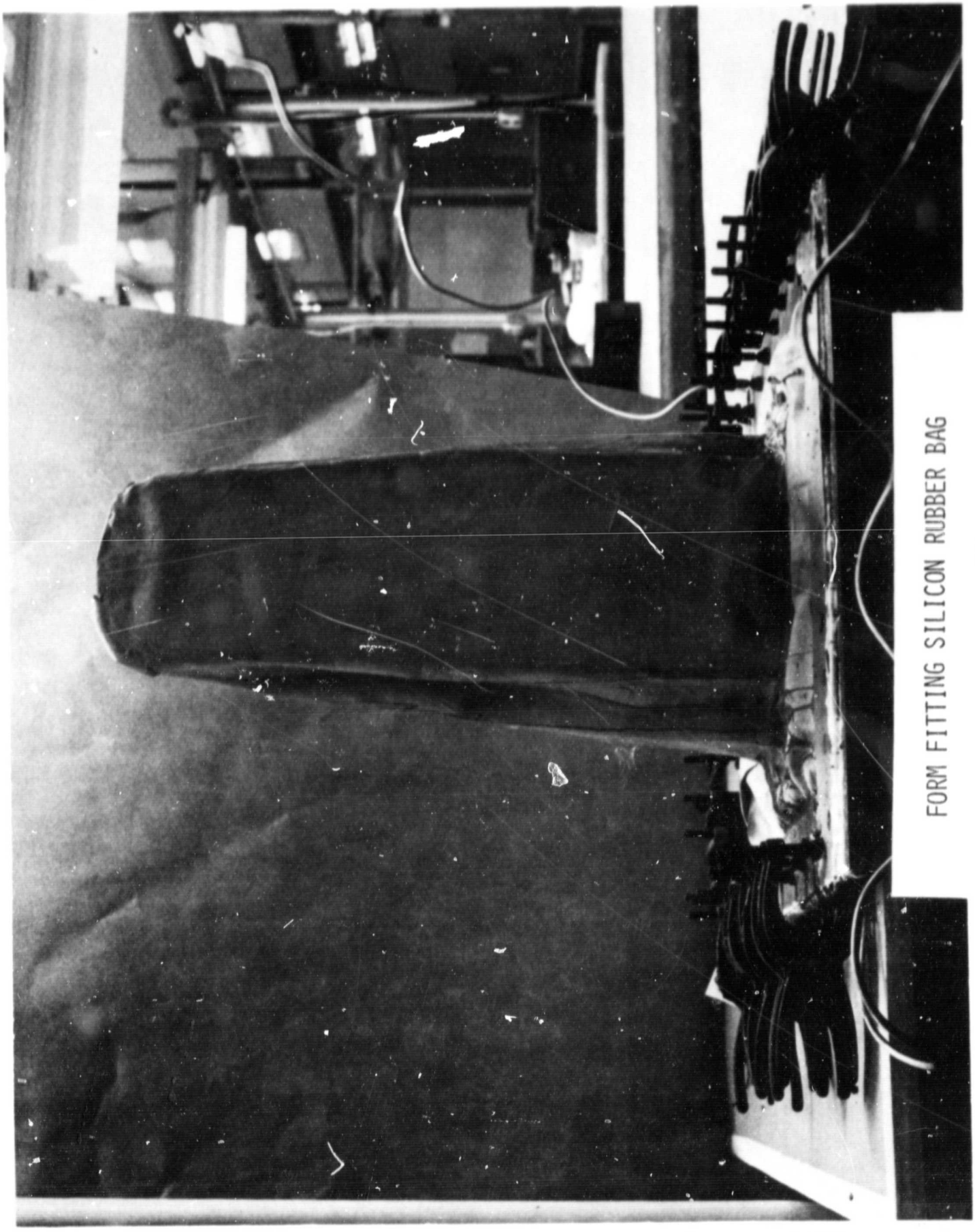

FORM FITTING SILICON RUBBER BAG

Figure 60

COMPACTED LAYUP
Figure 62

 93+94

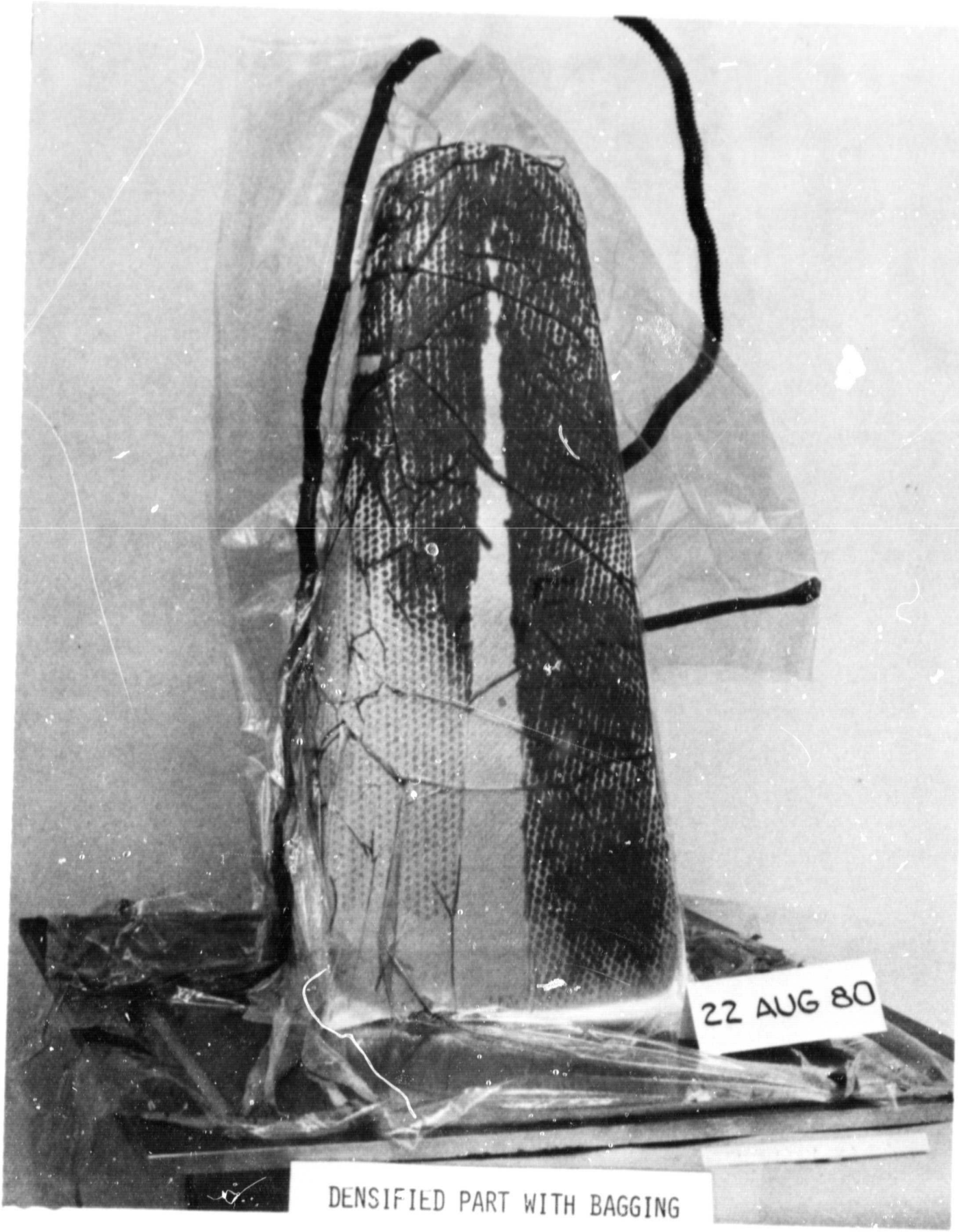

DENSIFIED PART WITH BAGGING

Figure 64

DENSIFIED FAIRING

Figure 65

 9-7-98

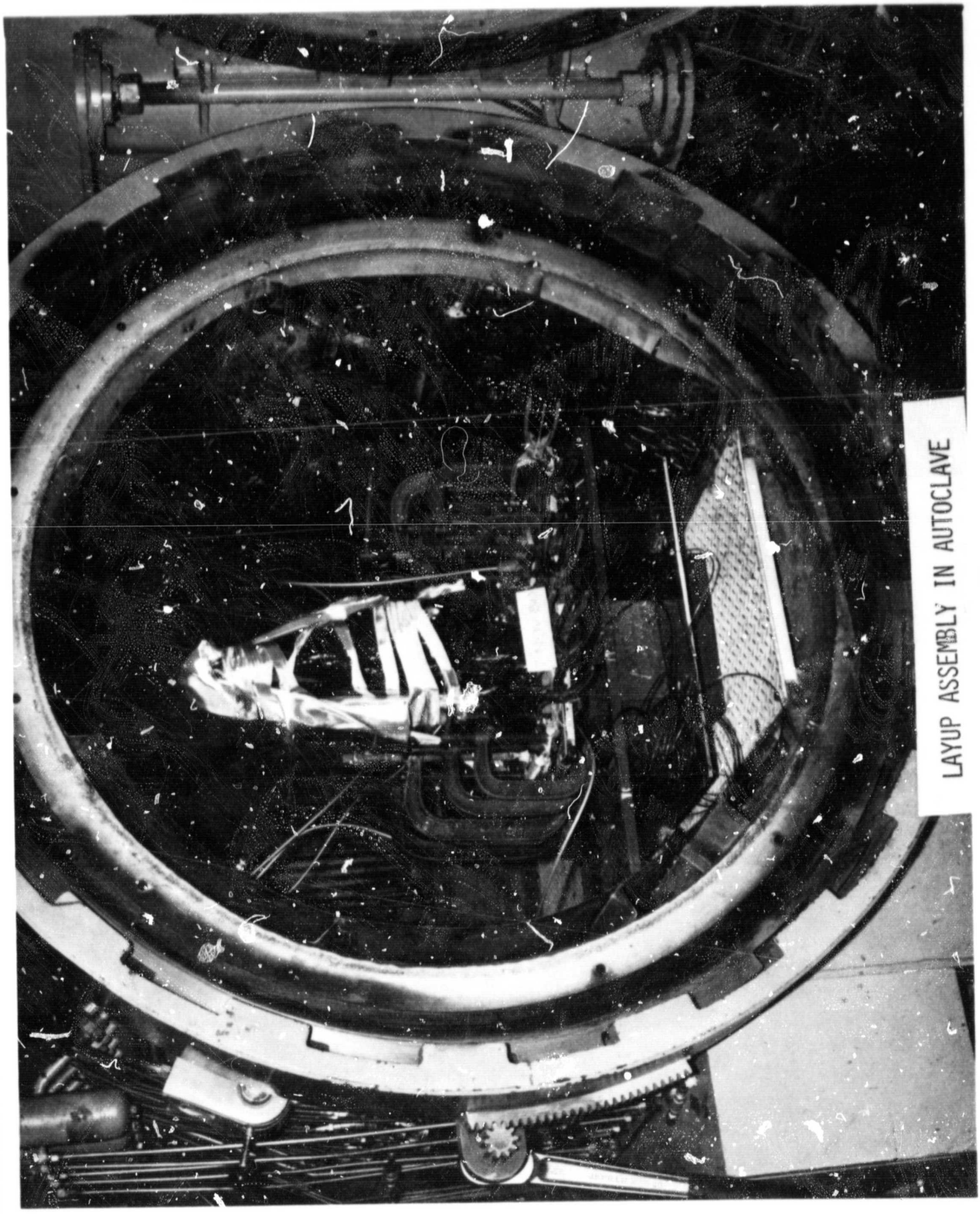

LAYUP ASSEMBLY IN AUTOCLAVE

Figure 68

CURED ASSEMBLY WITH BAGGING

Figure 69

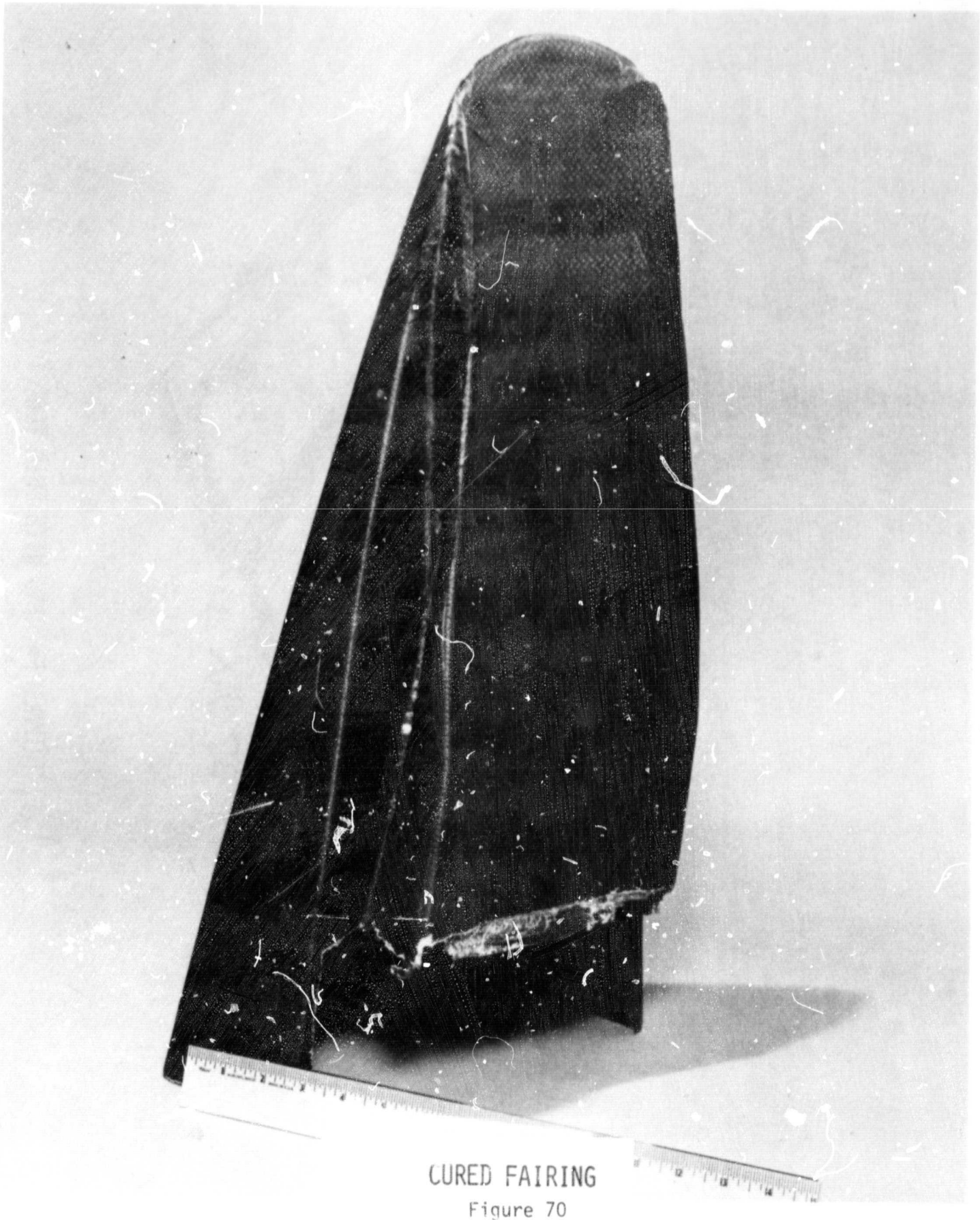

CURED FAIRING

Figure 70

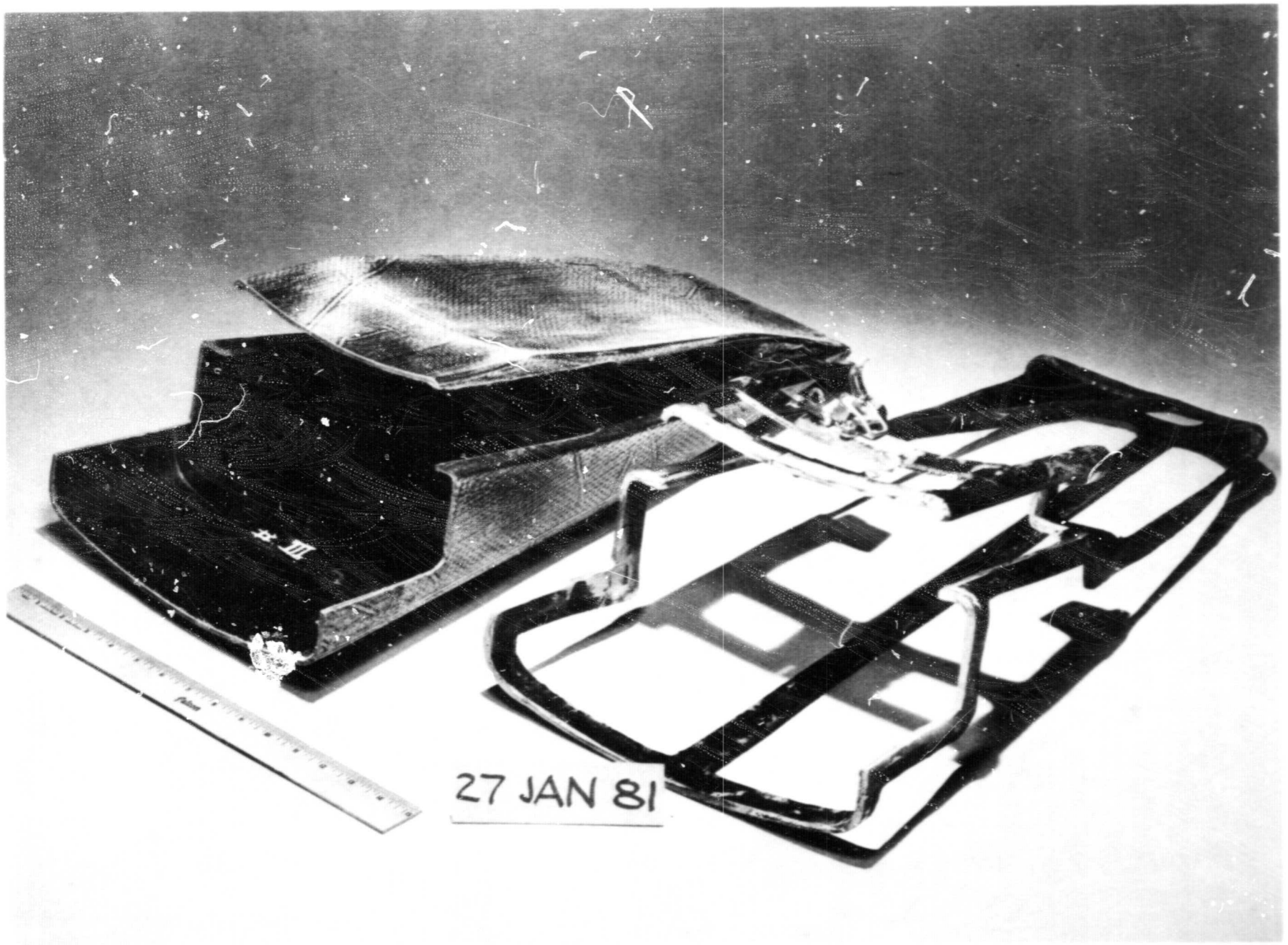

TRIMMED FAIRING WITH TRIM TOOL

Figure 71

Figure 72

4.6 Installation

Proper installation was established by fit checking a set of fairings on a reverser. This was done on the production line at Rohr Industries. Initial checking showed that the trim lines had to be changed to avoid mechanical interference. The fairings were re-trimmed and again fit checked on a reverser at Rohr Industries. The fit check showed that the fairings were satisfactory for installation on a DC-9 reverser. The composite fairing is shown on the right side in Figure 73 during the fit check. The aerodynamic improvement minimizing base area is evident.

A service change drawing was made for installation of the fairings on a reverser. Figure 74 shows the overall installation. Figure 75 shows a side view section of the service change drawing. Figure 76 shows a vertical section view.

Existing mechanical fastener locations are used on the freestream flow side. A metal bracket is used to attach the exhaust flow side because the improved fairing stands off from the stang surface.

The fitted fairings were primed and then painted with a polyurethane paint. The polyurethane finish will withstand flash heating to 561°K (550°F). A finished fairing compared to a production baseline fairing is shown in Figure 77.

The fairings are to be installed on a Texas International DC-9. The in-service evaluation of the fairings will be conducted on a follow-on effort outside of this contract.

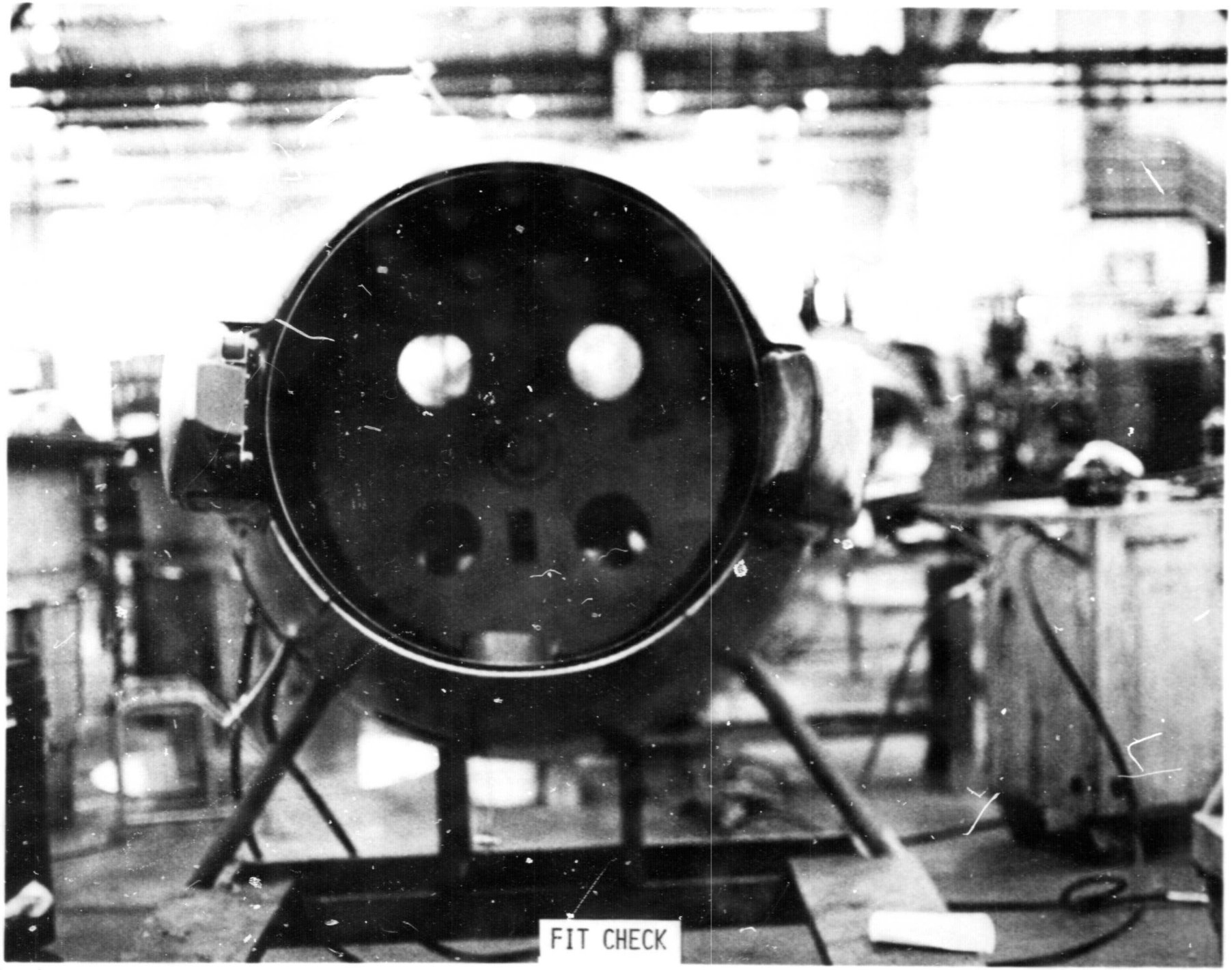

Figure 73

ORIGINAL PAGE IS
OF POOR QUALITY

INSTALLATION DRAWING

Figure 74

ORIGINAL PAGE IS
OF POOR QUALITY

NOTE: Dimensions are in inches

INSTALLATION HORIZONTAL VIEW

Figure 75

ORIGINAL PAGE IS
OF POOR QUALITY

NOTE: Dimensions are in inches

INSTALLATION VERTICAL VIEW

Figure 76

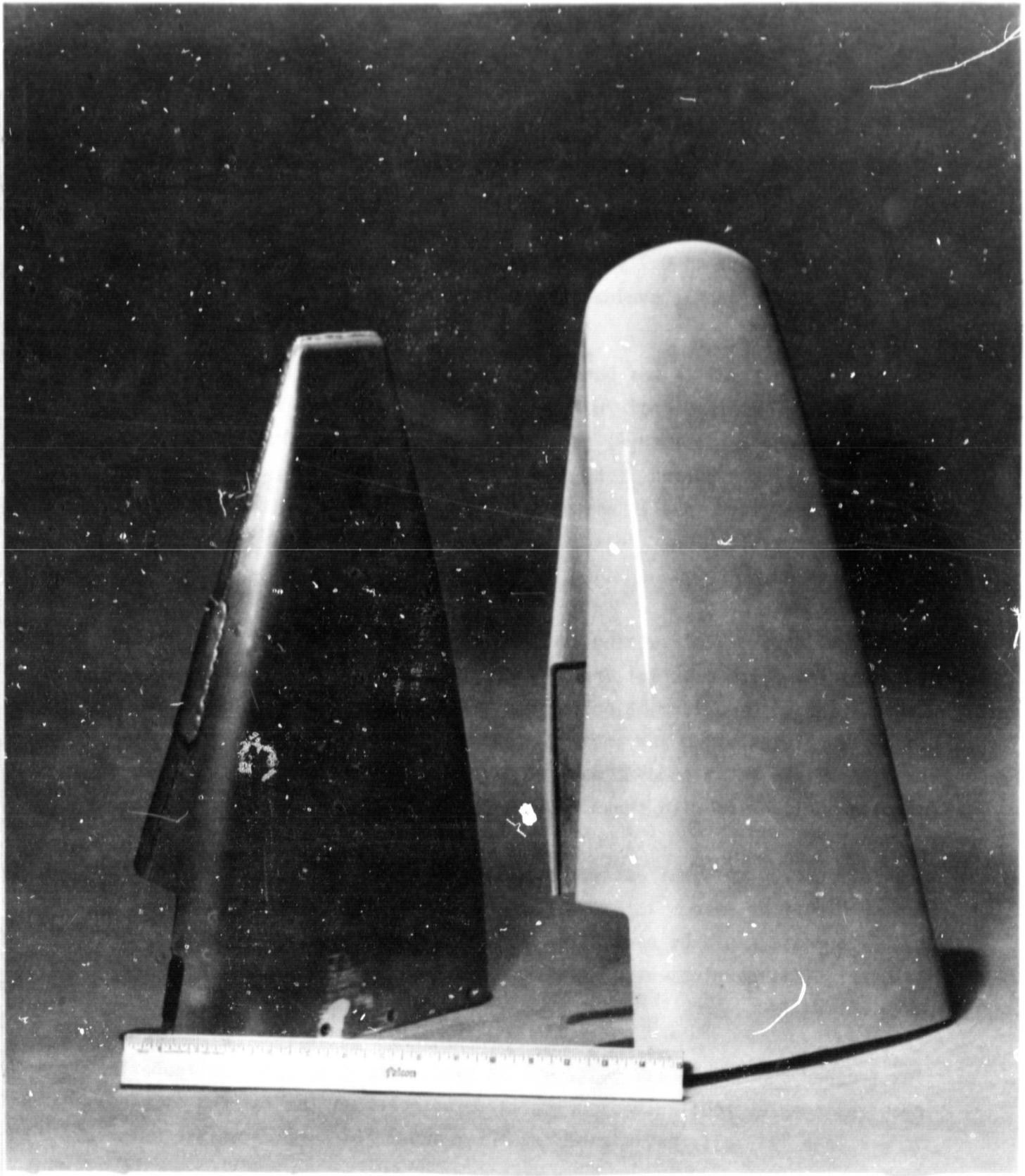

FINISHED FAIRING

Figure 77

SECTION 5

ECONOMIC ASSESSMENT

The original economic assessment that was conducted, is reported in Reference 3. In that evaluation, as shown in Figure 78, a 1/2% reduction in airplane drag was predicted for the initial modification. This resulted in a payback period of 0.7 years. Since then, a number of considerations that effect an economic evaluation have changed.

The economic evaluation was based on a domestic fuel price of 35 cents per gallon and an international fuel price of 45 centers per gallon. Since fuel is currently close to $1 per gallon, the difference in price will reduce the payback period. The aerodynamic development program conducted here, also resulted in a 1% airplane drag reduction as to the 1/2% used in the economic evaluation. This improved performance further shortens the payback period.

There are, however, offsetting factors. A continuing high rate of inflation has increased material and fabrication costs. Higher fuel prices, in conjunction with government noise regulations, has stimulated development of new airplanes using new engines which in turn reduces the amortization base for fixed costs on JT8D powered airplanes since the projected new airplane deliveries with these engines has been reduced.

The fabrication cost was estimated for the initial modification which was a simple part to make. It was believed at that time that the trapped rubber process could be used allowing inexpensive tooling with curing in an over. This development program has shown that these initial premises were not valid.

The trapped rubber process could not be used. The developed configuration requires complex tooling and curing in an autoclave. The fairing is also larger than initially envisioned requiring about 70% more composite material.

FROM REFERENCE 3

DC-9 NACELLE DRAG REDUCTION
ENGINE DATA
Per Engine

Performance	TSFC Reduction, %	EGT Reduction, °C
Takeoff	0	0
Climb	0.5	0
Cruise, Avg.	0.5	
Hold	0.5	
Weight Change, Kg (lb)	Neg.	
Price Change, $	1350	
Kit Price, $	1350*	
Maintenance Cost Change, $/Oper. Hr.		
Materials	0	
Labor @ $30 Per Man-Hr.		

* Subsequent check indicated that the kit price is higher than the nacelle price change.

DC-9 NACELLE DRAG REDUCTION
AIRLINE COSTS
Per Aircraft

Airplane Model	DC9-50	
Operating Cost Changes, $/Year		
Fuel	-4880	
Maintenance	0	
Block Speed Effect	- 210	
Total	-5090	
Type of Investment	New Buy	Retrofit
Required Airline Investment Changes, $		
Installed Stangs	2700	2700
Spare Engines	0	0
Spare Parts	700	700
Total	3400	3400
Payback Period, Years	0.7	0.7
DOC Change, %	-0.1	

TABLE 5-23
DC-9 NACELLE DRAG REDUCTION
FUEL SAVINGS

Fleet Fuel Saved, %	0.5			
Start of Service Date	1-79			
Investment Type		New Buy	Retrofit	Total
No. of Engines Affected		399	1165	1564
Cum. Fuel Saved, 10^6 Liters (Gal.)		117 (31)	204(54)	322(85)

PREVIOUS ECONOMIC ASSESSMENT

Figure 78

Compared to the economic assessment of Reference 3, higher fuel prices and a greater drag improvement reduce the payback period. Offsetting this are higher fairing costs due to inflation, a more complex shape, larger part size, the need for curing in an autoclave, and a reduced amortization base. Consequently, a re-evaluation is being conducted as a follow-on effort outside of this program activity to determine the most cost effective application of the performance improvement by evaluating alternative construction techniques.

C-2

SECTION 6

CONCLUSION

The reverser stang fairing program has been conducted up to the point a production decision can be made. An assessment on whether to introduce the reduced drag fairing into production is currently under way. A number of factors have changed since the original evaluation. The economic evaluation was based on domestic fuel at 35 cents per gallon and international fuel at 45 cents per gallon. The considerably higher fuel costs that have occured since then has made performance improvement more important. Consequently, when the original modification was found to be deficient, and the configuration development effort resulted in being able to reduce fuel consumption 1% rather than the original goal of 1/2%, this configuration was selected for composite development.

The initial modification envisioned was also a simple part to make and it was believed at that time that the trapped rubber process with simple, inexpensive tooling could be used. This development program has shown that these initial premises were not valid. The trapped rubber process could not be used and with the development of an aerodynamic shape that has a performance improvement twice the original goal, complex tooling is needed.

The current production application evaluation must therefore account for these differences and the impact of higher fuel costs on projected JT8D powered DC-9 deliveries. The more complex manufacturing and tooling results in a higher cost for composite fabrication while the projected amortization base for JT8D powered DC-9's has decreased. Consequently, the economics of the weight savings from composites has changed compared to the assessment made at the start of this program. The use of the reduced drag fairing is therefore being evaluated using alternative constructions to reduce tooling and fabrication costs.

6.1 Accomplishment of Goals

The original goal was to achieve a 1/2% reduction in total airplane drag. A 1% reduction has been achieved.

Using Kevlar-49/PMR-15 advanced composites, a weight savings of 40% has been accomplished relative to an aerodynamically similar part made from metal.

Production planning activities are currently underway.

Technical achievements accomplished as a part of this activity are summarized below:

Reverser Stang Fairing Environment

The temperature and dynamic pressure environment on the thrust reverser stang fairing of target reversers on low bypass ratio engines was determined. Noise levels of 165 db were found to occur. Maximum temperatures of about 530°K on the outer periphery of the trailing edge of the fairing during reverse thrust were found to occur.

Drag Reduction

The aerodynamic configuration to reduce drag on JT8D powered DC-9 engine installation nacelles by 1%, compared to the production baseline reference, has been accomplished.

Mechanical Properties of Kevlar-49/PMR-15

The mechanical properties for Kevlar-49/PMR-15 using a 561°K cure cycle have been determined and are presented in the Appendix. These data have been developed for temperatures from 219°K to 505°K for dry specimens and specimens subject to long term exposure to moisture and moisture/Skydrol.

Molding Complex Shapes

This program has demonstrated that complex shapes can be made using Kevlar-49/PMR-15 advanced composite material system. Parts can be made using an autoclave cure cycle with a retractable male mold.

Molding Simple Shapes

The feasibility of using zinc spray tooling for molding simple shapes using an autoclave cure cycle at 550°F was established. The tooling for a female mold can be readily made by using zinc spray over a plaster or wood pattern.

SECTION 7

PRODUCT ASSURANCE

The Product Assurance Program applied to Task I of this contract is as defined in detail in the plan ACEE-18-PL-8511B dated 11 September 1978 and submitted in response to data requirements of Article XXI of the Contract Schedule and Exhibit B. These procedures are essentially the same as used on the DC-9, DC-10, and KC-10 production programs. The Product Assurance Program is in compliance with applicable requirements of Parts 21 and 37 of the Federal Aviation Regulations, with interfacing requirements of MIL-Q-9858A and MIL-C-45662A, and with the requirements of NASA Lewis Research Center.

Documentation

Operating procedures included in quality manuals and functional standards and guides, have provided direction for quality continuity from development and material property testing through manufacturing research and procurement.

Objective evidence shown on Fabricated Outlines (FOs) are on file, verifying material property testing results. Verifications were made by Douglas engineers, quality assurance inspectors, and by FAA representatives.

Verifications of quality assurance control were recorded on the work instructions (FOs) issued to provide testing sequence and a record of in-process inspections and tests. Quality Assurance stamps were utilized on the foregoing documentations to substantiate the verification. The issuance and control of Quality stamps is a responsibility of the Quality Assurance organization.

Design Engineering provided surveillance during initial flight evaluation. The occurrence of any failures were to be reported in accordance with contractual requirements.

Process Control

The materials property testing and the development of fabrication processes by the Materials and Process Engineering Laboratory were accomplished under the surveillance of Quality Assurance. The maintenance of detailed records by Lab personnel enabled Materials and Process Engineering to draft a Douglas Material Specification (DMS) and a Douglas Process Standard (DPS) which can be finalized as inspection standards for a production release.

Supplier Control

Materials used for Task I were identified by Receiving Inspection and submitted to the M&PE labs for materials property testing. Suppliers were ascertained to have adequate inspection systems. Quality Assurance Planning verified that purchase orders referenced applicable technical and quality assurance requirements.

Drawing Change Control

Although a baseline configuration was not established, Design Engineering maintained control of all drawing releases. Quality Assurance verified that planning shop work instructions conformed to the proper engineering drawings.

Inspection and Tests

Inspection and tests were conducted in accordance with applicable specifications and quality requirements. Quality Assurance personnel conducted surveillance of engineering development and tests, and witnessed all materials property testing.

Equipment utilized for controlled material storage and testing is a part of the Quality Assurance Equipment Recall Data System (ERDS). The calibration and recertification of this equipment at prescribed intervals is controlled by a computerized system. All instrumentation utilized was serialized and calibrated in accordance with MIL-C-45662, which requires that reference standards be certified as being traceable to the National Bureau of Standards.

Non-Conforming Articles - Material Review

This program did not progress beyond the research and development of a manufacturing process utilizing Kevlar-49/PMR-15 composite material in the manufacture of DC-9 stang fairings. As a result, only engineering samples were produced and Review Board action was not required.

Equipment Log

Materials and Process Engineering Laboratory records for varying cure cycles and procedures were recorded and Quality Assurance verified recorded results of speciment testing.

In a production mode, each fairing would have been serially numbered and identified to a Fabrication Order which in turn would be identified to the applicable drawing number and change letter.

Reliability Considerations

The stang fairing is an aerodynamic enclosure that is secondary structure. Failure of the fairing would not affect flight safety. The primary reliability consideration was therefore long life without the need for any maintenance or repair. The baseline production fairings were experiencing cracking that was attributed to sonic fatigue because of the high noise environment that exists in the proximity of the engine exhaust flows. The fiberous nature of composites precludes stress concentrations developing at defects from which crack propagation results. The use of Kevlar fibers was therefore considered to offer improved service life from improved sonic fatigue resistance. Kevlar also exhibits superior impact resistance compared to graphite and this characteristic was considered to be an advantage in the selection of an advanced composite material.

The stang fairing is the aft closure for the thrust reverser hydraulic actuator housing and hence is subject to exposure to aircraft hydraulic fluid from leaks and seapage, and moisture due to weather. Available data on Kevlar indicated that the effects of these fluids on Kevlar would be nominal. Since

data was not available for the Kevlar/PMR-15 material systems, the environmental effects on mechanical properties were determined as a part of this program. The effects of Skydrol (aircraft hydraulic fluid) and moisture were confirmed to be nominal.

Kevlar is known to deteriorate from exposure to ultra violet light. The reverser stang fairing will, however, be painted to match the aluminum finish of the nacelle aft section. This precludes surface deterioration, which even if it occured, is not considered to be significant because the advanced composite fairing has a large strength margin.

Maintainability Considerations

Except for repainting due to weathering of the paint, the stang fairings are not expected to require any maintenance. Surface preparation for painting was determined to be readily accomplished. Although surface abrasion should be avoided when epoxy is used as the matrix material with Kevlar advanced composites because a fuzzy surface results, Kevlar composites using PMR-15 as the matrix does not exhibit this characteristic. It is believed that the 561°K (550°F) post cure may result in surface oxidation that effects the Kevlar such that a smooth surface results when the surface is lightly sanded.

For access for maintenance of the thrust reverser actuators, the stang fairings can be readily removed and reinstalled. The fairing is attached to the nacelle with mechanical fasteners which use the existing production baseline nut plates. The removal and replacement for access to the thrust reverser actuation system will be the same procedure as for the production baseline.

SECTION 7

REFERENCES

1. D.L. Nored, Planning a New Era in Air Transportation Efficiency - Propulsion. Astronautics and Aeronautics, pp. 47-54, July/August 1978.

2. W.L. Stewart, D.L. Nored, J.S. Grobman, C.E. Feiler, and D.A. Petrash, Preparing Aircraft Propulsion for a New Era in Energy and the Environment. Astronautics and Aeronautics, pp. 18-31, January 1980.

3. W.O. Gaffin and D.E. Webb, JT8D and JT9D Jet Engine Performance Improvement Program - Task 1, Feasibility Analysis, Final Report. NASA CR-159449, April 1979.

4. W.A. Fashing, CF6 Jet Engine Performance Improvement Program - Task 1, Feasibility Analysis. NASA CR-159450, March 1979.

5. T.T. Serafini, P. Delvigs, and G.R. Lightsey, Thermally Stable Polyimide From Solutions of Monomeric Reactants. Journal of Applied Polymeric Science, April 1972.

6. M.P. Hanson, Feasibility of Kevlar-49/PMR-15 Polyimide for High Temperature Applications. NASA Technical Memorandum 81560, prepared for Twelfth National SAMPE Technical Conference, October 1980.

7. P.J. Cavano, Fiber Reinforced PMR Polyimide Composites. NASA CR-135377, June 1978.

8. G.M. Lehman, Advanced Composite Rudder for DC-10 Aircraft. NASA CR-145068, April 1976.

APPENDIX

MECHANICAL PROPERTIES

OF

KEVLAR-49/PMR-15

NOTE:

Pages A-1, 5-9, 33-34, 36-40, 42-46, 48-51, and 53 have been deleted from this document to remove data that is restricted For Early Domestic Dissemination (FEDD).

MATERIAL PROPERTY TESTS

TABLE OF CONTENTS

		PAGE
1.0	INTRODUCTION	A-1
2.0	DESCRIPTION	A-2
3.0	TEST SPECIMENS	A-4
	3.1 FABRICATION	A-4
	3.2 ENVIRONMENTAL CONDITIONING	A-4
4.0	TEST SETUP AND PROCEDURES	A-10
	4.1 STATIC TENSION AND COMPRESSION	A-10
	4.2 FATIGUE	A-19
	4.3 SHEAR BEARING	A-22
	4.4 INPLANE SHEAR	A-25
	4.5 INTERLAMINAR SHEAR	A-28
	4.6 FIBER STRESS	A-29
5.0	MECHANICAL PROPERTIES	A-32
	5.1 TENSILE AND COMPRESSIVE PROPERTIES OF LONGITUDINAL LAYUP	A-32
	5.2 TENSILE AND COMPRESSIVE PROPERTIES OF ISOTROPIC LAYUP	A-35
	5.3 FATIGUE LIFE	A-47
	5.4 SHEAR BEARING STRENGTH	A-47
	5.5 TRANSVERSE SHEAR STRENGTH	A-47
	5.6 INTERLAMINAR SHEAR STRENGTH	A-47
	5.7 FIBER STRESS	A-52
6.0	REFERENCES	A-54

2.0 DESCRIPTION

Tests were conducted to obtain material properties data shown in Table 1.

Seven different tests were conducted:

1. Tensile and Compressive Properties Tests
2. Effects of Environmental Conditioning
3. Fatigue
4. Shear Bearing Strength
5. Inplane Shear Strength
6. Interlaminar Shear Strength
7. Flexural Strength

In general, six specimens were tested except for the short beam shear tests and flexure tests for which twelve specimens were used. Data from improper failures are not presented. For example, during compression tests of environmentally conditioned specimens, improper failure occured which was attributed to misalignment of the specimen in the test fixture introducing a transverse buckling load. These data have been excluded since they are not useful.

All specimens were made in the Material and Process Engineering (M&PE) Composite Laboratory at the Douglas Aircraft Company using material requirements specified in reference 1. All tests were conducted in the M&PE Composite Laboratory except for tests on the isotropic specimen at 505°K, the tests to determine effects of water and water/Skydrol, and the inplane shear tests which were conducted at Delsen Testing Laboratories in Glendale, California. The tests were conducted from late 1979 through early 1981, as a part of developing a Kevlar-49/PMR-15 reverser stang fairing for the DC-9 airplane.

TABLE 1

MATERIAL PROPERTY TEST MATRIX

TEST CONDITIONS													
		DRY			WATER			WATER/SKYDROL					
FIBER LAYUP	TEST PURPOSE	219°K	R.T.	394°K	505°K	219°K	R.T.	394°K	505°K	219°K	R.T.	394°K	505°K
Longitudinal	Strength												
	Tension	X	X	X	X	X	X	X	X	X	X	X	X
	Compression	X	X	X	Y	X	X	X	X	X	X	X	X
Isotropic	Environmental Effects												
	Tension	X	X	X	X	X	X	X	X	X	X	X	X
	Compression	X	X	X	X	X	X	X	X	X	X	X	X
	Fatigue		X				X				X		
	Shear Bearing Strength	X	X	X	X	X	X	X	X	X	X	X	X
Longitudinal	Shear	X	X	X	X	X	X	X	X	X	X	X	X
	Interlaminar Shear Strength		X				X				X		
	Fiber Stress		X				X				X		

3.0 TEST SPECIMENS

Test specimens were fabricated to suit the needs of the tests. They were fabricated from flat panels from two lots of prepreg using two different cure operations except for the environmental effects tests to determine relative strength which were from the same lot and cure cycle. The test specimens were initially used on sandwich beams for tension and compression strength tests, but the method of testing was changed and coupons used later because of bond delamination of sandwich beams conditioned by high humidity.

3.1 Fabrication

The test specimens were cut from flat panels that were made from a flat layup. The procedure is shown on Figure 1. The layup is shown schematically in Figures 2-4. The cure cycle used is shown in Figure 5.

3.2 Environmental Conditioning

The specimens conditioned for moisture tests were placed in a humidity chamber at 95 percent humidity and 333° K temperature for 30 days. Six control specimens were subjected to the same conditions.

Specimens conditioned in a Skydrol and water vapor environment were soaked in Skydrol at 333°K for a period of seven days and then placed in the humidity chamber at 95 percent humidity and 333°K for 30 days. Control coupons were used to monitor the absorption of Skydrol and water vapor. The control specimens were identical to those used in the water vapor conditioning process.

4.0 TEST SETUP AND PROCEDURES

4.1 Static Tension and Compression

Static tension and compression strength and initial tangent modulus were determined by conducting tests applying loads to beams and coupons. Tests were conducted initially with sandwich beams. The use of beams was developed as a means of achieving a uniform transverse stress in a fiberous advanced composite. This approach had been used with graphite/epoxy subjected to environmental conditioning by moisture and by Skydrol. With beams made with Kevlar-49/PMR-15, the beams debonded after moisture conditioning. The same adhesive previously used with graphite/epoxy was found to be unsuitable after moisture conditioning of the Kevlar-49/PMR-15. Specimen testing was then changed to use of coupons.

Sandwich Beams

Tension and compression sandwich beam tests were conducted according to the methods described in Reference 2. The construction of a test beam is shown in Figure 6. The beam specimen is comprised of an aluminum honeycomb core sandwich between two facings. One facing is a sheet 0.406 cm 4130 steel bonded to the honeycomb. This facing is designed to support the test load without failing. The composite facing tested is bonded to the opposite face of the honeycomb core. The basic allowable test beams had facings made using 8 plies with a 0°/90° layup and a 2.54 cm width. The beam test setup is shown in Figure 7. Beams used in environmental effects tests used an isotropic layup of 8 layers at 0°/90°, ±45° and a 3.81 cm width. They were identical to the fatigue test beams shown in Figure 12.

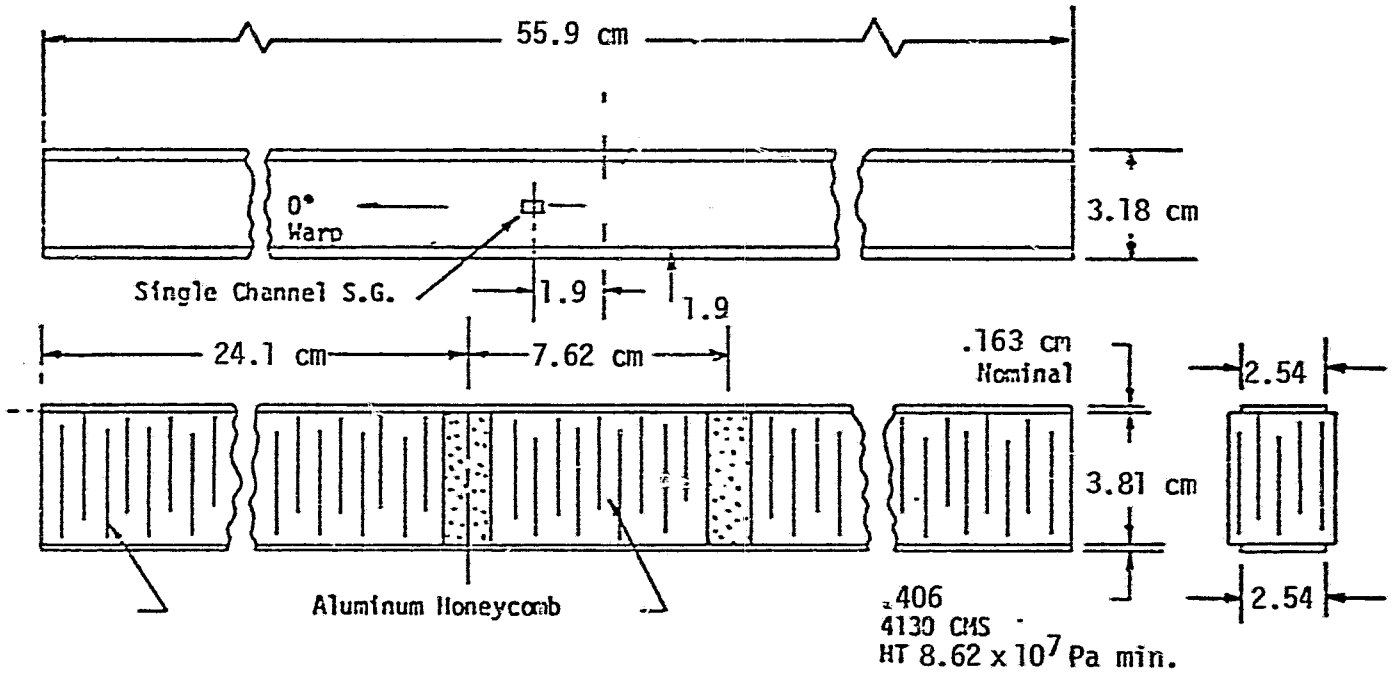

Dimensions in centimeters

SANDWICH BEAM BENDING SPECIMEN

FIGURE 6

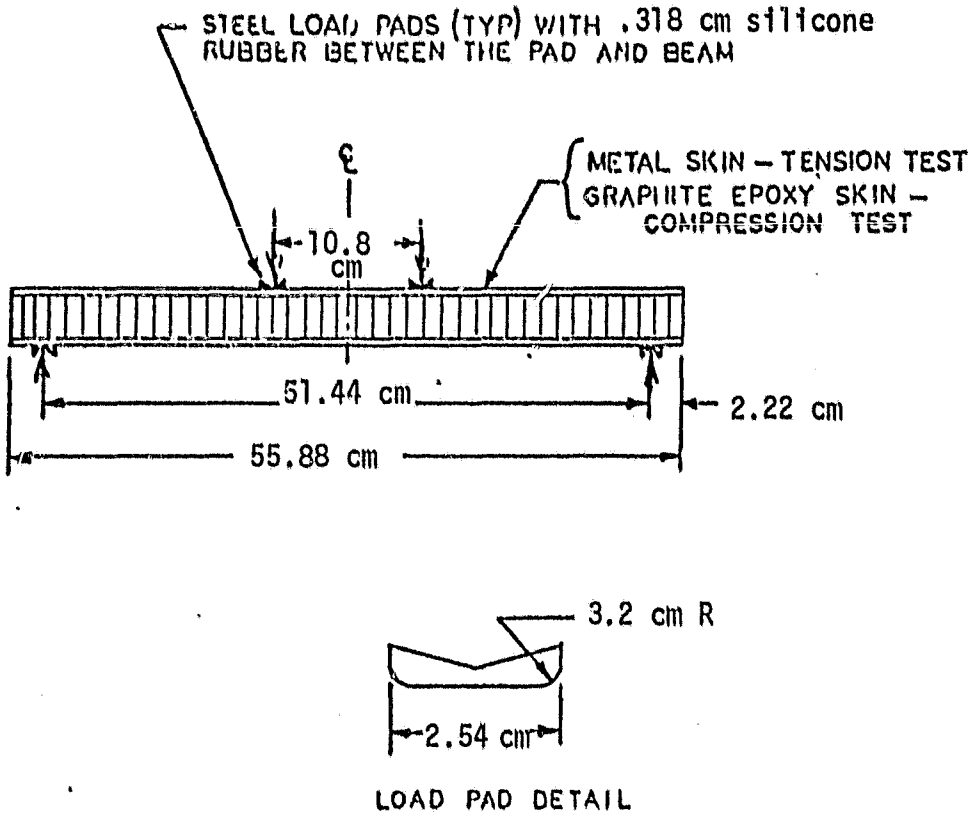

FIGURE 7 - SANDWICH BEAM SPECIMEN TEST SET-UP

Load/strain relationship was measured during the test. The strain was measured by an extensometer except where a measurement of Poisson's ratio is required. In this series of tests, one beam in each category is instrumented with strain gages to determine Poisson's ratio. For a given laminate, ply thickness can vary as much as 12 percent. This thickness variation is primarily a function of resin thickness which has little effect on the longitudinal strength of the laminate. Therefore, all stresses are calculated using the nominal ply thickness.

The stresses were determined by the method of Reference 2 corrected for the lower modulus Kevlar. The beam test was developed for use of high modulus graphite and an empirically determined correction for the lower modulus Kevlar was used. The correction was determined by correlating the apparent stress differences from beam and coupon tests with Kevlar.

Poisson's Ratio $\mu = \frac{E_T}{E_L}$

Where: E_T = Traverse Young's Modulus

E_L = Longitudinal Young's Modulus

Axial Tension

Axial tension coupons are made from flat panels as shown in Figure 8. These coupons were used for determining environmental effects and were made from isotropic layups using 8 layers of 0°/90°, ±45°. Axial tension specimens are mounted in a Universal testing machine as shown in Figure 9 and loaded until the specimen fails. Load-strain relationships were measured during the test by extensometers. Material properties are calculated by the following formulae:

$F_t = P/A$ Where: F_t is the gross tension stress; P is the failing load; A is the gross cross sectional area.

$E_t = \frac{F_t}{E}$ Where: E_t is Young's Modulus of elasticity in tension; F_t is the gross stress; E is the strain of the specimen at the above stress in length per unit length.

Axial Compression

Axial compression coupons were used for determining environmental effects and were made from isotropic layups using 8 layers of 0°/90°, ±45°. Axial compression coupons have fittings attached as shown on Figure 10. Axial compression specimens are mounted in a Universal testing

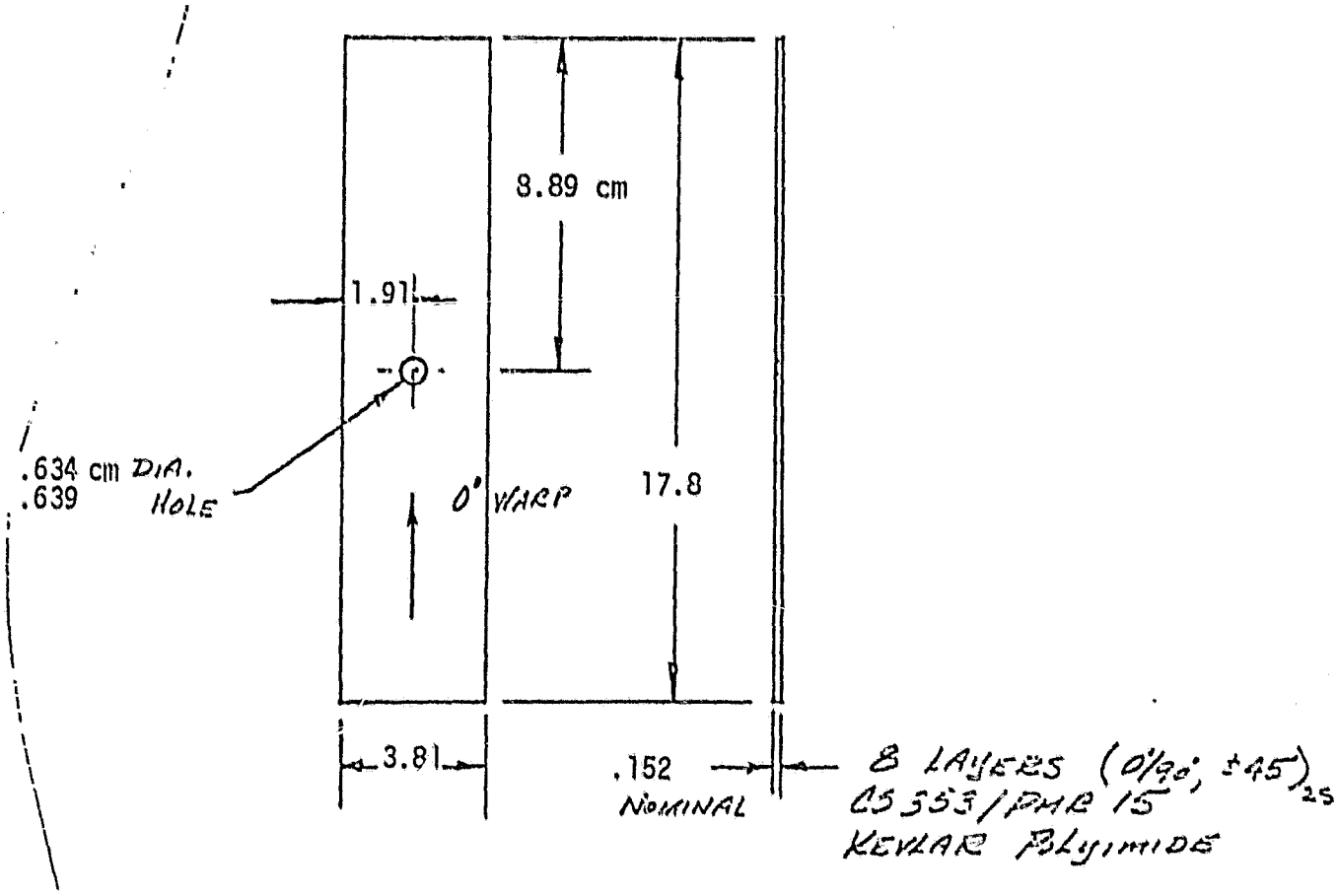

AXIAL TENSION SPECIMEN

FIGURE 8

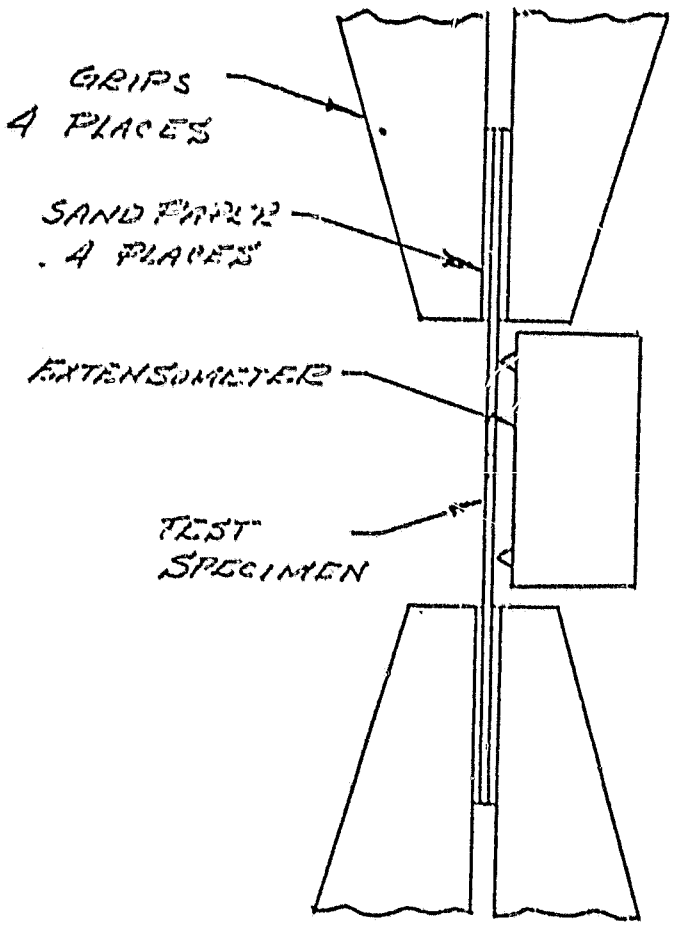

AXIAL TENSION TEST SETUP

FIGURE 9

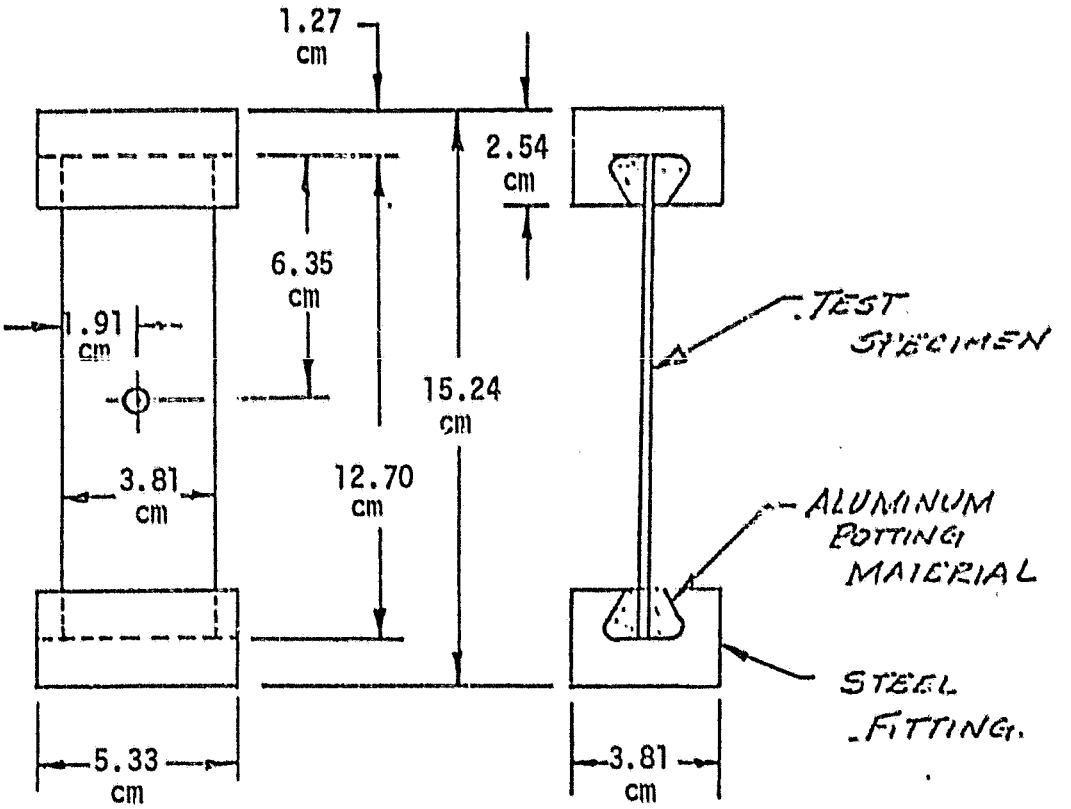

AXIAL COMPRESSION SPECIMEN

FIGURE 10

machine as shown in Figure 11 and loaded until the specimen fails. Load-strain relationship was measured during the test by a compressometer. Material properties are calculated by the following formulae:

$F_c = P/A$ Where:

F_c is the gross compression stress; P is the failing load; A is the gross cross sectional area.

$E_c = F_c/E$ Where:

E_c is Young's Modulus of Elasticity in compression; F_c is the cross compression stress; E is the strain of the specimen at the above stress.

4.2 Fatigue

The fatigue tests were conducted using sandwich beam specimens as shown in Figure 12. The fatigue test beams had an isotropic facing with a 3.81 cm width and a 0.635 cm open hole in the center of the test section. Eight specimens left in a room humidity state, eight specimens conditioned in water vapor, and eight specimens conditioned in a Skydrol and water vapor were tested. All tests were conducted at room temperature with an alternating stress amplitude of $R = \pm 1$. The test setup is shown in Figure 13. Fatigue load levels for test were determined from the failing loads of sandwich beams tested under similar conditions in the environmental effects tests. These loads are chosen to describe the S-N curve

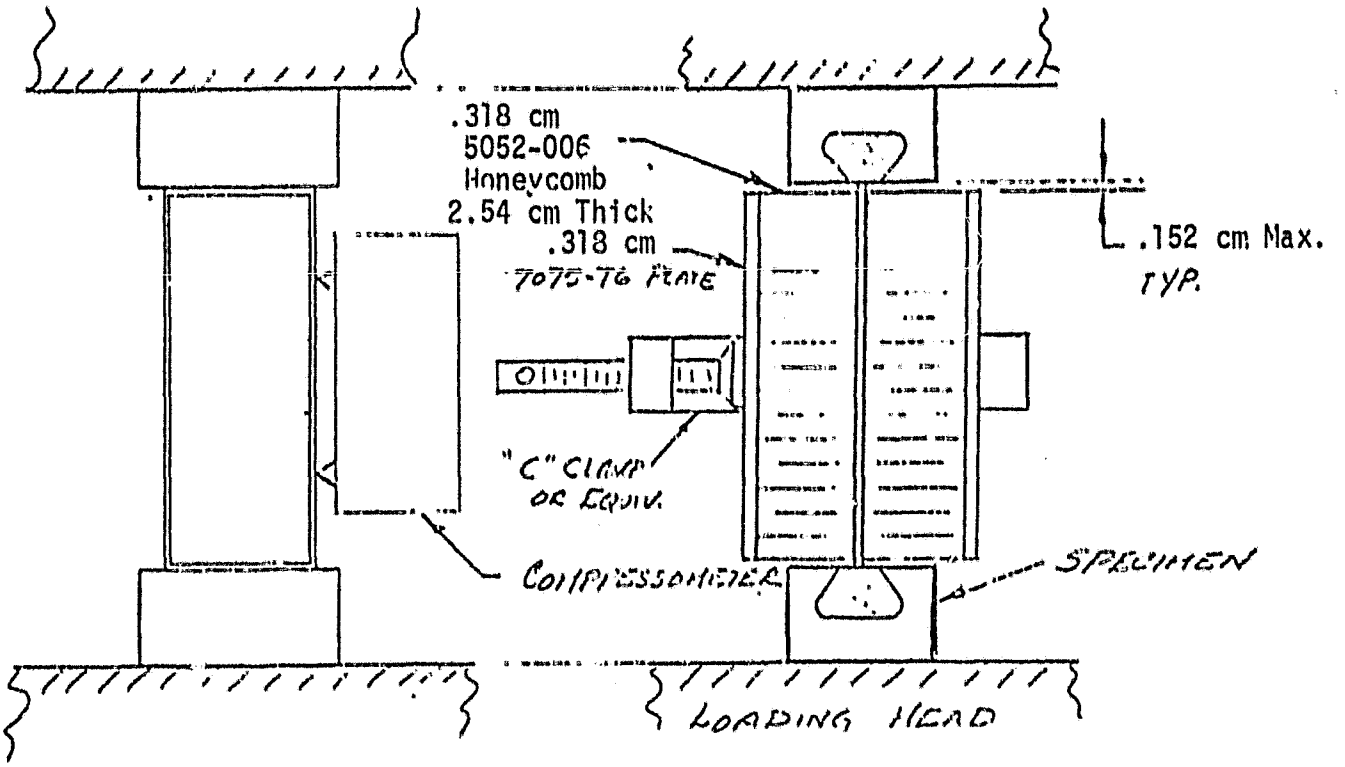

AXIAL COMPRESSION TEST SETUP

FIGURE 11

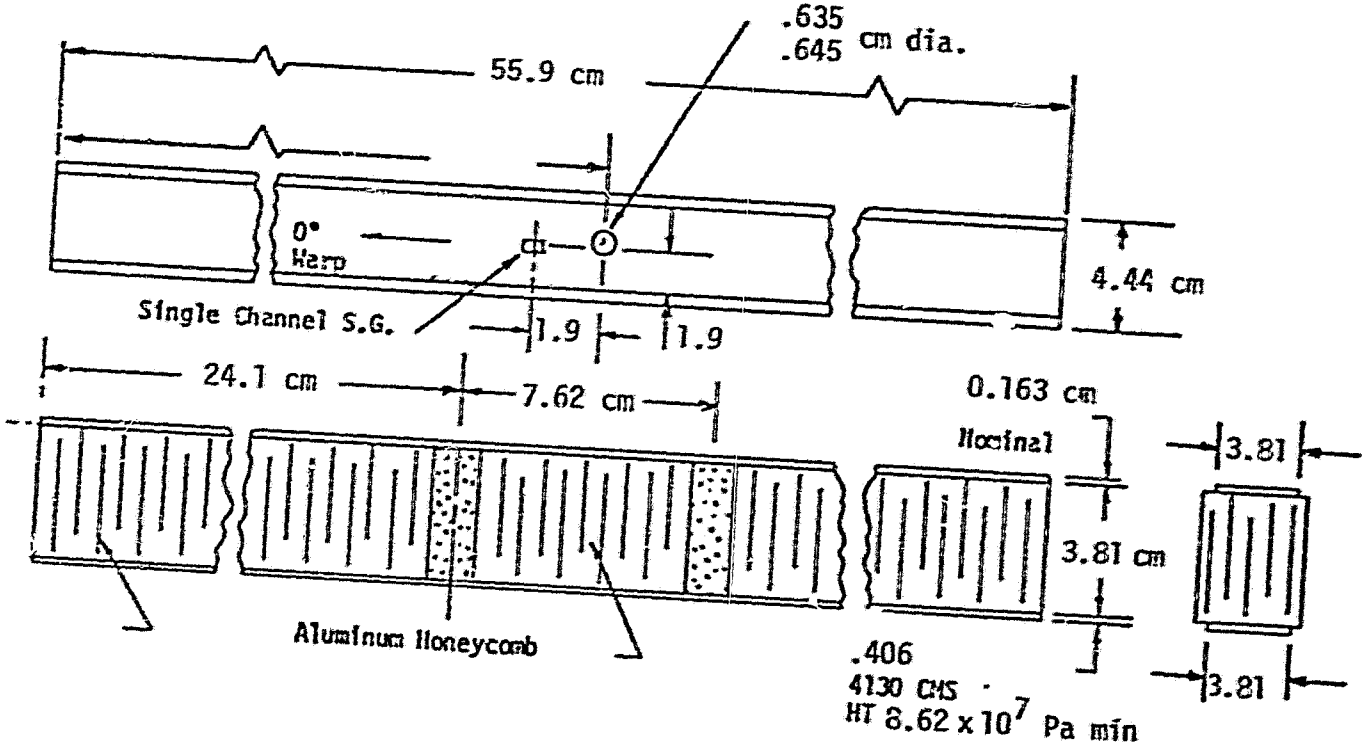

OWG. Z3943314 -501

Dimensions in centimeters

FIGURE 12- SANDWICH BEAM FATIGUE SPECIMEN

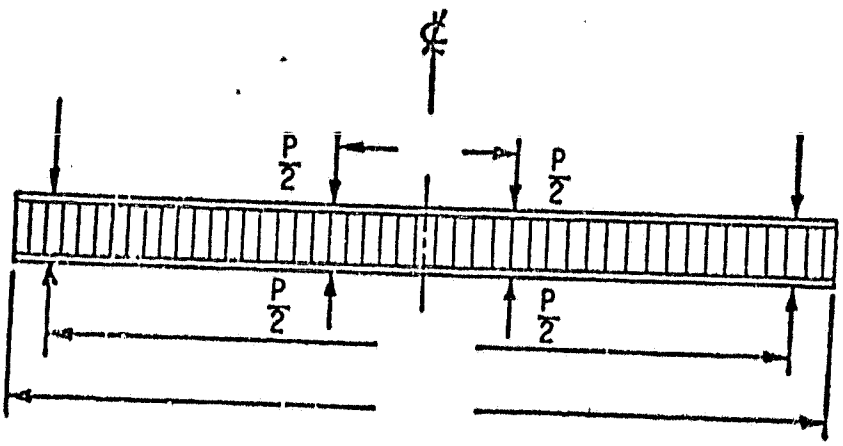

Load to be applied in either direction.

FATIGUE TEST SETUP

FIGURE 13

from approximately 10^3 cycles to the endurance limit. Gross stress can be determined by the methods described on Page 5 of reference 2. Stress is calculated using the nominal ply thickness.

3 Shear Bearing

The shear bearing test specimens are shown on Figure 14. The composite laminate thickness, width, and bolt hole diameter and hole location from the edge of the specimen are measured to the nearest 0.025 mm and recorded prior to testing. They were made from an isotropic laminate (0°/90°, ±45°). The specimens were made so that two tests can be accomplished on each test specimen. The specimens are symmetrical about the center bolt hold. The bolt in this hole reacts to the loads being applied at the test holes. Each test hole is loaded separately. The bearing specimens are mounted in a Universal testing machine as shown on Figure 15. Load is applied to the shear bolts until the laminate starts to yield. The load is recorded when the fibers first start to yield and again when the bolt hole no longer will support an increase in load.

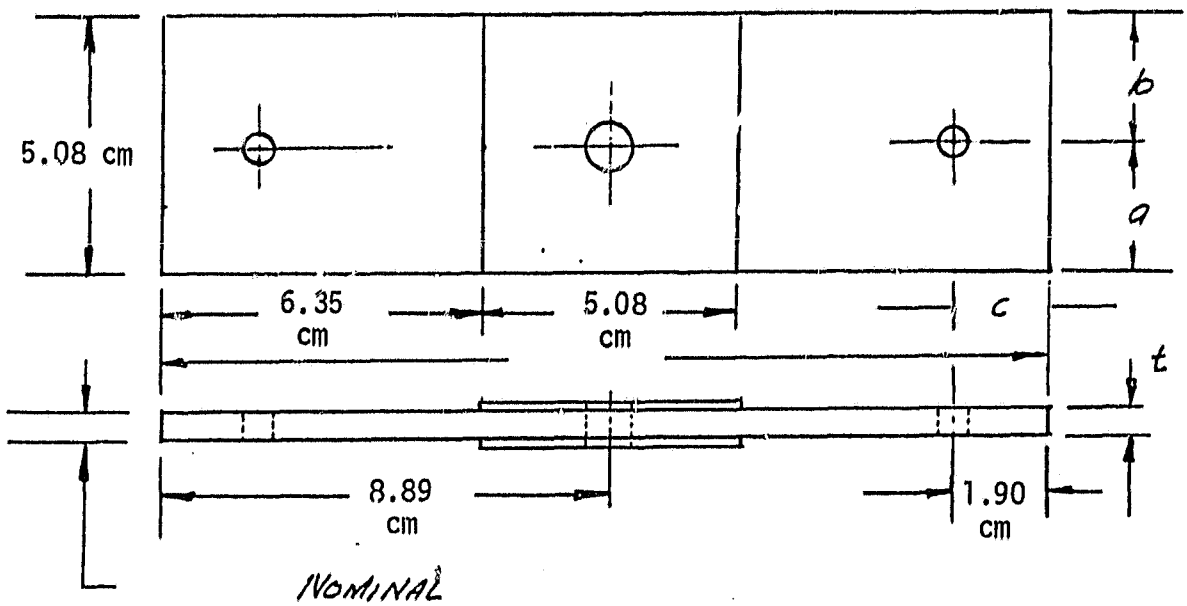

FIGURE 14 - SHEAR BEARING TEST SPECIMEN

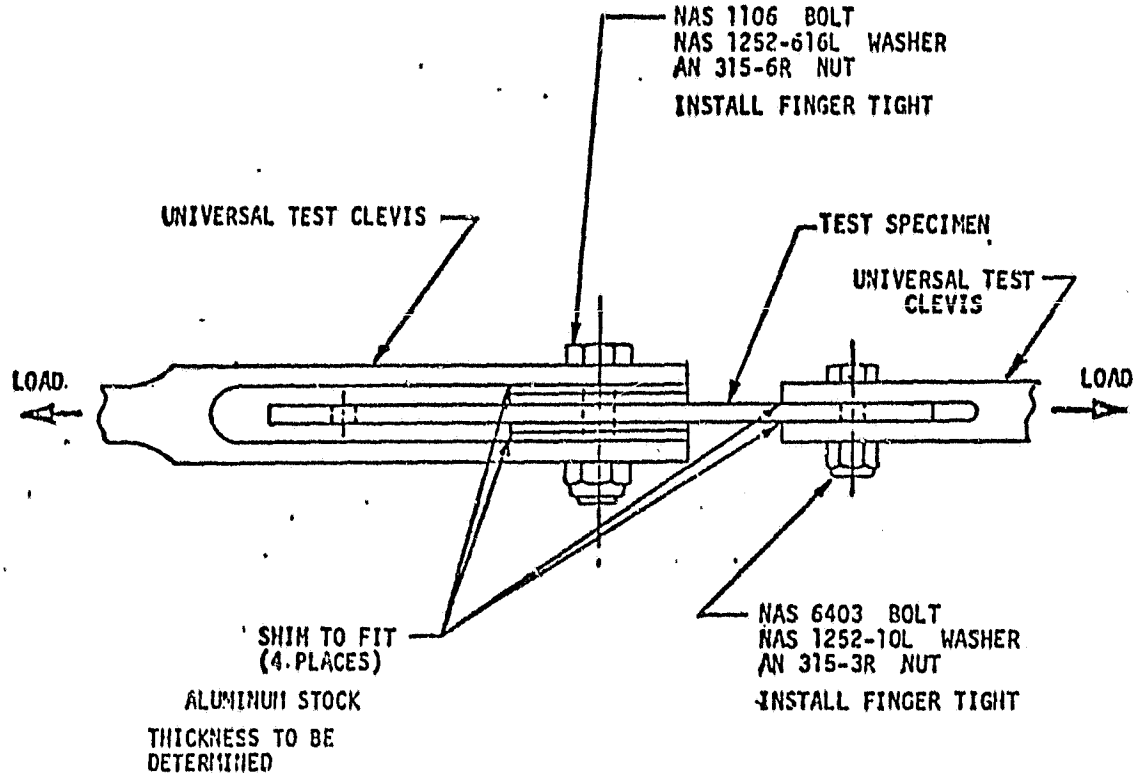

BEARING SPECIMENS MOUNTED IN UNIVERSAL TESTING MACHINE

FIGURE 15

The stress at failure is calculated by:

Actual Stress

$$F_{br} = \frac{P}{Dt}$$

Nominal Stress

$$F_{br} = \frac{P}{Dt_n}$$

Where:

P = Failing Load

D = Bolt Hole Diameter

t = Specimen Thickness

t_n = Specimen Thickness Based on Nominal Ply Thickness

4.4 Inplane Shear

Inplane shear strength was determined by conducting rail shear tests. The specimens with a nominal thickness of 0.152 cm are made up of eight plies of 0°/90° fabric. The specimens are 6.05 cm deep by 7.62 cm wide, and are assembled into test fixtures by bonding four tapered rails onto each surface of the shear specimen. A sketch of the assembled test specimen is shown in Figure 16.

A rosette strain gage is used to measure shear strain. The gage is mounted in the center of the test section with legs 1 and 3 located at 45 degrees to the shear plane. Leg 2 is located 90 degrees to the shear plane.

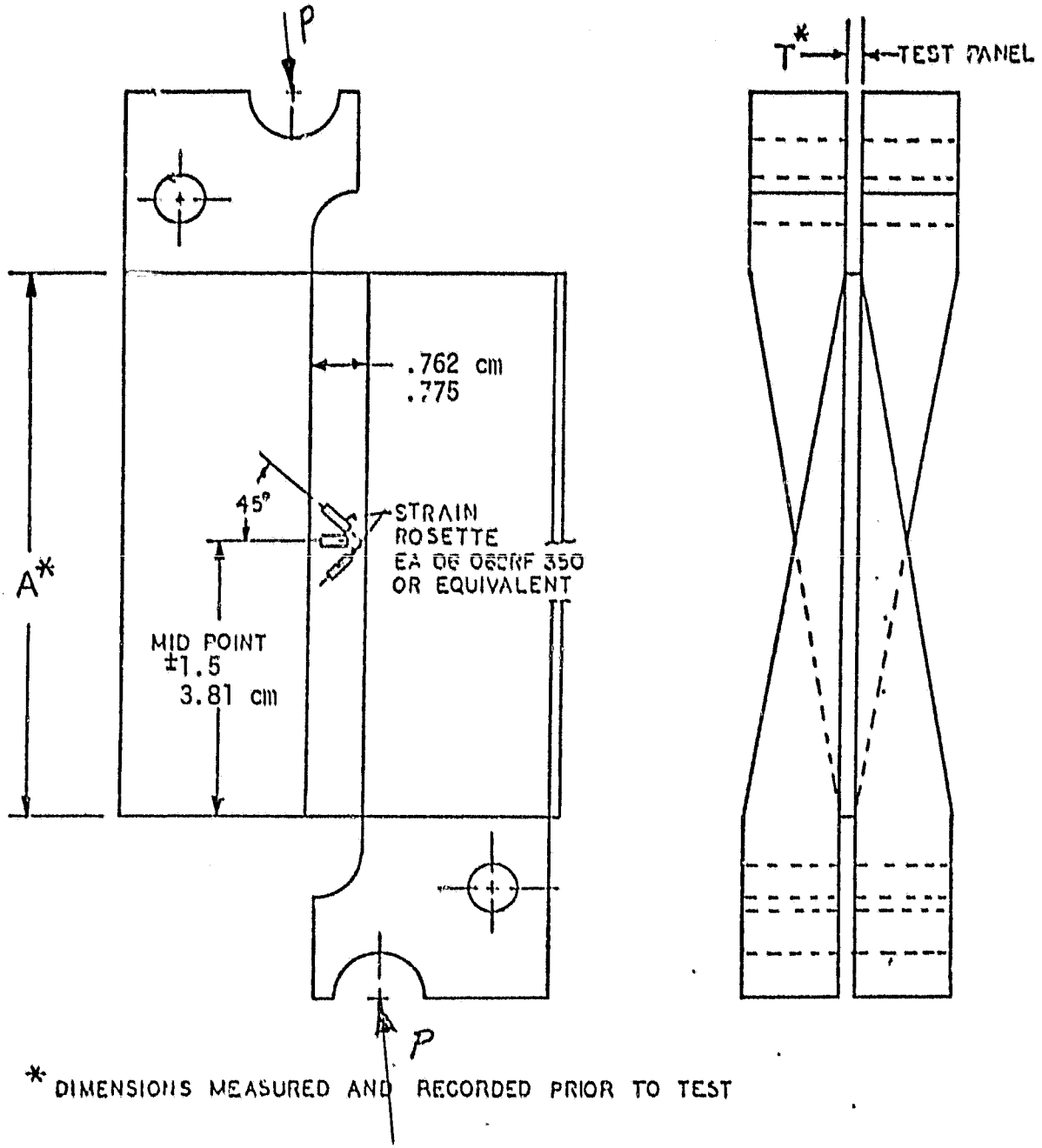

* DIMENSIONS MEASURED AND RECORDED PRIOR TO TEST

FIGURE 16 - RAIL SHEAR TEST SET-UP

Tests were conducted according to methods described in Reference 3. The load is introduced onto the rails through matched loading detents. Load/strain plots are recorded during the test. Load is measured through the standard load cells of the testing machine. Strain is measured by the two strain gages placed at 45 degrees to the load line. Total shear strain is the algebraic sum of the output of the two gages. The third leg, acting as a check on alignment, should read zero. The tests conducted at temperatures other than room temperatures were conducted in a Missimer's chamber.

Stress and strain is calculated as shown below by the methods from page 4 of Reference 2. Stress calculations are adjusted to the design thickness.

Actual Gross Stress (F_s)

$$F_s = \frac{P}{Lt}$$

Where:

P = Failing Load

L = Length of Speciman

t = Thickness of Specimen

Nominal Gross Stress (F_s^n)

$$F_s^n = \frac{P}{t_n L}$$

Where:

t_n = The Specimen Thickness Based on the Nominal Ply Thickness

Shear Modulus (G)

$$G = \frac{F_s^n}{M}$$

Where:

M = Slope of the Load-Strain Curve

4.5 Interlaminar Shear

The interlaminar shear stress is used to determine the quality of the resin system. This is determined by conducting short beam shear tests. Short beam shear test specimens and the test setup are shown in Figure 17. The specimens are laid up from 0° cloth. These tests are used to provide correlation data between the basic material properties derived in these tests and short beam shear tests for quality assurance inspection from other material lots.

The short beam shear tests were conducted according to the methods described in Reference 1. The specimen is loaded in a Universal testing machine as shown in Figure 17. Only the failing load is recorded. The method of calculating interlaminar shear stress is from Reference 1.

Interlaminar Shear Stress

$$F_{is} = \frac{3P}{4tW}$$

Where:

P = Failing Load

t = Thickness of Specimen

W = Width of Specimen

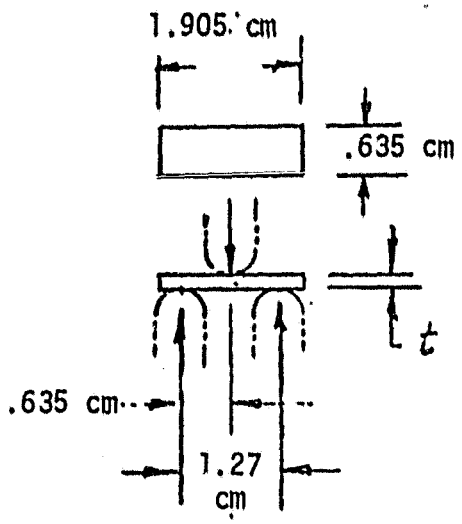

SHORT BEAM SHEAR TEST SPECIMEN AND TEST SETUP
FIGURE 17

4.6 Flexural Stress

Flexural stress measurements are made as a means of establishing quality control limits. Flexural stress and flexural modulus is measured by conducting flexural tests. The flexural tests are conducted according to the methods described in Reference 1. The specimen is loaded in a Universal testing machine as shown in Figure 18. Only the failing load is recorded. The methods of calculating flexural stress and flexural modulus are from Reference 1.

Flexural Stress

$$F_{fs} = \frac{3P}{2t^2W}$$

Flexural Modulus

$$E_f = \frac{L^3M}{4t^3W}$$

Where:

P = Failing Load

t = Thickness of Specimen

W = Width of Specimen

L = Distance Between Supports = 32t

M = Stress Divided by Strain

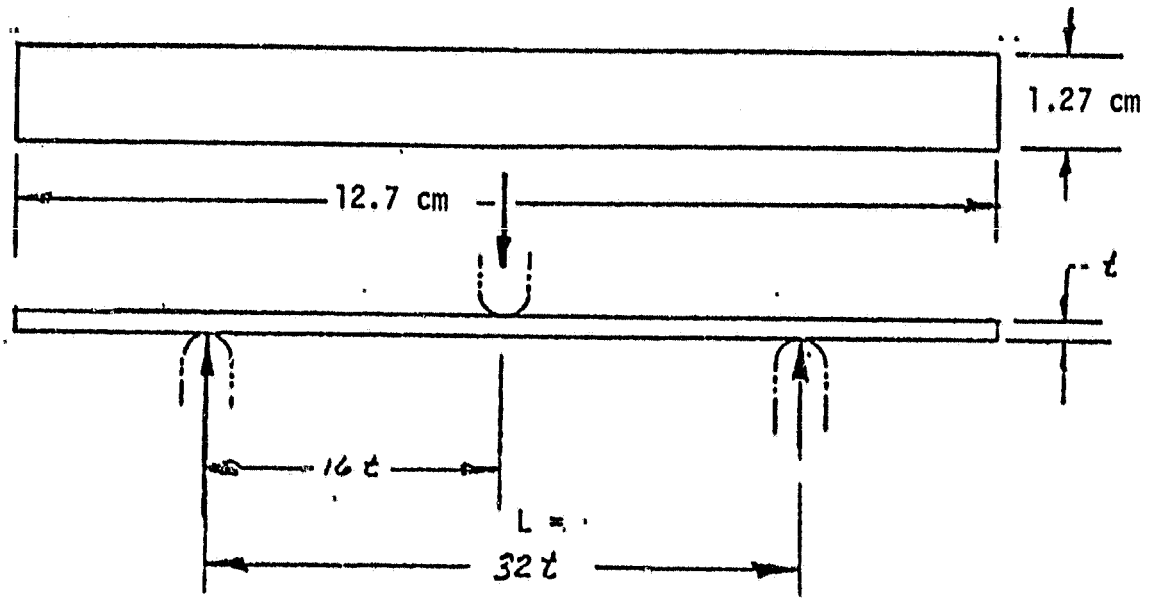

FLEXURAL TEST SPECIMEN AND TEST SETUP

FIGURE 18

5.0 MECHANICAL PROPERTIES

The mechanical properties were determined. The longitudinal fiber layup is for 353 style Kevlar cloth oriented 0°/90°. The isotropic layup is with the layup at 0°/90°, ±45°. Stresses are based on the nominal thickness of the specimen which is the average thickness for a given number of plies. This is more useful for design since strength will be primarily a function of the number of plies used as to thickness variations that occur after cure.

The initial tangent modulus is the initial slope of the stress-strain curve. Kevlar/PMR-15, particularly in compression, exhibits a decreasing modulus near failure stress. Room temperature is about 294°K to 297°K.

5.1 Tensile and Compressive Properties of Longitudinal Layup

Tensile and compressive properties of longitudinal bidirectional specimen were determined using sandwich beams with a specimen width of 2.54 cm.

The ultimate strength, initial tangent modulus, and Poisson's ratio for 0°/90° specimen in tension is shown in Table 2. The data is for tests at 219°K, room temperature, 394°K and 505°K. The Poisson's ratio data does not appear to be correct although there is no known reason for error.

The ultimate strength, initial tangent modulus, and Poisson's ratio for 0°/90° specimen in compression is shown in Table 3. This data is for 219°K, room temperature, 394°K and 505°K. Again, the Poisson's ratio data does not appear to be correct.

5.2 Tensile and Compressive Properties of Isotropic Layup

Tests conducted on isotropic layups with cloth fiber oriented at 0°/90°, ±45° were conducted using specimens that were 3.8 cm wide with a 0.64 cm hole. The gross stress is the value determined using the overall specimen width. The net stress is the value based on the net width which is the overall width less the diameter of the hole. For the data presented, except as noted, the failures occured at the hole.

The initial tangent modulus is based on the gross stress because a 2.54 cm or 5.08 cm extensometer was used to measure strain.

Effects of Temperature

The ultimate stress and initial tangent modulus in tension is shown in Table 4 for 219°K, room temperature, 394°K and 505°k from sandwich beam tests. The data from coupon tests conducted at room temperature and 505°K are shown in Table 5.

The ultimate stress and initial tangent modulus in compression is shown in Table 6 for 219°K, room temperature, 394°K and 505°K from sandwich beam tests. The data from coupon tests at room temperature and 505°K are shown in Table 7.

Effects of Moisture

The ultimate stress and initial tangent modulus in tension after conditioning in 95% humidity at 333°K for 30 days is shown in Table 8.

These data are from coupon tests conducted at 219°K, room temperature, 394°K and 505°K.

The ultimate stress and initial tangent modulus in compression after conditioning in 95% humidity at 333°k for 30 days is shown in Table 9. These data are from coupon tests conducted at 219°K, room temperature, 394°K and 505°K.

Effects of Skydrol

The ultimate stress and initial tangent modulus in tension after conditioning by soaking in Skydrol at 333°K for 7 days followed by 95% humidity at 333°K for 30 days is shown in Table 10. These data are from coupon tests conducted at 219°K, room temperature, 394°K and 505°K. The values from Skydrol conditioned sandwich beam tests conducted at 219°K and room temperature are shown in Table 11.

The ultimate stress and initial tangent modulus in compression after conditioning by soaking in Skydrol at 333°K for 7 days followed by 95% humidity at 333°K for 30 days is shown in Table 12. These data are from coupon tests conducted at 219°K, room temperature, 394°K and 505°K. The data from Skydrol conditioned sandwich beam tests conducted at 210°K and 394°K are shown in Table 13.

5.3 Fatigue Life

The fatigue life tests were conducted with isotropic beams subjected to alternating tension and compression loads in the composite face sheet. The tests were conducted at room temperature on dry, humidity conditioned, and Skydrol conditioned beams. The results are shown in Table 14. Specimen K-150 failed at the start of the test.

5.4 Shear Bearing Strength

The shear bearing strengths as shown in Table 15 were calculated for the nominal thickness of 0.488 cm (0.192 in.). The initial bearing failure stress is that for when the first peak occurs in the load. The shear out stress is that for the last peak. The anomaly in the initial bearing failure stress at 394°K (250°F) is not understood. The shear out stress at 394°K (250°F) appears to follow the expected trend with temperature.

5.5 Transverse Shear Strength

The transverse shear strength was determined from in plane shear tests. Tests were conducted at 219°K (-65°F), room temperature, 394°K (250°F), and 505°K (450°F). The rails debonded from the composite specimen during the tests at 505°K and the data are not presented since they are not valid. The remaining data are shown in Table 16.

5.6 Interlaminar Shear Strength

The interlaminar shear strength was determined from short beam shear tests. The test results are shown in Table 17.

5.7 Fiber Stress

The fiber stress was determined by measuring the flexural stress and flexural modulus. The results are shown in Table 18.

6.0 REFERENCES

1. Douglas Material Specification 2193, "Aramid Fabric, High Temperature Polyimide Impregnated", November 17, 1978.

2. Douglas Aircraft Company Report No. MDC J7148, "IRAD Report - Method of Test for Compressive or Tensile Strength Properties of Composite Laminates", C.Y. Kam, October 1976.

3. Douglas Aircraft Company Report No. MDC J7149, "IRAD Report - Method of Test for Inplane Shear Strength Properties of Composite Laminates", C.Y. Kam, October 1976.